HspB8 Protein Expression in Pregnant Rat Myometrium throughout Pregnancy

By

© Noelle Lillian Marsh

A thesis submitted to the School of Graduate Studies in partial fulfilment of the requirements for the degree of Master of Science (Medicine).

Division of BioMedical Sciences
Memorial University of Newfoundland

May 2014

St. John's Newfoundland & Labrador

Abstract

Heat shock protein (Hsp) B8 is highly expressed in smooth muscle, but the expression and function in uterine smooth muscle, or myometrium, during pregnancy remains unknown. The goal of this project was to characterize the myometrial expression of HspB8 protein in pregnant rats during myometrial programming.

Immunoblot analysis determined that HspB8 and the co-chaperone Bcl2-associated athanogene (Bag) 3 protein expression was elevated at mid-gestation at day (d)15 and d17 ($p<0.05$; $n=4$). The intracellular localization of HspB8 and Bag3 has not been well characterized; therefore, spatiotemporal expression in pregnant rat myometrium was also determined by immunofluorescence analysis. HspB8 and Bag3 were predominantly localized to the cytoplasm of myometrial cells and were not found in nuclei. To determine whether an HspB8-Bag3 complex existed in myometrial cells during pregnancy, co-immunoprecipitation assays were performed. The results demonstrated that an HspB8-Bag3 complex was present *in vitro* and *in vivo,* at non-pregnant, d15 and d23. This investigation provides valuable insights into the spatiotemporal expression of HspB8 and Bag3 and evidence of formation of a heteromeric signaling complex, HspB8-Bag3, in uterine musculature during pregnancy. With known roles of these proteins in macroautophagy activation, these results suggest that HspB8 and Bag3 could have similar function(s) during myometrial hypertrophy.

Acknowledgements

First of all, I would like to thank my supervisor Dr. Daniel MacPhee for giving me the opportunity to work in his reproductive biology lab for the past 2 years. It has been an amazing experience that has helped me develop into the person that I am today. His patience, advice and guidance were greatly appreciated throughout the completion of my master's degree. In particular, I would like to thank him for his mentoring and encouragement throughout the year, above and beyond his role as a supervisor. I will certainly miss trying to teach him the "proper" way to say St. Anthony. I would also like to show my appreciation to my labmates Joanne Delaney, Sarah Dinn, Gina Hamilton, Trina Kirby, Ewa Miskiewicz, Justin Pater, Mandy Peach and Bryan White for all of their help while I was becoming accustomed to the new lab techniques. To Joanne Delaney, thank you for helping make Team Uterus number one! To Sarah Dinn, for being the best friend a girl could ask for. We have shared so many laughs together and I certainly could not have done this without you. Remember our first day in the lab alone with those glass pipettes. Go Team Uterus! To Gina Hamilton, Geebs, thank you for all the great laughs that we have shared, most importantly Bridesmaids. I hope Team Placenta is not too jealous of Team Uterus. To Trina Kirby, thank you for helping me become accustomed to all the new lab techniques. To Ewa Miskiewicz, thank you for all of your help in the lab. I would never have been able to make TAE buffer without you! To Justin Pater, J Biebs, thank you for letting me teach you some newfie slang and for listening to Carly Rae Jepsen 24/7. Also, if you ever need hair advice I am always here for a consult. To Mandy Peach, thank you for teaching me the ropes of the lab and for being such a great mentor.

To Bryan White, thank you for the awesome glasses from the “mystery office”. To Brian MacPhee, thank you for all your technological advice, I would have never been able to purchase my Mac without you! I would also like to thank my supervisory committee, Drs. Ann Dorward and Noriko Daneshtalab, for all their support and excellent suggestions. Finally, I would like to thank my family and friends for their love and support throughout the year; I could not have done this without your daily words of encouragement!

This research was supported by an operating grant from NSERC (National Sciences and Engineering Research Council) and an Alexander Graham Bell Canada Graduate Scholarship from NSERC.

Table of Contents

List of Tables

List of Figures

List of Appendices

Abbreviations

4EBP1	Eukaryotic initiation factor 4E (eIF4E)-binding protein
2-ME	2-methyoxymethylestradiol
4EBP1	Eukaryotic initiation factor 4E binding protein 1
A	Absorbance
A260	Absorbance at the wavelength 260 nm
A280	Absorbance at the wavelength 280 nm
ADH	Alcohol dehydrogenase
AMPK	5’ adenosine monophosphate-activated protein kinase
Ang II	Angiotensin II
ANOVA	Analysis of variance
A-RAF	A- rapidly accelerated fibrosarcoma
Atg	Autophagy-related gene
ATP	Adenosine triphosphate
AUG^{START}	Methionine start codon
Bag	Bcl2-associated athanogene
Bcl2	B-cell lymphoma 2
Bcl2l1	Bcl2-like 1
bp	Base pairs
BSA	Bovine serum albumin
BrdU	5’-bromo-2’-deoxyuridine
$[Ca^{2+}]_i$	Intracellular calcium concentration
cAMP	Cyclic adenosine monophosphate
CAPs	Contraction associated proteins
cDNA	Complementary DNA
CHIP	C-terminus of Hsc70-interacting protein
CMA	Chaperone-mediated autophagy
Ctrl	Control
Cx	Connexin
Cy5	Cyanine 5
d	Day
DAG	Diacylglycerol
DAPI	4’,6-Diamidino-2-Phenylindole
ddH_2O	Double deionized water
Dm	Drosophilia melanogaster
DEM	Glutathione-depriving agent diethylmaleate
DMEM	Dulbecco’s modified Eagle’s medium
DNA	Deoxyribonucleic acid
ECL	Electrochemiluminescence
ECM	Extracellular matrix

EDTA	Ethylenediaminetetraacetic acid
EGF	Epidermal growth factor
eIF	Eukaryotic initiation factor
eIF4E	Eukaryotic initiation factor 4E
ER	Endoplasmic reticulum
ER-α	Estrogen receptor alpha
ERK	Extracellular signal-regulated kinases
FAK	Focal adhesion kinase
FBS	Fetal bovine serum
FIP200	Focal adhesion kinase family interacting protein of 200 kilodaltons
FITC	Fluorescein isothiocyanate
FP-receptor	Prostaglandin F receptor
FSC	Forward scatter
G	Gravid
GAPDH	Glyceraldehyde 3-phosphate dehydrogenase
GTP	Guanosine-5'-triphosphate
Hr	Hour
HRP	Horseradish peroxidase
Hsc	Heat shock cognate
HSE	Heat shock element
HSF-1	Heat shock factor protein 1
Hsp	Heat shock protein
sHsp	Small heat shock protein
hTERT-HM	Human Telomerase Reverse Transcriptase- Human myometrial cells
Htt43Q	Huntingtin exon 1 fragment with 43 CAG repeats
IB	Immunoblot
IF	Immunofluorescence
IGF-1	Insulin-like growth factor 1
Igfbp1	Insulin-like growth factor binding protein 1
IGF-1R	Insulin-like growth factor 1 receptor
IgG	Immunoglobulin G
Ile	Isoleucine
IP	Immunoprecipitation
IP_3	Inositol 1,4,5-triphosphate
IPV	Isoleucine-Proline-Valine
IRS	Insulin receptor substrate
kDa	Kilodalton
KFERQ	Lysine-Phenylalanine-Glutamate-Arginine-Glutamine
LAMP2A	Lysosome-associated membrane protein 2
LC3	Microtubule associated protein light chain 3
LC3I	Microtubule associated protein light chain 3 I

LC3II	Microtubule associated protein light chain 3 II
LIR	LC3II interacting region
MII	Myosin motor II
MAPK	Mitogen activated protein
MLC_{20}	Myosin light chains
MLCK	Myosin light chain kinase
min	Minutes
mRNA	Messenger ribonucleic acid
mTOR	Mammalian target of rapamycin
mTORC1	Mammalian target of rapamycin complex 1
NG	Non-gravid
nm	Nanometers
O	Oil
NP	Non-pregnant
NP-40	Nonidet-P40
OTR	Oxytocin receptor
P	Phosphorylation
P4	Progesterone
PBS	Phosphate-buffered saline
PDZ	Post synaptic density protein, Drosophila disc large tumor suppressor and zonula occludens-1 protein
PE	Phosphatidylethanolamine
Pen/Strep	Penicillin/streptomycin
PFA	Paraformaldehyde
$PGF_2\alpha$	Prostaglandin $F_2\alpha$
PGI_2	Prostaglandin I_2
PGIS	Prostacyclin synthase
PI3K	Phosphoinositide-3-kinase
PIP_2	Phosphatidylinositide biphosphate
PKB	Protein kinase B
PLCγ	Phospholipase C-gamma
PMCA	Plasma membrane Ca^{2+} ATPase
PP	Post-partum
PR	Progesterone receptor
Pro	Proline
pSer15-HspB1	Serine15-phosphorylated HspB1
PTK2	Protein tyrosine kinase 2
P-Tyr	Tyrosine phosphorylation
PXXP	Proline-rich repeat
rcf	Relative Centrifugal Force
RHEB	Ras homolog enriched in brain

RIPA	Radioimmunoprecipitation assay
RT	Room Temperature
RT-PCR	Reverse transcription polymerase chain reaction
RU486	Mifepristone
s.c	Subcutaneously
SC buffer	Saline sodium citrate buffer
SDS	Sodium dodecyl sulfate
SDS-PAGE	Sodium dodecyl sulfate polyacrylamide gel electrophoresis
SEM	Standard error of the mean
Ser	Serine
SERCA	Sarco/endoplasmic reticulum Ca^{2+}-ATPase
SK6	S6 Kinase
SOD1	Superoxide dismutase 1
SQSTM1	Sequestome 1
Src	Sarcoma
SSC	Side scatter
TBST	Tris-buffered saline-tween
Thr	Threonine
TORC1	Target of rapamycin complex 1
TSC2	Tuberous sclerosis complex 2
Tyr	Tyrosine
ULK	Unc-51-like kinase
Val	Valine
WW	Tryptophan domain

Chapter One

Introduction

1.1 Preterm Birth: Clinical Significance

Preterm labour in humans can be defined as childbirth occurring prior to the optimal human gestation period of 37-42 weeks [1]. Currently, there is no diagnostic indicator of preterm labour and following initiation there is no effective method to significantly inhibit the process [2]. This is of major concern as premature birth is a key factor associated with neonatal mortality and morbidity and has serious long-term health-related consequences [3]. Premature babies are at high risk of life-long developmental disabilities, mental retardation, cerebral palsy, cognitive impairment, cardiovascular disease, vision impairment, diabetes and early death [4-6]. United States statistics indicate that preterm birth contributes to approximately 85 % of all perinatal deaths and approximately ten percent of newborns each year are preterm infants, weighing less than 2500 g [7]. In Canada, premature birth constituted 7.8 % of all births in 2011-2012 [8]. Of all provinces, Alberta and Newfoundland and Labrador showed the highest preterm birth rates, 8.3 % and 8.2 %, respectively [8]. Multiple-fetus pregnancies are predisposed to delivering prematurely; over 52.2 % of multiple births occur prior to 37 weeks and 10.7 % before 32 weeks of gestation [9].

Preterm labour causes substantial economic burdens on families, communities, and the health care system. In 2001, a preterm infant required an average hospital stay of 12.9 days and a cost of $15,100, whereas an uncomplicated newborn remained in hospital

for only 1.9 days with a much lower cost of $600 [10]. The total cost due to preterm/low birth weight deliveries in 2001 totalled $5.8 billion in the United States. This figure does not include any treatments that were required after parturition with respect to developmental disabilities or other health concerns [10].

Major causes of preterm birth fall into three main categories: the first is delivery for maternal or fetal complications and labour is induced or the infant is delivered by pre-labour caesarean section; the second is due to premature rupture of the fetal membranes; and the final category is termed idiopathic preterm labour and arises from an unknown cause [1]. About 30% of preterm births are due to maternal or fetal infections, 25–30% follow premature rupture of fetal membranes and 40–45% are idiopathic [11]. Aside from the three main categories, there is also evidence indicating that the increased use of obstetric interventions (iatrogenic), including both induction of labour and caesarean sections, may result in early delivery [4, 9].

Despite intensive research efforts in obstetrics, the mechanisms resulting in preterm birth largely remain unknown; however, it is now clear that the causes of preterm birth are multifactorial. According to the literature, the fetal genome contributes signals that initiate parturition, ultimately leading to phenotypic changes in the uterine smooth muscle or myometrium [12]. Throughout most of a normal gestation period, the myometrium remains in a quiescent state but at term switches to an active state that is capable of producing contractions forceful enough to expel the fetus. This thesis aims to increase our understanding of the mechanisms underlying normal labour, including myometrial adaptation and function during pregnancy. This knowledge of normal

function may help us acquire a more complete comprehension of the causes of signaling asynchrony between mother and fetus in pre-term labour. Future research efforts will help to develop effective treatment and prevention strategies for preterm birth.

1.2 Uterus: The Myometrium

The human uterus is a pear-shaped, muscular organ that is composed of smooth muscle and is found in the midline between the bladder and rectum of a woman. This hollow reproductive organ is unique to viviparous female mammals and is responsible for protecting and nourishing the developing embryo and fetus [13]. The uterus undergoes extensive physiological changes throughout the gestational period as it accommodates the developing fetus, placenta and amniotic fluid [14]. During gestation, the uterus dramatically expands superiorly into the abdominal cavity. A 75 g non-pregnant uterus may become a 1300 g uterus at term. In comparison to the non-pregnant uterus, which typically has a capacity of 10 ml, the uterus at term has an average capacity of 5 L [15].

The human uterus is composed of three different tissue layers: the serosa, a thin outer connective tissue covering; the myometrium, a thick middle layer of smooth muscle; and an inner layer known as the endometrium, comprised of epithelial cells and an underlying layer of thick connective tissue [16]. Implantation of the multicellular blastocyst normally occurs in the body of the uterus, more specifically into the endometrium. The rat myometrium is composed of two distinct muscle layers, the outer longitudinal layer and the inner circular layer that work together to generate strong waves of contraction to expel multiple fetuses at term (Figure 1.1A). When a cross section of the

rat myometrium is viewed under a microscope, the longitudinal layer appears as muscle bundles that often surround vascular channels whereas the circular layer is found circumferentially next to the endometrium [17].

The rat is an often-used model for studying the basic cellular mechanisms of smooth muscle contraction in the myometrium. The myometrium is easily obtainable from pregnant rats and their gestational period is shorter than the human gestational period. In addition, the rat can be manipulated endocrinologically and surgically as the rat uterus is bilateral with two horns that extend toward the kidneys (Figure 1.1B,C). The bicornuate uterus provides the opportunity to treat one horn differently from the other. The work presented in this thesis is based upon the rat model of pregnancy and further discussion will focus on the phases of rat myometrial differentiation throughout pregnancy (Figure 1.2).

1.3 Phases of Myometrial Differentiation

Throughout pregnancy the smooth muscle cells of the myometrium differentiate. This differentiation is required to activate the tissue and in turn drive the necessary myometrial contractions required for delivery of the fetus. Each distinct phase of pregnancy is regulated by mechanical (distension) influences, endocrine influences or both [1].

Figure 1.1(A) A diagrammatic representation of a cross section of a rat uterine horn. The rat myometrium is composed of two muscle layers, the outer longitudinal layer and the inner circular layer that work together to generate strong waves of contraction to expel the fetus at term. When a cross section of the myometrium is viewed under a microscope, the longitudinal muscle layer appears as muscle bundles that often surround vascular channels. The circular muscle layer is found circumferentially next to the endometrium. **(B)** A rat uterus dissected from a non-pregnant Sprague Dawley rat. **(C)** A cartoon image of a pregnant rat uterus demonstrating the two horns that extend toward the kidneys.

A

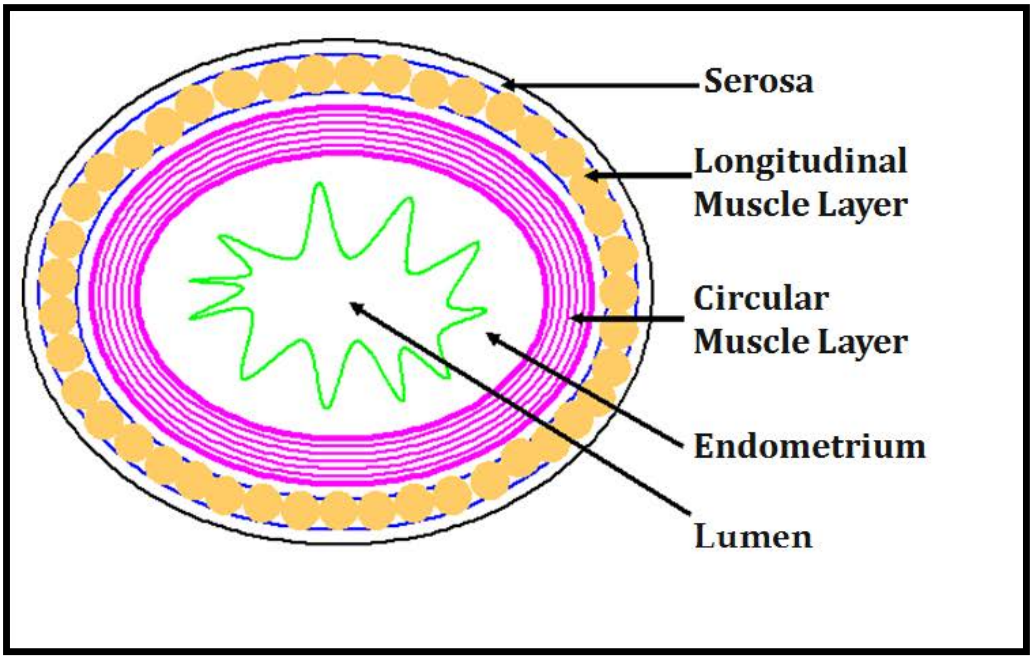
Serosa
Longitudinal Muscle Layer
Circular Muscle Layer
Endometrium
Lumen

B

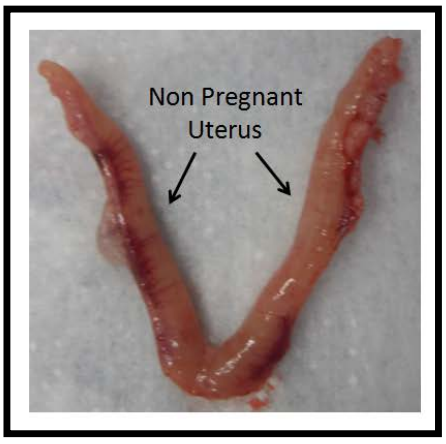
Non Pregnant Uterus

C

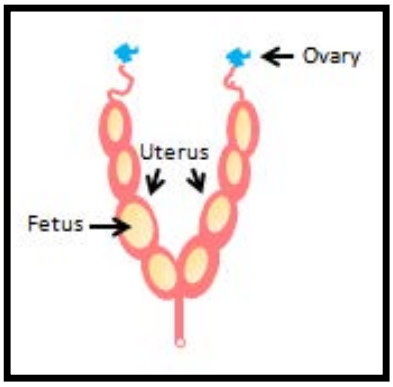
Ovary
Uterus
Fetus

Figure 1.2 The phases of rat myometrial differentiation throughout pregnancy. The initial proliferative phase of gestation, from the non-pregnant (NP) state to ~day (d) 14, is characterized by hyperplasia. Around d14 of gestation proliferation decreases and it is followed by a synthetic phase in which the myocyte growth switches to a phase of hypertrophic growth and it is associated with an increase in the extracellular matrix (ECM). At ~d21 of pregnancy the myocytes differentiate further to a contractile phenotype, which lasts until ~d23. During this time the myometrium becomes spontaneously active, excitable, and highly responsive to uterine agonists. Finally, the myometrium enters the labour phase, which is marked by an up-regulation of contractile associated proteins (CAP) that allow the myometrium to become activated and able to generate highly coordinated contractions that are capable of expelling the fetus. PP= post-partum.

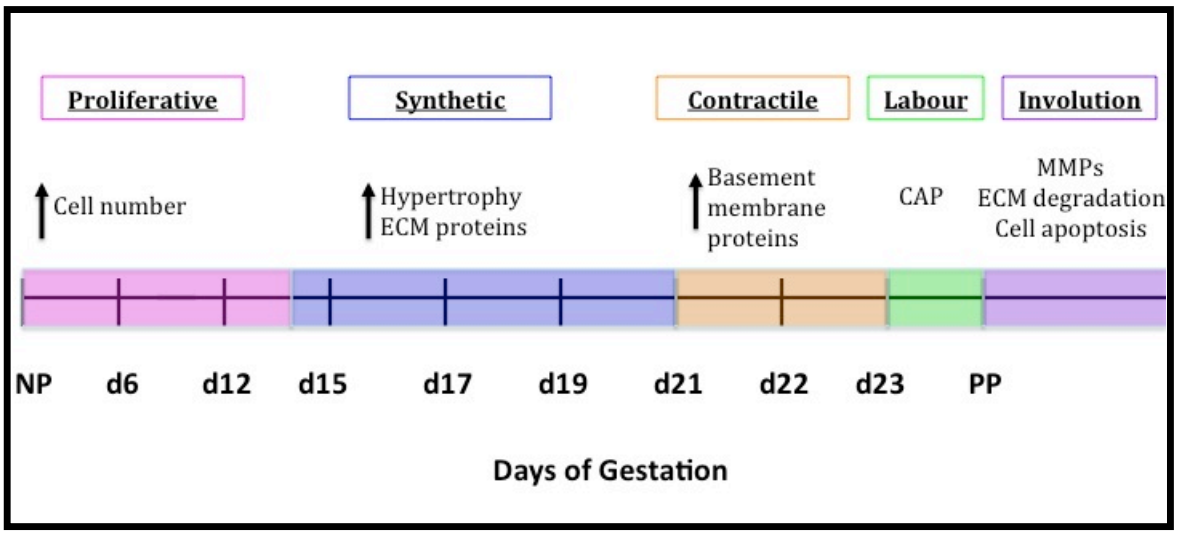
Proliferative
Synthetic
Contractile
Labour
Involution
Cell number
Hypertrophy
ECM proteins
Basement
membrane
proteins
CAP
MMPs
ECM degradation
Cell apoptosis
NP
d6
d12
d15
d17
d19
d21
d22
d23
PP
Days of Gestation

1.3.1 *Proliferation*

In the rat model, the initial proliferative phase of gestation is from a non-pregnant state to approximately day (d) 14 of gestation. This phase is characterized by an increase in cell number in the myometrium, also known as hyperplasia [18]. Initial studies on myometrial cell proliferation conducted by Shynlova et al. [19] indicated increased incorporation of 5-bromo-2'-deoxyuridine (BrdU), a nonradioactive analogue of thymidine and marker of individual cell proliferation, into uterine myocytes at d6 and d12 of pregnancy. Furthermore, they noted increased expression of proliferating cell nuclear antigen between d6 and d15 of pregnancy. Myocyte proliferation occurs very rapidly and predominantly in the longitudinal muscle layer in both the non-gravid and gravid horns of unilaterally pregnant rats [18]. Therefore, it has been suggested that the initial phase of proliferation is primarily under the control of endocrine signals. During this phase there is a significant increase in expression of anti-apoptotic factors, such as B-cell lymphoma 2 (Bcl2), which may contribute to the increase in cell number [19]. More specifically, myometrial proliferation is induced by estrogen-regulated growth factors including insulin-like growth factor 1 (IGF1) and epidermal growth factor (EGF) [19]. Shynlova et al. found that *Igf-1* and *Igfbp1* (its associated binding protein) mRNA levels were up-regulated in the rat myometrium during d6-d12 of gestation [20]. Cell proliferation has also been found to be modulated by the PI3K-PKB-mTOR (mammalian target of rapamycin) signaling pathway in many tissues, including the myometrium (Figure 1.3) [21, 22]. 17β-Estradiol and IGF-1 production result in activation of phosphoinositide-3-

Figure 1.3 Cell proliferation modulated by the PI3K-PKB-mTOR (mammalian target of rapamycin) signaling pathway. Once insulin or IGFs bind to their appropriate receptors, this leads to the recruitment and phosphorylation of the insulin receptor substrate (IRS) and successive recruitment of phosphoinositide-3-kinase (PI3K). Subsequent PI3K activation is the result of a cascade of phosphorylation reactions but ultimately the most prominent effector of PI3K activity is protein kinase B (PKB). PKB promotes target of rapamycin complex 1 (TORC1) signaling, by phosphorylating several sites on tumour suppressor tuberous sclerosis complex 2 (TSC2), which relieves inhibition of Ras homolog enriched in brain (RHEB; a member of the Ras superfamily of GTPases) and thus activates TORC1. The two most characterized targets of mTORC1 are eukaryotic initiation factor 4E (eIF4E)-binding protein (4EBP1) and ribosomal S6 kinase (SK6). 4EBP1 is inactivated by mTOR phosphorylation, resulting in the release of eIF4E to promote translation. Furthermore, activation of mTORC1 causes initiation of protein translation by phosphorylating S6K1. S6K1 then phosphorylates the S6 protein of the 40S ribosomal subunit and leads to increased ribosomal biogenesis and ultimately increased protein synthesis. Adapted from Russell et al., 2011 [22]. P= phosphorylation

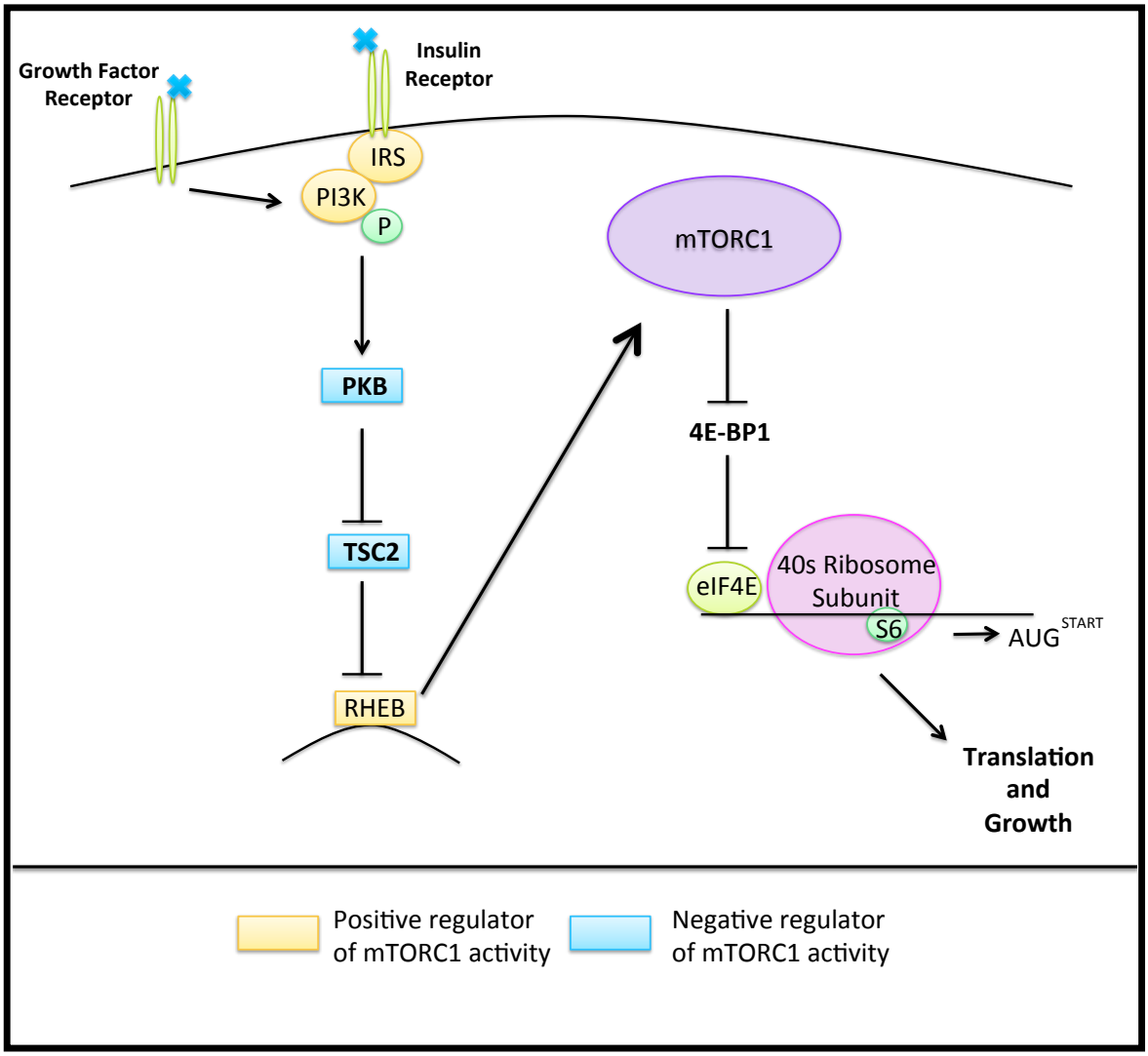
Growth Factor Receptor
Insulin Receptor
IRS
PI3K
P
PKB
TSC2
RHEB
mTORC1
4E-BP1
eIF4E
40s Ribosome Subunit
S6
AUG START
Translation and Growth
Positive regulator of mTORC1 activity
Negative regulator of mTORC1 activity

kinase (PI3K) signaling, which has been found to cause cell proliferation and growth in reproductive tissues [20, 23, 24]. Once insulin or IGFs bind to their appropriate receptors, this leads to the recruitment and phosphorylation of the insulin receptor substrate (IRS) and successive recruitment of PI3K [25, 26]. Subsequent PI3K activation is the result of a cascade of phosphorylation reactions but ultimately the most prominent effector of PI3K activity is protein kinase B (PKB) [21]. PKB is a serine (Ser)/threonine (Thr) kinase that is able to positively regulate mTOR [27-29]. PKB promotes target of rapamycin complex 1 (TORC1)- one of the two multiprotein complexes formed by mTOR- signaling, by phosphorylating several sites on tumour suppressor tuberous sclerosis complex 2, which relieves inhibition of Ras homolog enriched in brain (a member of the Ras superfamily of GTPases) and thus activates TORC1 [30-32]. Activation of the mTORC1 pathway results in activation of protein synthesis, metabolism, ribosome biogenesis and transcription. The two most characterized targets of mTORC1 are eukaryotic initiation factor 4E (eIF4E)-binding protein (4EBP1) and ribosomal S6 kinase (SK6). 4EBP1 negatively regulates the assembly of initiation factors as it binds and sequesters eIF4E, which inhibits the recruitment of the translation initiation complex required for protein synthesis [33, 34]. 4EBP1 is inactivated by mTOR phosphorylation, resulting in the release of eIF4E to promote translation [35]. Furthermore, activation of mTORC1 causes initiation of protein translation by phosphorylating S6K1. S6K1 then phosphorylates the S6 protein of the 40S ribosomal subunit and leads to increased ribosomal biogenesis and ultimately increased protein synthesis [36, 37]. Studies on proliferative uterine myocytes throughout gestation indicate that upstream regulators, including IRS-1, PI3K, PKB and downstream

effectors S6K1 and 4EBP1 - which are all involved in activation of mTOR - were significantly up-regulated during the proliferative phase of myometrium differentiation [21]. mTORC1 pathway activation can be blocked by the m-TOR-specific inhibitor rapamycin [25]. When rapamycin was used to inhibit mTOR signaling in pregnant rats there was a reduction in the number of proliferating cells in the pregnant myometrium [21]. P-mTOR, P-S6K1 and P-4EBP1 protein expression decreased significantly in these rapamycin rats, supporting the notion that myometrial hyperplasia is controlled by the PI3K-PKB-mTOR signaling pathway [21].

1.3.2 *The Synthetic Stage*

At approximately d14 of gestation, proliferation decreases and it is followed by a synthetic phase in which myocyte growth switches to a phase of hypertrophic growth [38]. Hypertrophy refers to an increase in cell size and it is associated with an increase in the synthesis of extracellular matrix (ECM) and cellular growth [38, 39]. The cause of the switch in myocyte growth from proliferation to hypertrophy is unknown, but the switch coincides with the activation of the apoptotic cascade machinery [18]. There is significant up-regulation of specific caspases, such as initiator caspase-9 and effector caspases 3, 6 and 7 at ~d14 of gestation, which are essential to apoptosis [18]. Even though the apoptotic cascade is activated during this window of time there are no physiological manifestations of myocyte apoptosis, indicating that it may be modulating other physiological processes [18]. Activation of the apoptotic pathway may be due to a period of hypoxia around mid-pregnancy in the rat that results from the growing fetus reaching a

maximal spherical radius and consequently, impeding maternal blood flow and oxygen supply [40]. Once the shape of fetal growth switches to ellipsoid, this relieves the tension and restores maternal blood flow throughout the uterus [40]. Evidence of myometrial hypoxia is shown by the presence of two different markers, hypoxia-inducible factor-1α and the hydroxyprobe pimonidazole hydrochloride, primarily in the circular muscle layer of the rat myometrium on d14 of gestation [41].

The synthetic phase of myometrial differentiation is characterized by an increase in the protein: DNA ratio in the pregnant rat myometrium, and a concomitant increase in the synthesis and deposition of interstitial matrix forming the ground substance of the myometrium [18]. The synthetic phase is also characterized by a marked increase in ECM proteins such as collagen I, collagen III and elastin, and reorganization of the ECM to ensure that cells are properly anchored throughout gestation [38, 42]. There is significant remodelling of cell matrix contacts through structures known as focal adhesions in cultured cells.

Focal adhesions are clusters of integrin molecules within the cell membrane that have extracellular domains that interact with the ECM surrounding the cell and cytoplasmic domains that interact with complexes of cytoplasmic and cytoskeletal proteins [43]. Extracellular ligands are coupled to cytoplasmic F-actin, by their integrin receptors, and thus mediate cell-matrix adhesions. The intracellular domain of integrin proteins interact with the cytoskeleton by adaptor proteins, such as talin, actinin and vinculin [44]. Focal adhesions are responsible for sensing mechanical forces and facilitating force transmittance generated through contractile proteins to the ECM and

muscle bundles [14, 43, 45]. Two key players in the focal adhesion signaling network include focal adhesion kinase (FAK) and paxillin, as they have been associated with turnover and remodelling of focal adhesions. Focal adhesions may allow cells to maintain critical cell-matrix interactions as cells increase in size during the synthetic phase of myometrial programming, as phosphorylated (activated) FAK, or PTK2, is found in the gravid myometrium during the synthetic phase [46]. In the synthetic phase the expression of γ-smooth muscle actin and I-caldesmon also begin to increase, a finding characteristic of a relatively undifferentiated contractile state [47].

Induction of myometrial hypertrophy requires an increase in uterine tension and the presence of progesterone. Progesterone appears to play a key role in pregnancy as it is required by almost all species for both the establishment and maintenance of pregnancy [48]. The circulating levels of progesterone in rat maternal serum have been found to peak specifically between d15-d19 after which there is a dramatic decline until labour [49]. Progesterone is known to suppress the initiation of labour as the removal of progesterone, via ovariectomy early in pregnancy or administration of a progesterone antagonist (mifepristone, RU486), results in early termination of pregnancy [50]. Administration of RU486 to pregnant animals on d17 resulted in attenuation of hypertrophy, thus indicating that progesterone circulation is essential for cell growth [19]. Progesterone is also important in the synthesis of ECM proteins, including collagen I and II and elastin. After progesterone levels decreased at term or following administration of RU486, the secretion of these proteins decreased significantly. Administration of RU486

also results in a premature increase in collagen IV, fibronectin and laminin expression [38]. In contrast, administration of exogenous progesterone at d23 delayed the onset of labour by reducing the level of fibronectin and laminin mRNA and preventing a decrease in collagen III mRNA [19, 38]. Fibronectin and laminin are ECM molecules that surround myometrial smooth muscle cells during the contractile stage [14, 38].

1.3.3 *The Contractile Stage*

At approximately d21 of pregnancy the myocytes differentiate further to a contractile phenotype, which lasts until d23 (labour). During this phase, hypertrophy is stabilized and there is a marked increase in the interaction between the myocyte and the underlying matrix. At this time, the myometrium becomes spontaneously active, excitable and highly responsive to uterine agonists [14]. Instead of synthesis of interstitial matrix, which is characteristic of the synthetic phenotype, there is significant up-regulation of matrix proteins such as fibronectin, laminin β2 and collagen IV, which form the basement membrane surrounding each smooth muscle cell [14, 38]. This reorganization of uterine tissue architecture is crucial for extensive uterine hypertrophy [14]. In order to study the effects of stretch Ou et al. (1997) performed experiments in which virgin female rats underwent unilateral tubal ligation and therefore, the rat was only able to implant the conceptus in one horn [51]. This procedure provides an internal control allowing for separation of hormonal and mechanical influences. In unilaterally pregnant animals, the expression of matrix proteins (fibronectin, laminin β2 and collagen IV) was only found in the gravid horn, suggesting that uterine distension may be

regulating their expression [38]. Furthermore, increased expression of basement membrane proteins is associated with decreased levels of progesterone. Administration of RU486 to rats on d19 of gestation induced a switch from interstitial to basement membrane, as measured by the pre-mature increase in messenger ribonucleic acid (mRNA) levels of collagen IV, fibronectin and laminin, normally reached on day 23 during labour [38]. In the reciprocal experiment, exogenous progesterone was administered to pregnant rats to prevent a normal drop in circulating hormone, it was able to block changes in matrix synthesis and the transition to the contractile phenotype [38].

The contractile phenotype is also characterized by changes in the expression of contractile protein isoforms within smooth muscle cells. There is a transition in the expression of α-smooth muscle actin to the γ-actin isoform, which is more characteristic of a contractile phenotype, in conjunction with the expression of smooth muscle-specific contractile forms of tropomyosin and myosin heavy chain [47]. Lastly, there is a notable increase in H-caldesmon expression, an actin binding protein that is capable of inhibiting actomyosin interaction *in vitro* [52, 53]. Li et al., performed immunostaining using a phospho-*H*-caldesmon antibody and noted that phospho- H- caldesmon increased ~40-fold in staining during labour, compared to little staining of phospho-H- caldesmon in nonpregnant myometrium [53]. Thus, as H-caldesmon is involved in increasing smooth muscle contractility through thin filament mechanisms, caldesmon phosphorylation may reverse the inhibition of acotmyosin interactions by caldesmon which leads to increased contractility. [54, 55].

1.3.4 *The Labour Phase*

Just prior to d23 of gestation in the rat, the myometrium is activated and able to generate highly coordinated contractions that are capable of expelling the fetuses. This switch to an active state can occur as a result of signals produced by the maturing fetuses, including an up-regulation of corticotrophin-releasing hormone by the placenta, as well as an increase in mechanical stretch of the uterus [9]. At this point in gestation uterine growth is much slower than fetal growth, ultimately resulting in significant myometrial tension. Activation of the myometrium is defined biochemically as an increase in the expression of "contraction-associated proteins" (CAPs), such as the sodium channel, oxytocin receptor (OTR), prostaglandin F2α receptor and connexin 43 (Cx43; gap junction protein) and occurs as a result of the mechanical and endocrine signals [19, 50, 56, 57]. Ou et al. (1998) determined through semi-quantitative reverse transcription-polymerase chain reaction (RT-PCR) that OTR expression increases significantly with the onset of labour and thus oxytocin is able to stimulate uterine contractions [50]. Prostaglandin F2α ($PGF_2\alpha$) receptor is thought to play an important role in myometrial contractility as endogenous $PGF_2\alpha$ is capable of inducing labour and administration of the cyclooxygenase inhibitor, indomethacin, is able to inhibit uterine contractions and the onset of labour [56, 57]. To further support the role of prostaglandin F (FP) receptors in uterine contractility, there was a significant increase in FP-receptor protein expression towards the end of gestation, with a marked increase at the onset of labour [58]. In unilaterally pregnant rats, the increase in CAPs is only found in the gravid horn,

consistent with the notion that stretch plays an important role in the labour-associated up-regulation of these genes [50]. However, stretch is not the only requirement for expression of these genes as insertion of a polyvinyl tube into the non-gravid horn on d17 of gestation, a time when the circulating levels of progesterone are high, did not result in an increase in CAP gene expression [19]. Therefore, the differentiation of the myometrium to the labour phenotype appears to require both mechanical and endocrine influences.

Stretch of uterine muscle has been found to induce transient myogenic contractions. *In vitro* studies on smooth muscle strips from rat uterus indicate that stretch of uterine muscle results in an intracellular influx of Ca^{2+}, promoting stretch-induced contractions [59]. The increase in tension also results in an increase of CAPs, which results in activation of the myometrium and facilitates the coordinated contractions necessary for labour [5, 9]. Ou et al. (1997) found that an up-regulation of CAPs only occurred in the gravid (stretched) horns of unilaterally pregnant animals, which suggested that stretch had an important role in CAP activation [51]. Work performed by Shynlova et al. (2007) that focused on the same stretch model, further supported the role of uterine stretch on CAP activation as the artificially stretched horn showed higher OTR, Cx43, Cx26 and fibronectin expression in comparison to the non-gravid horn [14]. Furthermore, Ca^{2+} influx and PKC translocation from the cytosolic compartment to the membrane compartment, as a result of EGF, induced phosphorylation of Cx43 [60]. Phosphorylation of connexins is important for proper formation and modulation of

function of gap junction channels. Thus, Ca^{2+} influx, as a result of mechanical distension, may regulate Cx43 phosphorylation in the cytoplasmic domain [61]. These experiments indicate the importance of uterine distension on activation of the myometrium via coordinated expression of CAPs [1, 14]. Through the use of the unilateral pregnant rat model, it is evident that mechanical stretch plays a key role in regulating the synchronous, high-amplitude, high frequency contractions at labour [62]. In addition to animal data, a study on primary cultures of human uterine smooth muscle cells, from pregnant women before labour, indicate that stretch results in up-regulation of OTR mRNA expression and increased OTR gene promoter activity [63]. Also, prostaglandin I_2 (PGI_2), a potent vasodilator has been shown to be a major prostaglandin secreted before the onset of labour [64]. The effects of labour-like cyclic mechanical stretch on PGI_2 production has been analyzed in cultured human myometrial cells and the results suggest that cyclic mechanical stretch may be responsible for increased PGI_2 concentration towards the end of gestation. More specifically, cyclic mechanical stretch up-regulated prostacyclin synthase (PGIS) expression, a synthase responsible for regulating biosynthesis of $PGI_{2,}$ via activation of the transcription factor activator-protein-1 (AP-1) [65].

During labour, changes that must occur in the interaction between smooth muscles cells and the underlying matrix via focal adhesions. In screening rat myometrial stretch samples by anti-phosphotyrosine immunoblotting, Li et al. (2007) show an increase in the tyrosine phosphorylated bands identified as FAK, A- rapidly accelerated

fibrosarcoma (A-RAF), paxillin and Src in response to stretch [66]. MacPhee & Lye however, show a slightly different pattern of phosphorylated FAK expression [46]. Although tyrosine phosphorylation (P-Tyr) of myometrial FAK and its downstream substrate paxillin increase during late pregnancy (d15-d22), they found that there is a significant decrease in P-Tyr on d23 during the onset of labour [46]. Following administration of exogenous progesterone, pregnant animals show no decrease in FAK-P-Tyr enzyme activity on d23 and consequently, the labour process is inhibited. These findings indicate that progesterone is involved in modulating FAK activity/focal adhesion signaling [46]. The fall in FAK-P-Tyr enzyme activity may allow for stabilization of smooth muscle cells and ECM interactions resulting in stable focal adhesions, connecting ECM and actin cytoskeleton via integrin molecules [14]. Together these results support the notion that focal adhesions are responsible for force transduction and modulation of myometrial contractility, ensuring that the myometrium works as a mechanical syncytium through each contraction [45].

1.3.5 *The Involution Phase*

Following fetal delivery the myometrium undergoes significant tissue remodelling as a result of induction of matrix metalloproteinases, ECM degradation, and cell apoptosis to return the tissue to the non-pregnant state [18]. This phase, known as the involution phase, completes the reproductive cycle following pregnancy. Following parturition there is an increase in IGF-I and IGFBP-5 gene expression and IGF-1R, the receptor that binds to both IGFs, which may be associated with uterine tissue recovery

[20]. Eighty five percent of the collagen of an involuting rat uterus is resorbed in the first four days following parturition, representing one of the fastest known rates of collagen degradation in any connective tissue [67]. Immune scavenging is an important component of myometrial remodelling enhanced by the expression of chemokines. Monocyte chemotactic protein-1 and other cytokines such as, monocyte chemotactic protein-3, eotaxin, fractalkine, and macrophage inflammatory protein -1β are required for postpartum decidual breakdown and myometrial involution [68].

1.4 Regulation of Myometrial Contraction

Two different pathways initiate labour from fetal signals. One pathway is the fetal hypothalamic-pituitary-adrenal-placental axis and is primarily an endocrine cascade, whereas the other pathway is mechanical as the growing fetus creates tension on the uterine wall inducing changes within the uterine smooth muscle cells. As already described in section 1.3, it is thought that both of these pathways increase CAPs, as well as ECM proteins, cell matrix adhesion complexes, and contractile proteins to control the synchronized and temporally coordinated contractions of uterine myocytes at the onset of labour [43].

Uterine smooth muscle cells are specialized cells that are packed with contractile myofilaments that are ready for contraction [12]. Excitability of uterine myocytes ultimately depends on the movement of Na^{+}, Ca^{2+} and Cl^{-} ions into the cytosolic compartment from the extracellular space, and of K^{+} ions into the extracellular space

from the cytosolic compartment. Intracellular Ca^{2+} concentrations ($[Ca^{2+}]_i$) increase due to Ca^{2+} entry via plasma membrane cation channels, as well as release from intracellular stores in the endoplasmic reticulum. Also, a number of myometrial contractants interact with a specific G-protein coupled receptor in the myocyte plasma membrane which activates a trimeric G-protein containing a $G_{\alpha q}$ subunit to increase $[Ca^{2+}]_i$ [69]. $G_{\alpha q}$ activates phospholipase Cβ isoforms, causing the hydrolysis of phosphatidylinositide biphosphate (PIP_2) to generate inositol 1,4,5-triphosphate (IP_3) and diacylglycerol (DAG) [70]. IP_3 binds to its receptors on the ER causing an increase in release of ER Ca^{2+} and a subsequent rise in $[Ca^{2+}]_i$ [71, 72]. Similar downstream intermediates are also generated by an alternative pathway involving receptor tyrosine kinases that activate PLC_{Υ} and generate IP_3, ultimately increasing $[Ca^{2+}]_{i.}$ [73]. Upon labour, contractant hormones can also indirectly cause depolarization of smooth muscle cell plasma membranes leading to the entry of extracellular Ca^{2+} into the myometrial cells via L-type voltage-gated Ca^{2+} channels, resulting in an increase in $[Ca^{2+}]_i$ [74, 75]. When the membrane potential is depolarized to approximately −40 mV, the L-type voltage-gated Ca^{2+} channels open allowing a substantial influx of Ca^{2+} into the intracellular space [76]. Calmodulin, a calcium binding protein, requires binding of four calcium ions for its activation and thus a marked increase in Ca^{2+} is the key trigger for its activation [77]. The interaction between calcium and calmodulin then activates the key enzyme myosin light chain kinase (MLCK) by inducing a conformational change [1, 7]. Activation of MLCK results in phosphorylation of Ser^{19} on myosin light chains ($MLC_{20)}$ and causes a conformational change, ultimately increasing the angle in the neck domain of the two heavy chains of

myosin motor (MII) and the formation of a cross bridge between actin and myosin filaments (Figure 1.4). A marked increase in phosphorylation of MLC_{20} is important for activating the contractile machinery of the cell. MII undergoes a conformational change from the folded to extended state to become activated, allowing myosin and actin to move approximately 10 nm with respect to each other, resulting in a power stroke. Phosphorylation of the regulatory light chains of myosin also activates the myosin head domain, which constitutes the ATP hydrolysis site, to provide the mechanical energy required for contraction [17, 74]. Another mechanism of increasing the ATPase activity of MII is through phosphorylation of Thr^{18} on MLC_{20} [78-80].

The force transmission between smooth muscle cells throughout the uterus may occur by conduction of action potentials through gap junctions [81]. Gap junctions are structurally differentiated areas of the plasma membrane of a cell that are composed of an array of small channels formed by proteins termed connexins [82]. Connexins are arranged into hexameric hemichannels, which become aligned across adjacent cells to form an interconnecting pore that permits electrical or ionic coupling between the cells and provides a pathway for small molecules to shuttle from one cell to another, directly linking the interior of adjacent cells [83]. Gap junctions allow electrical and metabolic coupling among cells as signals initiated in one cell can readily propagate to neighboring cells, thus allowing synchronous muscle contractions. Accordingly, during the last 12 hours (h) of gestation in the rat, gap junctions between myometrial cells increase over 200-fold creating an electrical syncytium allowing coordinated contraction

Figure 1.4 Steps involved in contraction of uterine smooth muscle. A marked increase in Ca^{2+} activates calmodulin, which then allows activation of the key enzyme MLCK by inducing a conformational change. Activation of MLCK results in phosphorylation of Ser^{19} on MLC_{20} and causes a conformational change; ultimately increasing the angle in the neck domain of the two heavy chains of myosin motor II (MII) and the formation of a cross bridge between actin and myosin filaments. MII undergoes a conformational change from the folded to extended state to become activated resulting in a power stroke and contraction. Based on figure from Wray, 1993 [75].

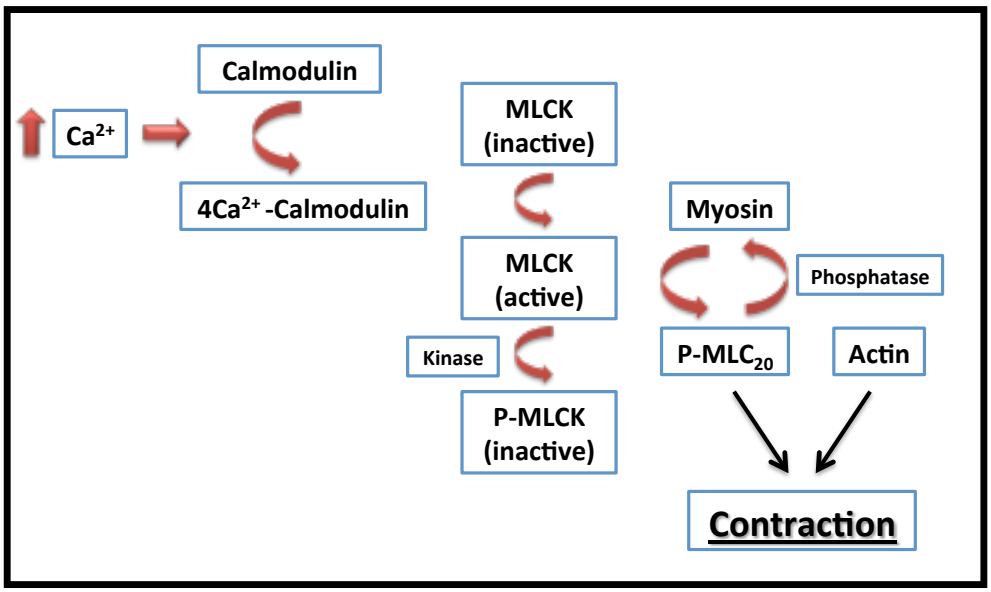
Calmodulin
Ca2+
4Ca2+ -Calmodulin
MLCK (inactive)
MLCK (active)
Kinase
P-MLCK (inactive)
Myosin
Phosphatase
P-MLC20
Actin
Contraction

capable of delivering the fetus [81].

Following muscle contraction, in order to induce relaxation of the smooth muscle, Ca^{2+} must be removed from the cytosol. Relaxation occurs by several mechanisms, including actions of the plasma membrane (PMCA) and SR/ER (SERCA) Ca^{2+-} ATPases and Na/Ca^{2+} exchangers, activation of K^{+} channels causing hyperpolarization of the cell and decreased voltage-mediated Ca^{2+} entry [17].

1.5 Autophagy

During myometrial differentiation there is a period when the myometrium transitions from a state of hyperplasia to hypertrophy. This transition is associated with significant protein turnover. The main pathway for cells to degrade misfolded proteins is the ubiquitin-proteasome system. Recent evidence suggests that lysosomal degradation pathways (known as ‘autophagy’) also have essential roles in cellular protein quality control [84]. Autophagy or “self-eating”, is a ubiquitous and evolutionary conserved process and is found in yeast and mammals [85]. Three distinct types of autophagy have been described: macroautophagy, microautophagy and chaperone-mediated autophagy (CMA). Each autophagy type differs mechanistically from the others, but all types share a common role in degrading cytosolic components by lysosomal hydrolases (Figure 1.5) [86-88].

Macroautophagy refers to a multi-step process in which intact organelles and portions of the cytosol are initially sequestered into a phagophore or isolation membrane, a crescent shaped double membrane, that expands and fuses to form a double-membrane

vesicle known as an autophagosome. The isolation membranes are acquired from various intracellular membranes including the endoplasmic reticulum, Golgi apparatus, mitochondrial outer membrane and plasma membrane [89-92]. Subsequently, the autophagosome matures once the outer membrane of the autophagosome fuses with an endosome and/or lysosome, resulting in the formation of an autolysosome/autophagolysosome. The autolysosome results in the degradation of the luminal material, as well as the internal membrane. The resulting macromolecules are then released through membrane permeases and recycled in the cytosol [93]. More specifically, initiation of autophagosome formation requires the formation of a Unc-51-like kinase (ULK) protein complex, which is composed of ULK1, autophagy-related gene (Atg)13, FIP200 and Atg101, along with other Atg proteins. mTOR–dependent and mTOR-independent pathways are the primary regulators of the assembly of the ULK protein complex [94]. mTOR-independent mechanisms alter the transcription of macroautophagy genes or they decrease the amount of 1,4,5-triphosphate [95, 96]. The next step involves nucleation and elongation of the isolation membranes to generate vesicular structures. Nucleation requires the assembly of the Beclin1/class III phosphatidylinositol 3-kinase (PI3K) complex [97, 98]. Elongation of the phagophore membrane is dependent on the Atg12 and microtubule associated protein light chain 3 (LC3) conjugation system. A complex comprised of Atg5, Atg12 and Atg16L1 along with other autophagy-related genes regulate the conjugation of PE to LC3I to form LC3II, resulting in translocation of LC3 from the cytoplasm to the membrane of the pre-autophagosomes [99-101]. Following nucleation and elongation, autophagosome

Figure 1.5 Scheme showing the relationship among the three known types of autophagy: Chaperone-Mediated Autophagy, Microautophagy and Macroautophagy. Adapted from Crotzer & Blum 2009 [88].

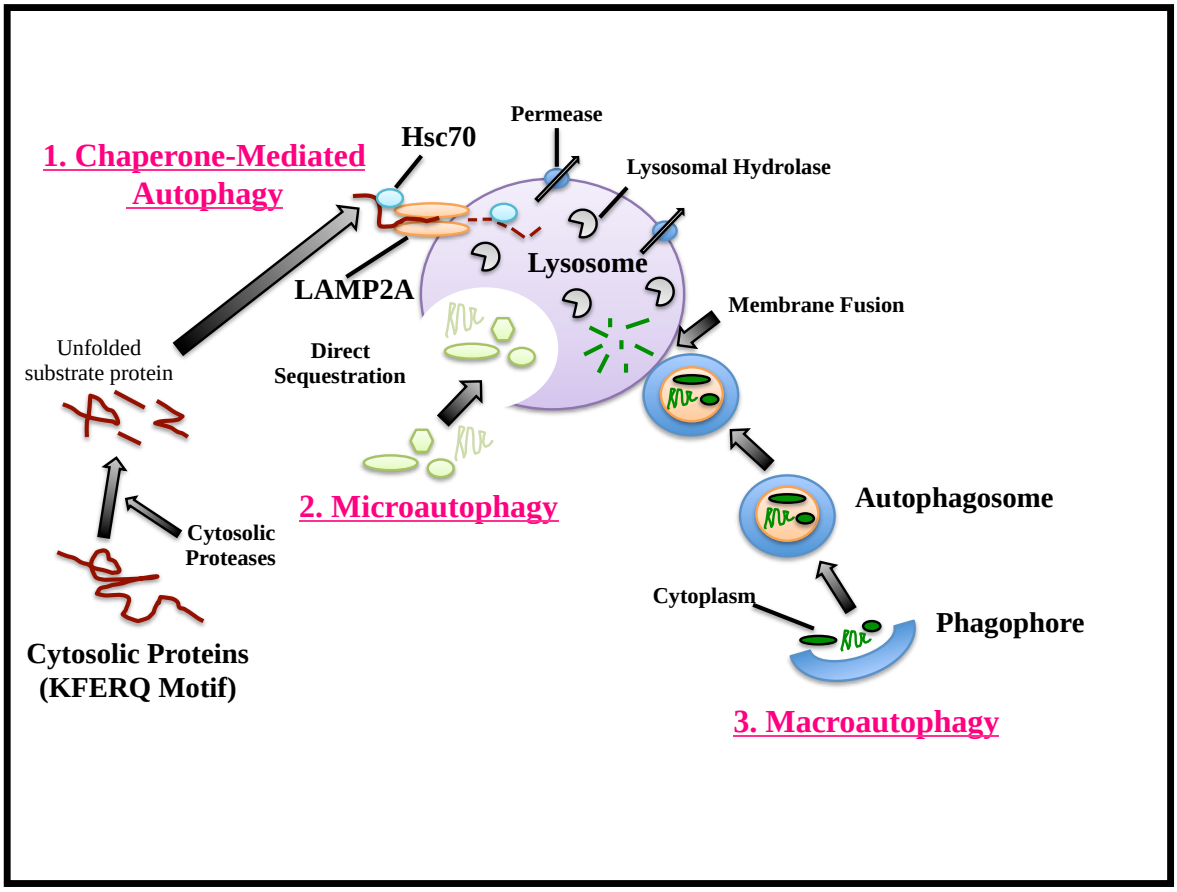
1. Chaperone-Mediated Autophagy
Hsc70
Permease
Lysosomal Hydrolase
LAMP2A
Lysosome
Membrane Fusion
Unfolded substrate protein
Direct Sequestration
2. Microautophagy
Autophagosome
Cytosolic Proteases
Cytoplasm
Phagophore
Cytosolic Proteins (KFERQ Motif)
3. Macroautophagy

undergo a process termed maturation in which they fuse with late endosomes and lysosomes for degradation of their contents [102, 103]. Maturation and degradation have been found to require late endosome marker protein Rab7 and lysosomal membrane protein LAMP-2 [104-106]. The constitutive or basal level of macroautophagy appears crucial for maintaining cellular homeostasis as it is responsible for the removal of damaged/old organelles, protein aggregates and the turnover of long-lived proteins. If cells encounter environmental stressors then the level of macroautophagy can increase significantly as a cytoprotective measure [107].

Microautophagy involves direct sequestration of cytosolic components by invagination of the lysosomal membrane in the form of single-membrane vesicles [108]. A dynamin-related GTPase Vps1p regulates microautophagic invagination [109]. CMA is a selective lysosomal pathway that is responsible for degradation of single soluble cytosolic proteins that contain a pentapeptide lysosome-targeting motif, KFERQ. When the motif is exposed during protein misfolding or disassembly of protein complexes, it is recognized by heat-shock cognate (Hsc)70 and the cytosolic proteins are directly translocated into the lysosome after unfolding by a chaperone complex, comprised of Hsc70, Bcl2-associated athanogene (Bag)1, Hip, Hop and Hsp40/DNAJB1[110, 111]. In order for complete translocation into the lumen to occur the substrate proteins must bind to the cytosolic tail of LAMP-2A [112]. Binding of the substrate proteins to monomers of LAMP-2A stimulates its multimerization to form the approximately 700-kDa LAMP-2A complex necessary for substrate translocation [113]. The LAMP-2A complex is then disassembled into monomers in an Hsc70-dependent manner when substrates are no

longer available, thus initiating a new cycle of binding and translocation [113].

1.6 Small Heat Shock Proteins

Heat shock proteins (Hsps) have been found in Prokaryota and Eukaryota and are generally classified based on their molecular masses, properties and structures [114]. There are five classes of heat shock proteins: Hsp100, Hsp90, Hsp70, Hsp60 and the small heat shock proteins [115]. Heat shock proteins are known to act as molecular chaperones that block the aggregation of unfolded proteins and have a cytoprotective function under stressful situations [116]. The chaperone activities of Hsp100, Hsp90, Hsp70 and Hsp60 are regulated by the binding of ATP and subsequent hydrolysis; however, small heat shock proteins, in contrast to the major chaperones, show ATP-independent chaperone-like activity [117].

The human genome encodes ten different small heat shock proteins (sHsps) termed HspB1-HspB10 [118]. The sHsps form a ubiquitous family of molecular chaperones that have low molecular masses that normally range between 12 and 42 kDa [115]. This diverse family of proteins is characterized by a conserved C-terminal region consisting of 80-100 amino acids, termed the α-crystallin domain, a more variable N-terminal sequence, and in most cases a short and variable C-terminal tail [119]. The α-crystallin domain is often involved in the formation of dimers, whereas the N-terminal domain is involved in the formation of stable oligomeric complexes [115, 120-123]. The secondary structure of sHsps is a compact β-sheet sandwich composed of two layers of

three and five anti-parallel strands that are connected by a short interdomain loop [115, 124].

sHsps are widely expressed chaperone proteins whose two main functions are to bind denatured proteins (in order to prevent stress-induced aggregation) and to maintain the solubility of denatured proteins until they can refold to their native conformation. sHsps are able to help promote the proper folding of these proteins, upon removal of the stress, by binding to exposed hydrophobic patches on protein substrates [125-127]. As sHsps exist in high molecular mass oligomers, substrate binding sites appear to correspond to temperature related exposure of hydrophobic interface sites, following dissociation of oligomeric complexes or an increase in subunit exchange between complexes [120, 128-130]. Unlike larger stress response chaperones**,** sHsps are ATP-independent chaperones and are extremely important under stress conditions when the levels of ATP have been significantly depleted [116, 124, 126, 130, 131].

One of the key features of sHsps is their ability to form large oligomeric complexes. sHsps may form complexes composed of 2-40 subunits that are either homomeric or heteromeric [118, 121, 130-134]. Oligomerization of sHsps is a dynamic process that becomes more rapid under stressful conditions [135-137]. The formation of oligomeric structures plays an important role in the chaperone functions of sHsps and may be a method of storage for inactive or partially active sHsps [126]. Oligomerization may also lead to the formation of several different homo- and hetero-oligomers, each with different binding properties to chaperone an extensive array of substrates [138-140].

There are several known factors that result in the dissociation of sHsp oligomers including: temperature, ionic strength, pH, Ca^{2+} concentration, tissue age, or protein concentration [126, 128, 141-143]. One mechanism of sHsp activation is through temperature-dependent dissociation of oligomers [128-130]. Changes in the oligomeric organization of αB-crystallin increases the exposure of hydrophobic surface area and result in increased chaperone activity [144]. Regulating the exposure of hydrophobic surfaces through oligomeric organization may provide the molecular mechanism for sHsp regulation [144].

Many sHsps undergo phosphorylation via various protein kinases and this may affect their chaperone activity. Most sHsps have phosphoralatable serine residues and phosphorylation has been found to modulate oligomerization and hence the function of these proteins within the cell [119, 145-152]. Phosphorylation affects sHsp cellular distribution [119, 153, 154].

Expression of sHsp genes depends on the organism and the cell type. Some sHsp genes are ubiquitously expressed while others are only expressed in specific tissues. sHsps are often induced when cells and tissues respond to various stress signals including: heat, oxidative or osmotic stress, cold shock and heavy metals [126, 155-160]. These stress signals result in increased expression of sHsps through the binding of heat shock transcription factors (HSF1-4) to heat shock promoter elements, upstream of sHsp genes (Figure 1.6). Therefore there are two mechanisms to activate the Hsp response: detachment from oligomeric structures and novel transcription/translation.

Figure 1.6 Conditions that induce a heat shock response. Expression of sHsp genes depends specifically on the organism and the cell type; however, they are often induced when cells and tissues respond to various stress signals including: heat, oxidative or osmotic stress, cold shock and heavy metals. These stress signals result in an up-regulation of sHsps through the binding of HSF-1 to heat shock promoter elements, upstream of sHsp genes, resulting in increased gene transcription of Hsps. Adapted from Hu et al., 2007 [160].

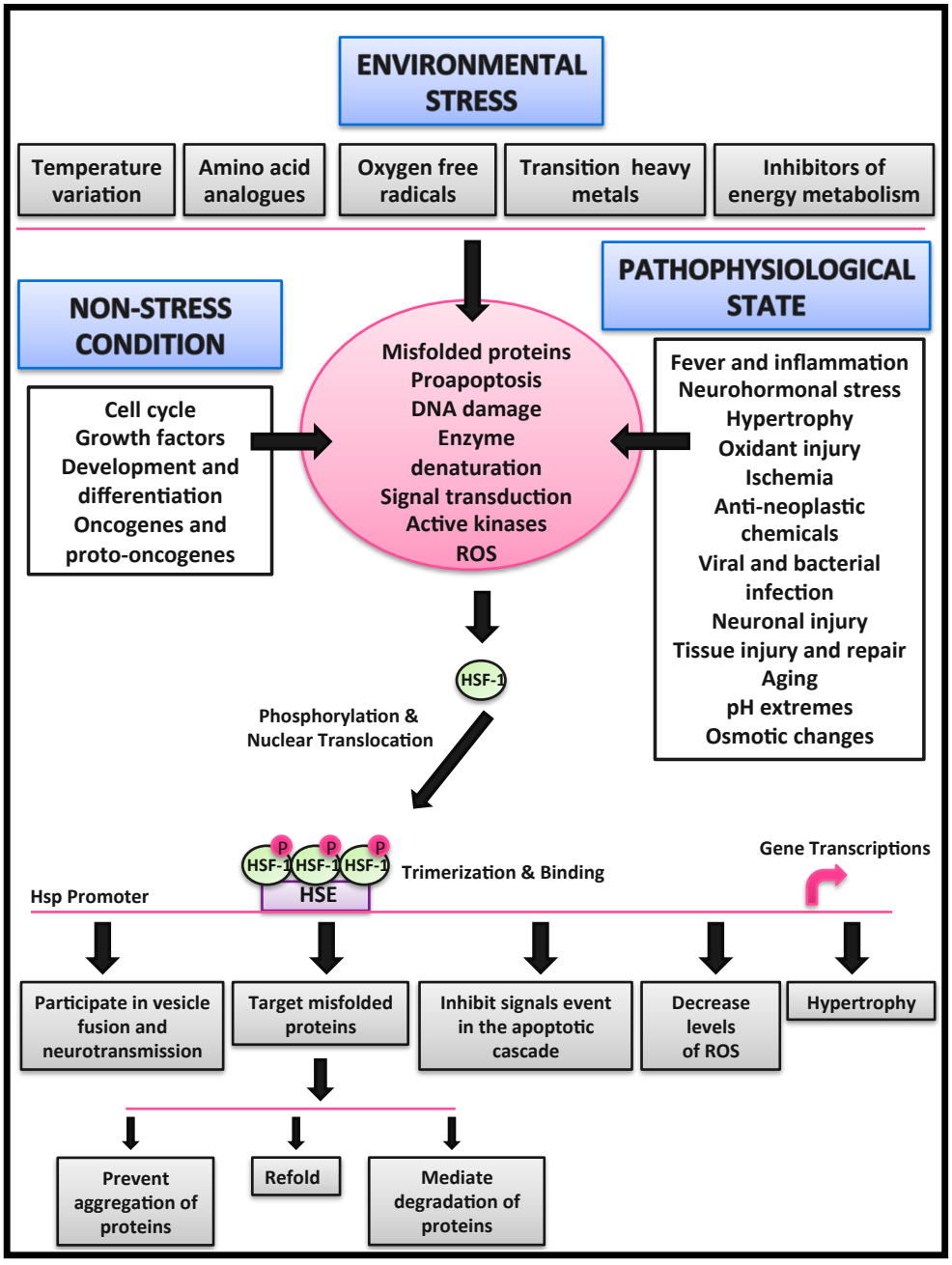
ENVIRONMENTAL STRESS
Temperature variation
Amino acid analogues
Oxygen free radicals
Transition heavy metals
Inhibitors of energy metabolism
NON-STRESS CONDITION
PATHOPHYSIOLOGICAL STATE
Cell cycle
Growth factors
Development and differentiation
Oncogenes and proto-oncogenes
Misfolded proteins
Proapoptosis
DNA damage
Enzyme denaturation
Signal transduction
Active kinases
ROS
Fever and inflammation
Neurohormonal stress
Hypertrophy
Oxidant injury
Ischemia
Anti-neoplastic chemicals
Viral and bacterial infection
Neuronal injury
Tissue injury and repair
Aging
pH extremes
Osmotic changes
HSF-1
Phosphorylation & Nuclear Translocation
P
HSF-1
HSF-1
HSF-1
HSE
Trimerization & Binding
Gene Transcriptions
Hsp Promoter
Participate in vesicle fusion and neurotransmission
Target misfolded proteins
Inhibit signals event in the apoptotic cascade
Decrease levels of ROS
Hypertrophy
Prevent aggregation of proteins
Refold
Mediate degradation of proteins

1.7 HspB8 Protein

HspB8 (also known as Hsp22, H11 and E2IG1) possesses the structural motif of the alpha-crystallin family of Hsps and is considered to be a member of the superfamily of sHsps [118, 160, 161]. HspB8 has a very low molecular mass of approximately 21.6 kDa and consists of 196 amino acids [162]. HspB8 protein is predominantly expressed in skeletal and smooth muscles, heart and brain, with moderate expression in cervix, prostate, lung, kidneys, heart, placenta and spleen [132, 162]. HspB8 has been found to possess two putative HSF1 binding sites (HSEs) 1000 bases upstream of the translation start site, suggesting that it may be stress-inducible [132].

The secondary structure of HspB8 is randomly coiled, and *in vitro* is monomeric. According to Kim et al. (2004) 36 % of human HspB8 is β-structured, 5 % is alpha helices and about 58 % is comprised of turns and unordered structures [163]. HspB8 also lacks the β2 strand detected in many sHsps [164, 165]. Thus, HspB8 is a member of the group of intrinsically disordered proteins, which are known to play vital roles in recognition, regulation and cell signaling [166]. The aromatic amino acids of HspB8 are in a chiral environment that is comparable with those of αβ-crystallin and the sequence of HspB8 includes three cysteine residues, but no disulphide bonds [132]. HspB8 is resistant to thermal denaturation but highly susceptible to proteolysis [164, 165, 167].

HspB8, like other intrinsically disordered proteins is phosphorylated by several protein kinases. *In vitro*, protein kinase C phosphorylates Ser14 and Thr63, ERK1

phosphorylates Ser27 and Thr87 whereas casein kinase 2 phosphorylates a number of unidentified sites [162]. HspB8 is also phosphorylated by cAMP-dependent protein kinase at Ser24 and Ser57 *in vitro*; however, Ser57 is the primary site of phosphorylation [148]. Phosphorylation by cAMP-dependent protein kinase affects the structure and decreases the chaperone-like activity of HspB8 *in vitro* [148]. HspB8 is phosphorylated at Ser24 and Ser(Thr)87 *in vivo* [168-170]. Furthermore, HspB8 is phosphorylated at Tyr118 in non-small-cell lung cancer cells [171]. Despite this information, the effect of phosphorylation on the structure and properties of HspB8 has yet to be fully examined.

Although HspB8 is highly expressed in muscle, its exact function remains unclear. Originally HspB8 was reported to have protein kinase activity but the evidence has been inconsistent [172, 173] HspB8 protein kinase activity was analyzed using SDS-gel electrophoresis with alpha-casein and histone IIIS as the protein substrates [163]. The authors found that HspB8 was not capable of phosphorylating alpha-casein or histone IIIS; however, the substrates were phosphorylated by purified rat liver casein kinase II and by the catalytic subunit of cAMP- dependent protein kinase, respectively [163]. Furthermore, HspB8 only contains seven out of eleven motifs that are typically characteristic of protein kinases, indicating only weak similarity between the primary structure of HspB8 and protein kinase motifs [174]. Kim et al. (2004) attribute the previous protein kinase activity to protein kinases tightly bound to HspB8, as a result of sample contamination [163].

HspB8 has chaperone-like activity, similar to many other sHsps. It prevents

aggregation of partially unfolded or denatured proteins *in vivo* [132, 167, 175]. Heating results in aggregation of yeast alcohol dehydrogenase (ADH), particularly in the presence of reducing agents. Upon addition of HspB8 to ADH there was decreased aggregation [163]. A similar result was obtained when bovine liver rhodanese was used as a substrate. Thus, HspB8 was capable of preventing heat-induced aggregation of both ADH and bovine liver rhodanese, indicating chaperone activity similar to HspB6 [163]. HspB8 also prevents the formation of amyloid oligomers and aggresomes formed by the R120G mutant of αβ-crystallin, which causes desmin-related cardiomyopathy [176, 177]. Overexpression of HspB8 was accompanied by improved cardiac function and survival [176]. Furthermore, HspB8 was more effective than HspB1 and αβ-crystallin in preventing *in vivo* aggregation of polyglutamine containing proteins (polyglutamine protein Htt43Q and androgen receptor containing 65 glutamine residues). HspB8 also maintains Htt43Q in a soluble state allowing for its rapid degradation [178]. Together these results demonstrate that HspB8 has chaperone-like activity.

sHsps are able to interact with each other to form homo- and hetero-oligomeric complexes and suggesting that the formation of these complexes is essential for their function [123]. The conserved alpha-crystallin domain is involved in the formation of both homo- and hetero- dimers. HspB8 has at least two binding sites that permit interaction with itself, HspB7, myotonic dystrophy protein kinase binding protein, HspB1, αβ-crystallin and HspB6 [179].

HspB8 can form homo-dimers, which can subsequently dimerize to form tetramers [180]. Yeast tyrosine hydroxylase assays were performed to determine whether or not HspB8 was able to interact with itself. Both of the reporter genes (his+, gal+) indicated the presence of HspB8 dimers [180]. Size exclusion chromatography and chemical cross-linking with dimethylsuberimidate, were performed by Kim et al. (2004) and they also found that HspB8 is capable of forming stable dimers [163]. When HspB8 was incubated with increasing quantities of β- mercaptoethanol there was decreased intensity of the putative HspB8 band on immunoblots analogous to an HspB8 dimer (~40-45 kDa) and increased intensity of an HspB8 band corresponding to the monomeric form of HspB8 (22 kDa). There was also evidence of high molecular mass complexes on the top of the gel. Therefore, it was proposed that HspB8 is capable of forming disulfide cross-linked dimers, as well as unordered crosslinked oligomers having high molecular mass [163]. Following oxidation both the secondary and tertiary structures of HspB8 are disrupted, which affects the formation of intermolecular disulfide bonds and thus cross-linked dimers. To examine the formation of homo-oligomeric complexes Sun et al. transfected 293T cells to express FLAG-tagged HspB8 that was treated with different concentrations of glutaraldehyde, allowing cross-linking of cell proteins [180]. Bands were observed at ~30, 65 and 120 kDa, however, with increased glutaraldehyde concentration a band was observed having a molecular mass of 250 kDa [180]. This data indicated that HspB8 formed homo-dimers, as well as homo-oligomers [163, 180].

Significant sequence similarity exists between HspB8 and HspB1, which may account for their interaction. Human HspB1 has three sites of serine phosphorylation

including Ser15, Ser78 and Ser82 [180]. Originally, Benndorf et al. (2001) showed an interaction between HspB8 and a mimic of phosphorylated HspB1 (a triple aspartate mutant) [162]. However, in recent studies it has been shown that HspB8 weakly interacts with HspB1 without the need for HspB1 phosphorylation [180, 181]. The interaction between HspB8 and HspB1 involves the C-terminus of HspB1, which must interact with full-length HspB8 [179, 180, 182]. Although it is thought that hetero-oligomeric complexes are crucial for function, the significance of this interaction is still undefined.

Most recently, HspB8 has been found to interact with the adapter protein Bag3, a known stimulator of macroautophagy, in human cervical cancer (HeLa) and African green monkey kidney (COS-1) cells [183]. Currently there are two proposed methods for stimulation of macroautophagy via an HspB8-Bag3 complex. First, HspB8 is part of a multiheteromeric complex comprised of HspB8, Bag3, Hsc70 and C-terminus of Hsc70-interacting protein (CHIP). This complex is then responsible for the removal of misfolded proteins through macroautophagy activation [184]. However, there is also evidence that HspB8 and Bag3 are working independently of Hsc70 and CHIP to promote phosphorylation of the α subunit of translation initiator factor eIF2 and stimulation of macroautophagy [185, 186].

1.8 Bag Proteins

The human genome encodes six different members of Bag proteins including Bag1 (and its various isoforms), Bag2, Bag3 (CAIR-1; Bis), Bag4 (SODD), Bag5 and Bag6 (Scythe, BAT3) [187]. The Bag proteins are a family of co-chaperones, which are

capable of interacting with the ATPase domain of Hsc70/Hsp70 through their structural Bag domain (110-124 residues) [188, 189]. The Bag domain is an evolutionary conserved domain consisting of ~110 amino acids and three anti-parallel alpha-helices, each ~30-40 amino acids in length [190]. The first and second helices interact with the serine/threonine kinase RAF-1 and the second and third helices are the sites of the BAG domain interaction with the ATPase domain of Hsc70/Hsp70 [190, 191]. The interaction between the Bag domain and the ATPase domain of Hsp/Hsc70 is reported to regulate the ATP-driven activity of the chaperone complex [192]. All members of this family contain one Bag domain, which is located in the C-terminal portion of the molecule, except Bag5, which contains five putative Bag domains [188, 190]. The N-terminal regions of the family members vary in both length and composition [188, 190].

Bag1 has several isoforms which interact with several molecular targets including Bcl2 apoptosis regulator, constitutively expressed Hsc70, heat-inducible Hsp70, nuclear hormone receptors, the RAF-1 kinase, components of the proteasome machinery and DNA [191, 193, 194]. Bag1, along with its binding partners, is involved in diverse cellular functions [195, 196]. Bag1 has been found to serve as an anti-apoptotic molecule by suppressing apoptosis upstream of caspase activation and thus, is involved in cell survival and proliferation [197, 198]. Another key role of Bag1 is to mediate protein quality control by targeting selected proteins for proteasome-mediated degradation [199]. Bag1 binds to Hsc/Hsp70 via its carboxy-terminal BAG domain and associates with the proteasome in an ATP-dependent manner, promoting binding of Hsc70 and Hsp70 to the

proteolytic complex [189]. Bag1 is considered a coupling factor between the Hsp70 chaperone system and the proteolytic complex. Bag1 and Bag3, however, appear to be reciprocally regulated during cellular aging and under acute oxidative or proteasomal stress (Figure 1.7) [200, 201]. Bag1 maintains protein quality control through Bag1-dependent proteasomal degradation of polyubiquinated proteins, mediated by the Hsp70 chaperone system. However, when there is an accumulation of misfolded proteins and a decrease in the efficiency of proteasomal degradation, there is an up-regulation of Bag3-mediated macroautophagy. This is referred to as a Bag1/Bag3 “switch” and is thought to be a physiological adaptation to the changing protein degradation demand during cellular aging and proteasomal stress [183, 184, 200, 202].

Bag 3 is another member of the Bag family co-chaperones and, in addition to the Bag domain, it possesses a tryptophan domain (WW) at its N-terminus and a proline-rich repeat (PXXP) at its central region [183]. The WW domain is a protein-protein interaction domain that has been found to bind to proline-rich ligands, including the adenovirus penton base protein and the PDZ domain containing guanine nucleotide-exchange factor 2 [203, 204]. The only known protein to interact with the Bag3 proline-rich region is Phospholipase C-gamma 1 (PLCγ-1), an SH3 containing protein involved in growth signal transduction [187, 205]. PLCγ-1 interacts with γ-tubulin and modulates the assembly of microtubules, which are essential for macroautophagy [206, 207]. The BAG domain of Bag3 is required for its interaction with Hsp70/Hsc70 and Bcl2, an anti-

Figure 1.7 The Bag1 to Bag3 switch. In order to maintain protein homeostasis in times of proteasomal stress there is an increase in the Bag3/Bag1 ratio, resulting in the recruitment of the macroautophagy pathway. The Bag1/Bag3 switch is thought to be a physiological adaptation to the changing protein degradation demand during cellular aging and proteasomal stress. Adapted from Behl, 2011 [201].

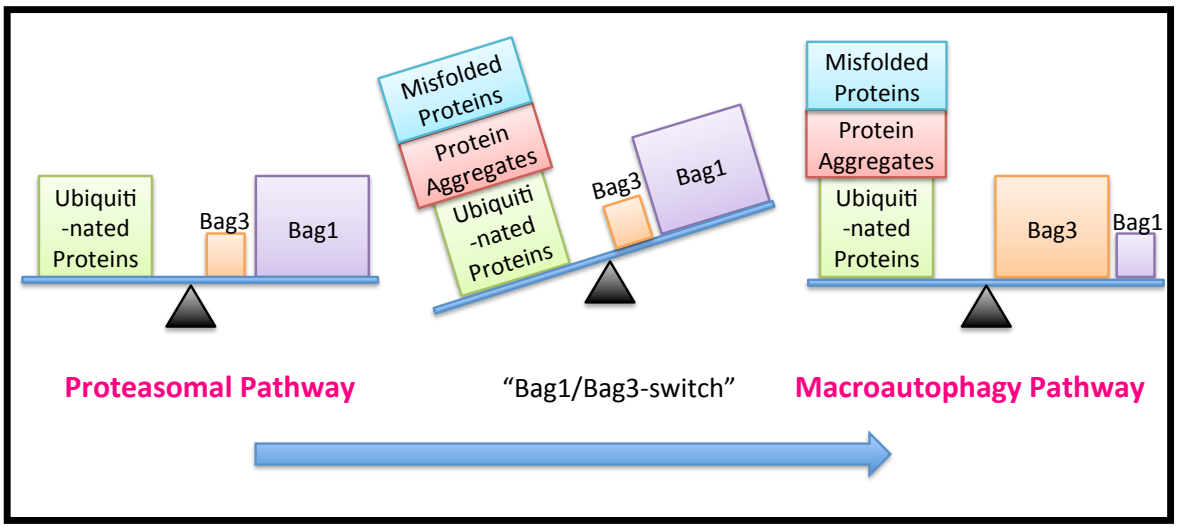
Misfolded Proteins
Protein Aggregates
Ubiquiti -nated Proteins
Bag3
Bag1
Ubiquiti -nated Proteins
Bag3
Bag1
Misfolded Proteins
Protein Aggregates
Ubiquiti -nated Proteins
Bag3
Bag1
Proteasomal Pathway
"Bag1/Bag3-switch"
Macroautophagy Pathway

apoptotic protein [187]. Hsp70/Hsc70 subsequently interacts with co-chaperones such as CHIP, an E3 ligase [208]. Bag3 is the only member of this family that can be induced by stressful stimuli, as a result of HSF1 binding to heat shock-responsive elements on the *Bag3* gene promoter [209]. It is known that the full-length product of the *Bag3* gene has an apparent mass of 74 kDa and is localized to the cytoplasm, however another form of Bag3 has also been described [188]. The shorter form of Bag3 (~40 kDa) has been characterized by immunoprecipitation and mass spectrometry in neural synaptosome homogenates yet it is unclear whether this form is due to alternative splicing or proteolytic processing [210].

According to Fuchs et al. (2010) two conserved Ile-Pro-Val (IPV) motifs in Bag3, located between the WW domain and the proline-rich domain, are crucial for mediating binding to HspB8 [211]. Furthermore, HspB8 binds to Bag3 through its hydrophobic groove, formed by β4 and β8 strands (Figure 1.8A). A filter-trap assay also determined that the HspB8-Bag3 complex is capable of stimulating the clearance of aggregation-prone Htt43Q (Huntingtin exon 1 fragment with 43 CAG repeats) through stimulation of the macroautophagy pathway (Figure 1.8B) [211, 212].

The multichaperone complex (Bag3-HspB8-Hsp70/Hsc70) is thought to mediate macroautophagy in cooperation with the macroautophagy receptor protein p62/SQSTM1 (sequestome 1). This protein is known to be a stress-regulated multi-adaptor protein that is capable of binding to ubiquitin and microtubule associated protein light chain 3 II (LC3II), the autophagosome membrane-associated protein, simultaneously [213]. p62

Figure 1.8 (A) The current model of sHsp structure. In the ribbon diagram of the *Triticum Aestivum* Hsp16.9 monomer N and C indicate the N- and C-terminal domains respectively. The amino acid residues that form the hydrophobic groove are shown as blue balls on β4 and as red balls on β8. The hydrophobic groove of HspB8 is crucial for the interaction between HspB8 and Bag3. Reproduced from Fuchs et al., 2010 [215]. **(B)** Two conserved Ile-Pro-Val (IPV) motifs in Bag 3, located between the WW domain and the proline-rich domain, are crucial for mediating binding to HspB8. The HspB8-Bag3 complex is capable of stimulating the clearance of aggregation-prone Htt43Q protein through Bag3-mediated macroautophagy stimulation. Based on figure from McCollum et al., 2010 [212].

A

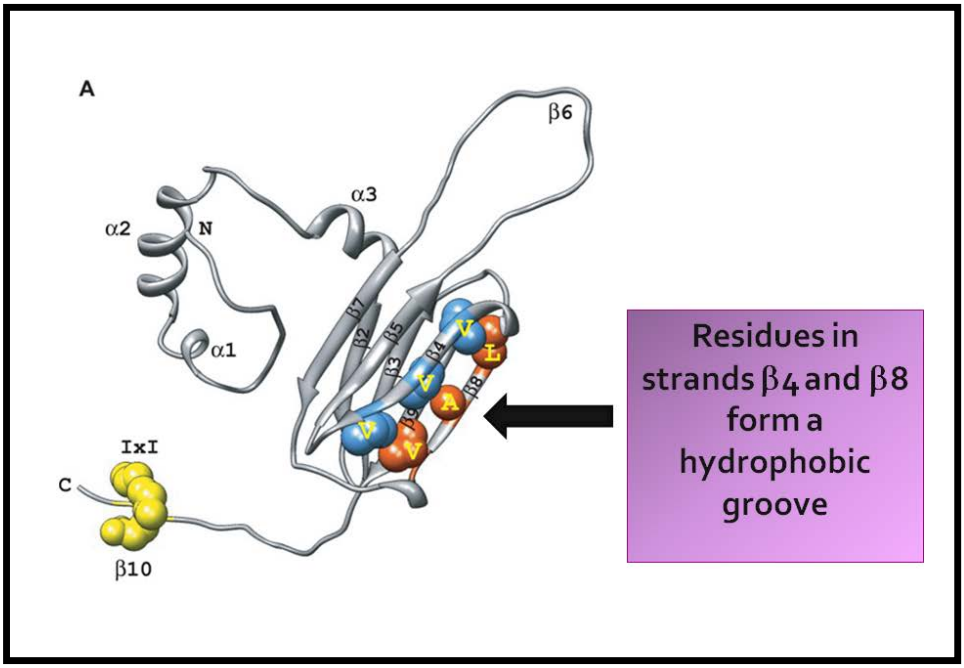
A
β6
α3
α2
N
α1
β7
β2
β5
β3
β4
β8
β9
V
L
V
A
V
V
IxI
C
β10
Residues in strands β4 and β8 form a hydrophobic groove

B

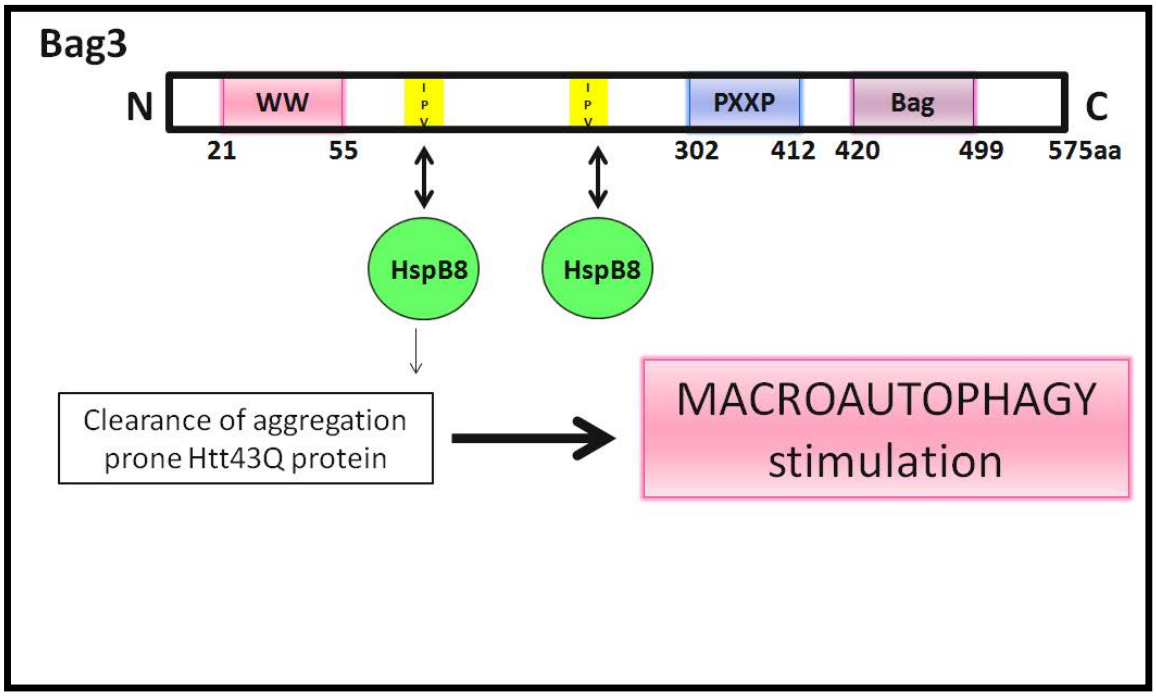
Bag3
N
WW
I P V
I P V
PXXP
Bag
C
21
55
302
412
420
499
575aa
HspB8
HspB8
Clearance of aggregation prone Htt43Q protein
MACROAUTOPHAGY stimulation

binds directly to LC3II by its LIR motif (LC3-interacting region), an 11-amino acid long linear motif [214, 215]. LC3II has been found to exist on autophagosomes and therefore it is often used as a marker for autophagosome accumulation [216, 217]. Nascent LC3 is initially processed at its C-terminus by autophagy-related protein (Atg) 4 and becomes LC3I, which possesses a glycine residue at its C-terminal end. LC3I is subsequently conjugated with phosphatidlyethanolamine, via an ubiquination-like enzymatic reaction, to form LC3II. LC3I is known to have cytoplasmic localization, whereas LC3II is associated with the outer and inner membranes of the autophagosome [218]. Following self-oligomerization of p62/SQSTM1, it is able to sequestrate ubiquinated substrates in the form of inclusion bodies, which are then engulfed by the autophagosome membrane through recruitment of LC3II [213].

Furthermore, Bag3-HspB8-Hsp70/Hsc70 and CHIP bind to mutated superoxide dismutase 1 (SOD1) and then target it for degradation through macroautophagy stimulation [184]. CHIP serves as a cochaperone, as well as an ubiquitin ligase and it is highly expressed in the heart, vascular cells and other cells [219]. CHIP, in possessing E3 ubiquitin ligase activity, is able to ubiquinate target proteins [220]. Thus, this multichaperone complex may ubiquinate-chaperoned substrates and then target them for degradation by p62/SQSTM1 and activation of the macroautophagy pathway (Figure 1.9) [202, 208, 221].

Figure 1.9 HspB8 and the macroautophagy pathway. HspB8 in, interacting with Bag3, is part of a multiheteromeric complex comprised of HspB8, Bag3, Hsp70/Hsc70 and CHIP. HspB8 is responsible for recognizing the misfolded proteins and subsequently the multichaperone complex mediates macroautophagy in cooperation with the macroautophagy receptor protein p62. CHIP ubiquinates target proteins and p62 is then capable of binding to ubiquitin and LC3II, the autophagosome membrane-associated protein, simultaneously. Thus, this multichaperone complex may ubiquinate-chaperoned substrates and then target them for degradation by p62 and activation of the macroautophagy pathway. Based on figure from Carra et al., 2009 and Mymrikov et al., 2011 [186, 221].

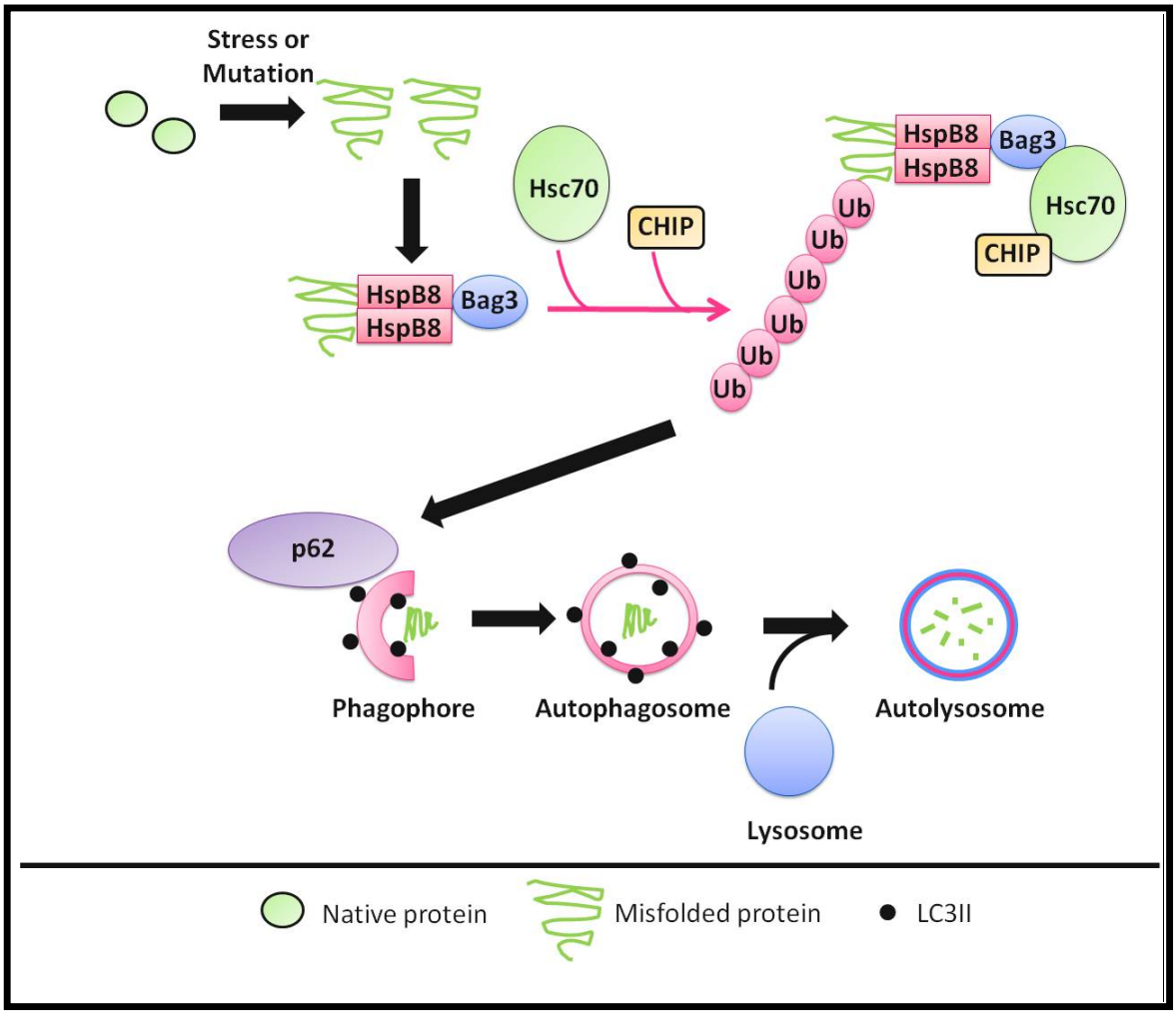
Stress or
Mutation
HspB8
HspB8
Bag3
Hsc70
CHIP
Ub
Ub
Ub
Ub
Ub
Ub
HspB8
HspB8
Bag3
Hsc70
CHIP
p62
Phagophore
Autophagosome
Autolysosome
Lysosome
Native protein
Misfolded protein
LC3II

1.9 Study Rationale and Hypotheses

Due to a preliminary immunoblot result in the MacPhee laboratory, which indicated that HspB8 may be expressed in the rat myometrium during gestation, the first hypothesis for this study was that HspB8 protein expression in rat myometrium will be elevated towards mid-gestation coincident with myometrial hypertrophy, as a means to regulate protein homeostasis. Throughout the stages of myometrial differentiation the myometrium transitions from a state of hyperplasia to hypertrophy. This transition is associated with significant protein turnover; thus, the second hypothesis is that HspB8, Bag3 and other members of a regulatory pathway, such as macroautophagy, should be expressed in the myometrium at this time to help maintain protein homeostasis.

To address these two major hypotheses I set out two main goals for this thesis project. The first goal was to characterize the expression of HspB8 protein and potentially associated autophagy machinery in the rat myometrium during pregnancy compatible with a functional significance for the HspB8 protein in myometrial hypertrophy. The second goal was to characterize the potential regulation of HspB8 protein expression in pregnant rat myometrium during pregnancy as the uterus changes from a quiescent tissue to a contractile tissue. In order to achieve these goals, four main experimental objectives were proposed:

Objective 1: To determine the spatial and temporal localization of HspB8 protein in the rat myometrium throughout pregnancy and labour.

Objective 2: To determine whether mechanical stretch, progesterone or a functional progesterone withdrawal (RU486) affects HspB8 protein expression in the rat myometrium.

Objective 3: To characterize the expression of proteins associated with HspB8 in the process of hypertrophy including: Bag3, Bag1, Hsp70, Hsc70, CHIP, LC3II, eIF2α and γ-actin.

Objective 4: To determine whether HspB8 and Bag3 form a complex during myometrial programming, particularly during the synthetic phase.

Some experiments used uterine tissue lysates and tissue sections which were collected by other students in the MacPhee laboratory including: Bryan White, Brandon Cross, Joy Williams and Mandy Peach. However, I collected additional samples throughout the duration of this thesis project and all experimental findings described in this thesis are the result of my own personal work in the laboratory.

Chapter Two

Materials and Methods

2.1 Animals

Sprague Dawley rats were acquired from Mount Scio Vivarium (Memorial University of Newfoundland, St. John's, NL, Canada) and used for all experiments. The rats were kept under the supervision of the Animal Care Unit at the Health Sciences Centre, Memorial University of Newfoundland and housed under standard environmental conditions of 12 h of light and 12 h of darkness. The rats had access to tap water *ad libitum* and were maintained on LabDiet Prolab RMH 3000 (PMI Nutrition International, Brentwood, MO, USA). For all experiments, virgin female rats weighing approximately 220-250 grams were mated with male rats. D1 of the gestational period was designated following the observation of a vaginal plug the morning after mating. The time of delivery under these standard conditions was d23 of the gestational period. All experiments were granted ethical approval by the institutional animal care committee under protocols 08-02-DM to 11-02-DM.

2.2 Experimental Design

2.2.1 *Tissue Collection*

Each animal was placed in a euthanasia chamber and exposed to increasing concentrations of carbon dioxide, resulting in death by asphyxiation within 5-10 minutes

(min). Uterine horns were then removed, excised and opened longitudinally, after which fetuses and placentae were discarded. Uterine tissue was then placed in ice cold phosphate-buffered saline (PBS; pH 7.4) and a scalpel blade was used to gently scrape away the endometrial layer [222-224]. All myometrial samples were flash-frozen in liquid nitrogen and stored at -80^{o}C. Each set of myometrial samples was composed of samples from ten time points throughout gestation including: non-pregnant (NP), d6, d12, d15, d17, d19, d21, d22, d23 (labour) and 1 day post-partum (PP). NP samples were not standardized to a given time of day or day in the ovarian cycle. Labour samples were collected during active labour, following the delivery of 2-3 pups [222-225]. For immunofluorescence detection a portion of rat uterine horn was fixed in 4 % paraformaldehyde (PFA) in PBS (pH 7.4) while shaking overnight at room temperature (RT). Tissues were processed, paraffin embedded, sectioned and mounted on microscope slides by the Histology Unit of Memorial University of Newfoundland School of Medicine. Cross sections of the uterine horn were used for immunofluorescence experiments and both the longitudinal and circular muscle layers of the myometrium were included in all sections. For each experiment all sections were treated at the same time under identical conditions.

2.2.2 *Unilateral Pregnancy Model*

Tissue samples from a unilateral pregnancy model were collected by Dr. Bryan White. Detailed procedures of tissue acquisition for this model are reported elsewhere [223]. Briefly, virgin female rats underwent general anesthesia followed by unilateral

tubal ligation through a flank incision so the rats were only able to become pregnant in one horn [223]. Animals were allowed a 7-day period after which the females were mated with male rats. The tissue samples were collected from both non-gravid (NG; empty) and gravid uterine horns on d15, d19 and d23 (n=4/day) of gestation. Labour samples (d23) were collected during active labour, following the delivery of 2-3 pups.

2.2.3 *Progesterone-delayed Labour*

The levels of serum progesterone peak between d15-d19, after which there is a dramatic decline leading into labour [49]. In order to investigate progesterone regulation of HspB8 protein expression, pregnant rats were given either a daily injection of progesterone (4 mg subcutaneously (s.c) in 0.2 mL of corn oil) to maintain elevated plasma levels of progesterone, or vehicle alone (0.2 mL of corn oil s.c.) beginning on d20 of gestation. Samples were collected from animals receiving injections of vehicle alone on d21, d22 and d23 (during labour), whereas samples from the progesterone-treated rats were collected on d21, d22 and d23; however, on d23 the rats were not in labour (n=4/day).

2.2.4 *RU486-induced Progesterone Withdrawal*

RU486 (Mifepristone) is a 19-norsteroid that blocks the action of the hormone progesterone, which is crucial for initiating and maintaining pregnancy [226]. Therefore, upon administration of RU486 to pregnant rats on d18 of gestation, preterm labour is induced within 24 h. On d18 of gestation two groups of rats were treated with either

RU486 (10 mg/kg, s.c, in 0.5 mL of corn oil containing 10 % ethanol, Mifepristone; 17β-hydroxy-11β-[4-dimethylaminophenyl]-17-[1-propynyl]-estra-4, 10-dien-3-one; (Sigma-Aldrich, St. Louis, MO, USA) or vehicle alone (0.5 mL of corn oil). Myometrial samples were collected from both treatment groups on d19 of gestation. RU486 treated rats were killed during active labour, following the delivery of 2-3 pups (n=4/day).

2.3 Immunoblot Analysis

Immunoblot analysis was performed for gestational profiles of protein expression as well as for stretch, progesterone, RU486 and IP experiments. Four independent sets of protein samples (n=4/day; i.e. 4 rats used per gestational time point) were used for all studies. Sample sizes of n=4/day are routinely used for immunoblot analysis within the field [14, 18, 45]. Frozen rat myometrial samples were pulverized under liquid nitrogen and homogenized with a Bead Mill (PreCellys, Markham, ON, Canada) in radioimmunoprecipitation assay (RIPA) buffer (50 mM Tris-HCL (pH 7.5), 150 mM NaCl, 1 % (vol/vol) Triton X-100, 1 % (wt/vol) sodium deoxycholate, and 0.1 % (wt/vol) sodium dodecyl sulfate (SDS)) containing Phosphatase Inhibitor Cocktail and Complete^{TM} Mini Ethylenediaminetetraacetic acid (EDTA)-free protease inhibitors (Roche Molecular Biochemicals, Laval, QC, Canada). Samples were centrifuged for 15 min at 15000 x g at 4 °C and supernatants collected. Protein concentrations of each sample were obtained using the Bradford Assay (Bradford, 1976). The Bradford Assay involves deducing the concentration of a protein sample from its spectrophotometric absorbance (A_{595}) when compared to a standard curve of A_{595} readings of protein

standards of known concentrations. A duplicate set of 7 protein standards (0, 2.5, 5, 10, 15, 20, 25 mg/ml) were prepared using bovine serum albumin (BSA) diluted in double deionized water (ddH_2O). One mL of 1X Bio-Rad protein assay dye reagent (Bio-Rad Laboratories, Mississauga, ON, Canada) was added to each sample and the absorbance was measured at 595 nm with a Shimadzu BioMini spectrophotometer. Samples for protein determination were prepared using a similar method. One μL of each protein lysate, of unknown concentration, was combined with 24 μL of ddH_2O and 1 mL of 1X Bio-Rad protein assay dye reagent. All samples were prepared in duplicate. The absorbance was measured at 595 nm and compared to the standard curve. Standard protein determinations were made according to the manufacturer's instructions (BioRad). Myometrial protein samples (40 μg/lane) were then separated by SDS-polyacrylamide gel electrophoresis (SDS-PAGE) in 10 %, 12 % or 15 % resolving gels, according to Laemmli [227], and proteins were electroblotted to 0.2 μm nitrocellulose membranes (BioRad, Mississauga, ON, Canada). A MemCode™ Reversible Protein Stain Kit was always used, according to the manufacturer's instructions, for detection of proteins on nitrocellulose membranes to confirm the efficiency and relative homogeneity of protein transfer in each lane.

After protein transfer, membranes were washed with Tris-buffered saline-Tween-20 (TBST; 20 mM Tris base, 137 mM NaCl, and 0.1% Tween-20; pH 7.6) followed by a 1 h block in 5 % milk powder/TBST or 5 % BSA/TBST, depending on antisera specifications, in order to prevent any non-specific binding of antibodies. Membranes

were probed with appropriate primary antisera (Table 2.1) and then washes (1X 20 min and 4X 5 min) were performed with TBST and constant shaking. Following primary antibody incubation, blots were probed with the appropriate secondary antisera (Table 2.2) and washes (1X 20 min and 4X 5 min) were repeated with TBST and constant shaking at RT. Protein detection was initiated by incubating the blot for 1 min in the Pierce SuperSignal West Pico chemiluminescent substrate detection system (MJS Biolynx, Inc., Brockville, Ontario, Canada). Multiple exposures of varying time lengths were conducted on Amersham ECL film (GE Healthcare Limited, Little Chalfont, BKM, UK) to ensure the film response was in the linear range and then the film was developed in an automated X-ray film developer. Calponin protein expression was used as a normalization control for rat myometrial tissue lysates, following probing with antisera raised against the protein of interest, as this protein is constitutively expressed in both pregnant and non-pregnant rat myometrial samples following RIPA lysis buffer protein extraction [45, 222]. Glyceraldehyde 3-phosphate dehydrogenase (GAPDH) protein expression was used as normalization control for cell lysates, as it is stably and constitutively expressed at high levels in most tissues and cells [228].

2.4 Immunofluorescence Detection

Slide-mounted tissue sections were de-waxed and rehydrated in a graded series of xylene (3X 100 % for 5 min each) and ethanol washes (1X 100 %, 95 %, 90 %, 80 %, 70 % and 50 % for 3 min each). Following rehydration, slides were washed in PBS (3X 7

Table 2.1 List of primary antibodies used for this study.

IF, immunofluorescence; IB, immunoblot; *Dependent on the concentration of the primary antisera used.

Antisera	Antibody type	Method	Dilution	Incubation	Catalogue Number
Bag1	Mouse monoclonal	IB	1:1000	1 hr RT	LS-C95531 Lifespan Biosciences, WA, USA
Bag 3	Mouse monoclonal	IB	1:1000	2 hrs RT	ALX-803-323 Enzo Life Science, NY, USA
Bag 3	Rabbit polyclonal	IB	1:10 000	1 hr RT	Generous gift from Dr. Jacques Landry Laboratory
Bag 3	Rabbit polyclonal	IF	1:100	Overnight at 4^{o}C	Generous gift from Dr. Jacques Landry Laboratory
CHIP (STUB1)	Rabbit monoclonal	IB	1:1000	1 hr RT	LS-C137950 Lifespan Biosciences, WA, USA
ChromPure rabbit IgG	N/A	IF	N/A*	N/A	011–000–003 Jackson ImmunoResearch Laboratories, PA, USA
γ-actin	Sheep polyclonal	IB	1:2000	1 hr RT	AB3265 Millipore, MA, USA
GAPDH	Rabbit polyclonal	IB	1:5000	I hr RT	Ab9485 Abcam Inc., Cambridge, MA, USA
HspB8	Rabbit polyclonal	IB	1:1000	2 hrs RT	LS-C81990 Lifespan Biosciences, WA, USA
HspB8	Rabbit polyclonal	IF	1:400	Overnight at 4^{o}C	LS-C81990 Lifespan Biosciences, WA, USA

Table 2.1 (cont.) List of primary antibodies used for this study.

IB, immunoblot; RT, room temperature

Antisera	Antibody type	Method	Dilution	Incubation	Catalogue Number
HspB8	Rabbit polyclonal	IB	1:1000	2 hrs RT	#3059 Cell signalling, ON, CA
HspB8	Rabbit polyclonal	IB	1:1000	1 hr RT	Generous gift from Dr. Jacques Landry Laboratory
Hsc70	Rabbit polyclonal	IB	1:1000	2 hrs RT	ADI-SPA-816 Enzo Life Sciences, NY, USA
Hsc70	Rabbit polyclonal	IB	1:1000	1 hr RT	SPC-102C/D StressMarq, BC, CA
Hsp70	Mouse monoclonal	IB	1:1000	2 hrs RT	ADI-SPA-810 Enzo Life Sciences, NY, USA
LC3II	Rabbit polyclonal	IB	1:1000	2 hrs RT	PA1-46286 Thermo Scientific, IL, USA
Myc-tag	Rabbit polyclonal	IB	1:1000	1 hr RT	06-549 Millipore, MA, USA
Phospho-EIF2α (Pser51)	Rabbit polyclonal	IB	1:1000	2 hrs RT	SAB4300221 Sigma-Aldrich, MO, USA
Smooth muscle calponin	Mouse monoclonal	IB	1:100 000	1 hr RT	C2687 Sigma-Aldrich, St. Louis, MO, USA

Table 2.2 List of secondary antibodies used for this study.

IB, immunoblot; IF, immunofluorescence; IP, immunoprecipitation; FITC, fluorescein isothiocyanate; HRP, horseradish peroxidase; RT, room temperature.

Antisera	Antibody type	Method	Dilution	Incubation	Catalogue Number
HRP-conjugated goat anti-rabbit IgG	Goat polyclonal	IB	1:10 000	1 hr RT	W401B Promega, Madison,WI, USA
HRP-conjugated goat anti-mouse IgG	Goat polyclonal	IB	1:10 000	1 hr RT	W402B Promega, Madison,WI, USA
HRP-conjugated rabbit anti-sheep IgG	Rabbit polyclonal	IB	1:5000	1 hr RT	AP147P Millipore, MA, USA
Rabbit IgG (whole molecule)-FITC	Sheep polyclonal	IF	1:250	30 min RT	F7512 Sigma-Aldrich, MO, USA
Rabbit TrueBlot: Anti-Rabbit IgG HRP	Goat polyclonal	IP	1:2000	1 hr RT	18-8816 eBioscience, CA, USA

min each) and then heat-induced epitope retrieval was performed using 0.01 M sodium citrate buffer (SC), pH 6.0. SC buffer was heated in a water bath at 95 °C, after which slides were immersed in the hot solution for 10 min and then transferred to a fresh solution at 95°C. Heat-induced epitope retrieval was repeated 4 times. Slides were air dried for 5 min then washed in PBS followed by a 15 minute incubation of sections in 1 mg/mL trypsin (4mM $CaCl_2$, 200mM Tris, pH 7.7; Sigma; Cat# T7168) at RT. Slides were rinsed with PBS. Tissue sections were blocked with 5 % normal goat serum/1 % horse serum in PBS for 1 h and incubated overnight with an HspB8 or Bag3 specific antibody, with agitation at 4 °C (Table 2.1). Both antibodies were diluted in blocking solution for all experiments and a non-specific IgG of the appropriate species, at the same effective concentration, served as a negative control (Table 2.1). Following incubation, sections were washed in PBS and incubated with fluorescein isothiocyanate (FITC)-conjugated sheep anti-rabbit IgG while shaking at RT for 30 min (Table 2.2). Sections were washed 3 times with cold PBS, which contained 0.02 % Tween-20, and mounted with Vectashield containing 4', 6-diamidino-2-phenylindole (DAPI) for nuclear staining (Vector Laboratories; Cat# H-1200 Burlington, ON, Canada). A Leica DMIRE2 microscope (Leica Microsystem (Canada) Inc., Richmond Hill, ON, Canada) equipped with epi-fluorescence optics and a QImaging Retiga EXi Camera (QImaging, Surrey, BC, Canada) was used to view sections and collect images. Images were collected and analyzed with Improvision Openlab 5 software (PerkinElmer, Waltham, MA, USA).

2.5 Immunoprecipitation (IP) Analysis

Human Telomerase Reverse Transcriptase- Human myometrial (hTERT-HM) cell lysates or rat myometrial tissue lysates from NP, d15 and d23 of gestation were diluted in RIPA buffer (containing Phosphatase Inhibitor Cocktail and Complete and Mini EDTA-free protease inhibitors) to a final concentration of 1 µg/µl. The lysates were then pre-cleared using 20 µl of Protein-A Sepharose 4B for 1 h at 4 °C. Following centrifugation at 200 rcf for 1 min, the pellets were discarded and 3 µl of a HspB8 or Bag3 specific antibody (generous gifts from Dr. Jacques Landry Laboratory; [178, 183]) were added to each sample. The lysates were incubated on a nutator overnight at 4 °C. Twenty microlitres of Protein-A Sepharose 4B was added to each antibody-lysate mixture and incubated overnight at 4 °C. Following centrifugation at 500 rcf for 5 min, the supernatants were discarded and the pellets were washed 4 times with RIPA buffer (containing Phosphatase Inhibitor Cocktail and Complete and Mini EDTA-free protease inhibitors), with repeated centrifugations at 500 rcf. Finally each pellet was resuspended in 4X SDS PAGE buffer, heated at 95 °C for 5 min and centrifuged at 1200 rcf. Samples were analyzed by SDS-PAGE and immunoblot analysis. Blots were processed using the immunoblot technique previously described (Section 2.3) with one exception: following primary antibody incubation blots were probed with TrueBlot™ HRP-conjugated Anti-rabbit IgG for 1 h with shaking at RT (Table 2.2).

2.6 Cell Culture

2.6.1 *Human Myometrial Cell Line hTERT-HM*

An immortalized human myometrial cell line, hTERT-HM, was a very generous gift from Dr. Ann Word (Southwestern Medical Center, Dallas, TX, USA) and was used for cell experiments. This line was derived from myometrial tissue of women undergoing hysterectomy. Retroviral infection was used to express the catalytic subunit of telomerase in these myometrial cells. The hTERT-HM cells retain morphological characteristics of proliferating smooth muscle cells in culture including: elongated cell shape with a central nucleus, a sheetlike growth pattern at confluence and expression of smooth muscle-specific actin [229]. This cell line expresses markers of uterine smooth muscle such as, the OTR, PR, calponin, caldesmon and smooth muscle α-actin and it maintains responsiveness to 17β-estradiol. The expression of these markers indicates that the hTERT-HM cell line retains the phenotypic characteristics of human myometrial smooth muscle cells and may serve as a useful model to study human myometrial function [229].

Cells were cultured in 75 cm^2 flasks at 37 °C under a 5 % CO_2 in air environment with Dulbecco's modified Eagle's medium (DMEM) nutrient mixture F-12 (Ham) 1X (DMEM/F12 1:1; (Invitrogen, Burlington, ON, Canada) which was supplemented with 10 % fetal bovine serum (FBS; PAA Laboratories, Etobicoke, ON, Canada) and 1 % pen/strep (100 U/ml penicillin, 100 μg/ml streptomycin; Invitrogen, Burlington, ON, Canada). Cells were cultured until they were 70-80 % confluent then used for various

experiments.

2.6.2 *Collection of Cell Protein Lysates*

Cells were washed in 5 mL of PBS and subsequently placed on ice. Nonidet-P40 (NP-40) lysis buffer (containing Phosphatase Inhibitor Cocktail and Complete^{TM} Mini EDTA-free protease inhibitors; Roche Molecular Biochemicals, Laval, Quebec, Canada; Cat# 04906837001, 12454800) were added to each dish and left on ice for ~2 min. Cells were removed from the dish using a cell scraper and placed into a 1.5 mL microfuge tube. Samples were then homogenized in NP-40 buffer using a bead mill and centrifuged at 11000 rcf for 15 min at 4 ^{o}C. Supernatants were collected and the protein concentrations of these samples were obtained using the Bradford Assay [230]. Samples were then stored at -80 ^{o}C.

2.6.3 *Angiotensin II-induced Hypertrophy Experiment*

Angiotensin II has been found to induce hypertrophy of human airway smooth muscle cells, vascular smooth muscle cells and cultured rat aortic smooth muscle cells [231-233]. For Angiotensin II (Ang II) experiments ~2.0 x 10^4 hTERT-HM cells were each seeded in four 25 cm^2 flasks. For the first night, cells were cultured in a 5 % CO_2 in air incubator at 37 °C in normal media supplemented with 10 % FBS and 1 % pen/strep. After 24 h, all cells were cultured in serum free media supplemented with 1 % pen/strep. After an additional 24 h, two flasks were cultured in serum free media supplemented with 1000 nM Ang II (05-23-0101, Calbiochem, San Diego, CA, USA) and 1 % pen/strep,

while the two vehicle control flasks were cultured in serum free media supplemented with an equivalent volume of ultrapure distilled water (DNAse, RNAse free; Invitrogen, Burlington, ON, Canada) and 1 % pen/strep. After an additional 24 h of culture in Ang II supplemented medium, protein lysates were collected (Section 2.6.2).

2.6.4 *Plasmids*

A mammalian expression vector encoding a myc-tagged human HspB8 cDNA construct (pCImycHspB8) and a mammalian expression vector encoding a myc-tagged human Bag3 cDNA construct (pCImycBag3) were very generous gifts from the laboratory of Dr. Jacques Landry [178, 211].

To cultivate the acquired plasmids, 50 µL of DH5α competent cells were thawed on ice and transferred to a 15 mL Falcon tube. Plasmid (25 ng) was added to the DH5α cells and the mixture was incubated on ice for 30 min. The mixture was heated at 42 °C for 90 s and subsequently incubated on ice for 2 min. One mL of pre-warmed cell culture media (without antibiotic) was added to the mixture and the culture agitated at 220 rpm for 1 h at 37 °C. The culture was spread on pre-warmed agar plates containing ampicillin (100 µg/mL) and plates were inverted and incubated overnight at 37 °C. Single colonies were selected for inoculation of 3 mL mini-cultures containing ampicillin and were left shaking overnight at 220 rpm at 37 °C. Plasmid DNA was purified using a PureLink Quick Plasmid Miniprep Kit (Invitrogen, Burlington, ON, Canada) according to the manufacturer's instructions and then the DNA concentrations of all samples were

determined using a NanoDrop Spectrophotometer. After determining the DNA concentration, samples were prepared for restriction endonuclease digestion. Each digestion contained 1 μg DNA, 1 μL 10X buffer (depending on restriction enzymes), 10 μg/μL restriction enzyme and had a total volume of 10 μL, made up with water. Restriction endonuclease digestions of DNA were conducted at 37 °C for 1 h, except for the uncut plasmids. Before loading samples on to an agarose gel, 1 μL of 6X loading dye was added to each sample. Digestions were analyzed on a 1% agarose gel prestained with SYBR safe by electrophoresis at 100 V for approximately 40 min. Next, a GeneElute HP Plasmid Midiprep Kit (Sigma-Aldrich, MO, USA) was used to purify the plasmid DNA in larger scale according to the manufacturer's instructions and restriction endonuclease digestion of all samples was conducted as described above.

The cDNA of myc-tagged human HspB8 was inserted at the EcoRI/XbaI restriction sites of pCI (Promega) (Figure 2.1). Therefore, following purification of the plasmid DNA the plasmid was verified by restriction endonuclease digestion using restriction enzymes EcoRI, NotI, and BamHI (Invitrogen, Burlington, ON, Canada). EcoRI and NotI were used to verify that the plasmid was present, as NotI is also found in the multiple cloning site. Finally, to verify that the plasmid was the correct size and to verify the orientation of the insert, BamHI was used as the restriction enzyme. BamHI

Figure 2.1 pCI mammalian expression vector encoding cDNA of human myc-tagged HspB8 or Bag3. The cDNA was inserted at the EcoRI/XbaI restriction sites of pCI (Promega).

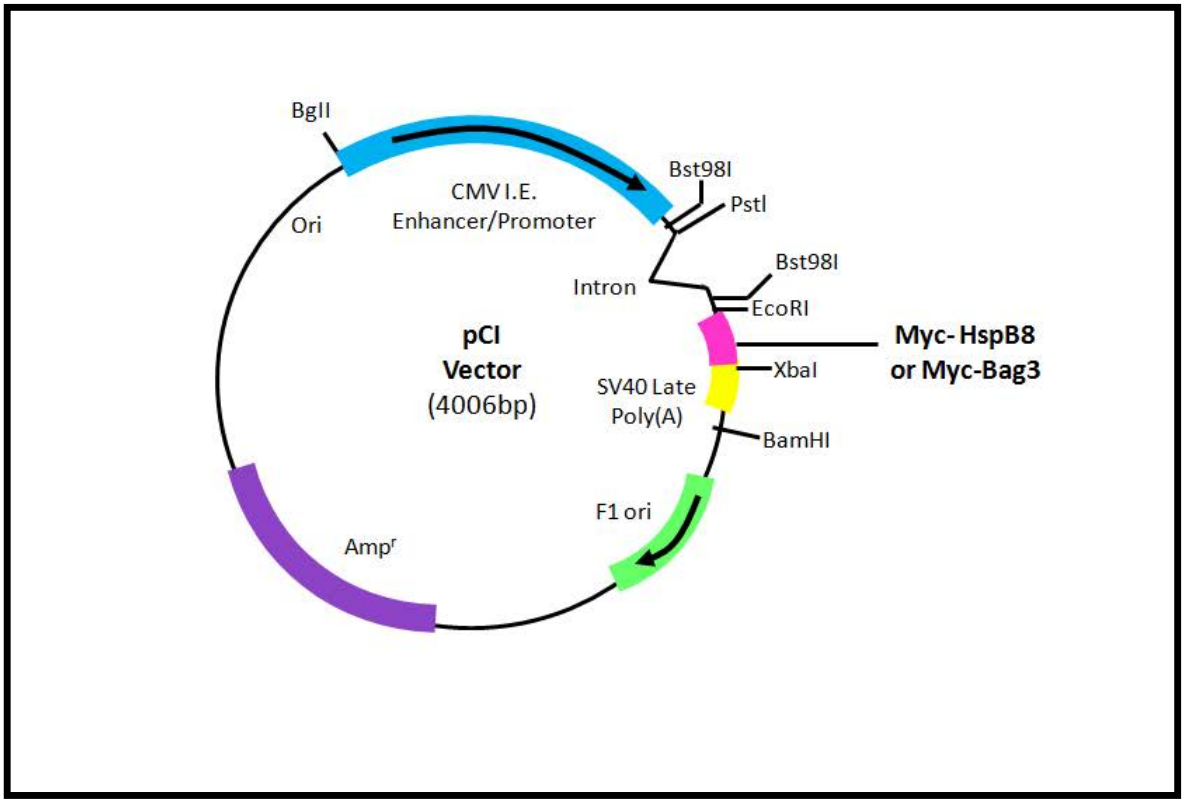
BglI
Bst98I
PstI
CMV I.E.
Enhancer/Promoter
Ori
Bst98I
Intron
EcoRI
pCI
Vector
(4006bp)
Myc- HspB8
or Myc-Bag3
XbaI
SV40 Late
Poly(A)
BamHI
F1 ori
Ampr

cuts both the insert and the vector once and the expected band for the cDNA insert was 465 base pairs (bp).

The cDNA of myc-tagged human Bag3 was inserted at the EcoRI/XbaI restriction sites of pCI (Promega) (Figure 2.1). Therefore, following purification of the plasmid it was verified by restriction endonuclease digestion using the restriction enzymes EcoRI and XbaI (Invitrogen, Burlington, ON, Canada). As the cDNA was inserted at the EcoRI/Xba1 restriction sites of pCI initially, the restriction enzymes XbaI and EcoRI were appropriate for verification.

2.6.5 *Optimization of Cell Transfection*

pEGFP-C3 expression vectors were transiently transfected into hTERT-HM cells using an Amaxa basic nucleofector kit for primary smooth muscle cells (Lonza, Mississauga, ON, Canada; Cat# VPI-1004). First, cells were cultured until approximately 70-80 % confluent, then washed in 5 mL of PBS followed by addition of 1 mL of trypsin to each 75 cm^2 dish for 5 min at 37°C. One mL of media was then added to each dish to inactivate the trypsin and cells from all dishes were pooled into a single 15 mL centrifuge tube. Cells were counted and approximately 1 x 10^6 cells were added to different 15 mL tubes. Each tube was centrifuged at 700 rpm for 10 min and the excess media was removed. The pellet was resuspended with 100 µL Nucleofector solution (82 µL Nucleofector solution + 18 µL Supplement) and 4 µL of pEGFP-C3 expression vector was added. The solution was then transferred to a cuvette and a Lonza nucleofector was

used to transfect the cells using the appropriate program (A-033, D-033, P-013, P-042, U-025, B-017) or no program to serve as a control. Following transfection, 0.5 mL of pre-warmed media was added to the cuvette and the entire solution then subsequently transferred to 6 mL of pre-warmed culture media in a 25 cm^2 tissue culture flask. Each flask was incubated for 10 min at 37 ^oC in a tissue culture incubator. Finally, the contents of each 25 cm^2 flask were equally distributed among each well of a 6 well plate (~2 mL per well) and placed in a tissue culture incubator, containing 5 % CO_2 in air, at 37 ^oC for 72 h. Cells were photographed at 24 h and 48 h under brightfield and epi-fluorescence illumination for assessment of transfection efficiency and cell numbers.

2.6.6 *Transfection of cells*

pCImycHspB8, pCImycBag3 and pEGFP-C3 expression vectors were transiently co-transfected into hTERT-HM cells, using an Amaxa basic nucleofector kit for primary smooth muscle cells, in order to assess their sufficiency to induce cellular hypertrophy. Following transfection optimization, program A-033 was utilized for all transfection experiments. Three 75 cm^2 tissue culture dishes of hTERT-HM cells were used for each transfection experiment, using the methods described above (section 2.6.5). For co-transfection experiments of a single expression vector and transfection indicator plasmid, a total of 2 μg of plasmid DNA was added to each cell sample. For co-transfection experiments with two transfection vectors (pCImycHspB8 and pCImycBag3) and transfection indicator plasmid, a total of 2.5 μg of plasmid DNA were added to each cell

sample. After transfection, cells were cultivated for 72 h followed by collection of protein lysates.

2.7 Flow Cytometry

Cells to be analyzed by flow cytometry (see Sections 2.6.3 and 2.6.6) were labeled with far-red fluorescent reactive dye (Cy5) using a LIVE/DEAD® Fixable Dead Cell Stain Kit (L10120, Invitrogen, Burlington, ON, Canada) according to the manufacturers' instructions. This assay is based on the reaction of a fluorescent reactive dye with cellular amines. The reactive dye can permeate the compromised membranes of necrotic cells and react with free amines in the interior and on the cell surface, resulting in intense fluorescent staining. However, the reactive dye can only react with the cell-surface amines of viable cells, resulting in dim fluorescent staining. The difference in intensity between live and dead cell populations is usually greater than 50-fold. Briefly, cells were trypsinized and then a sample of cells in suspension containing at least 1 x 10^6 cells was centrifuged, washed and resuspended in PBS. One microlitre of reconstituted fluorescent reactive dye (far red fluorescent reactive dye) was then added to 1 mL of the cell suspension and incubated on ice for 30 min, protected from light. Subsequently, cells were washed in PBS and resuspended in 900 µl of PBS and 100 µl of 37 % formaldehyde. Cells were incubated at RT for 15 min and then washed in PBS with 1 % BSA. Finally, cells were resuspended in 1 mL of PBS with 1 % BSA and then analyzed by flow cytometry using a BD FACSCalibur™ flow cytometer (far red fluorescent reactive dye: 633/635 nm excitation and ~665 nm emission).

2.8 Protein/DNA ratio

Protein/DNA ratios were determined using a SurePrep^{TM} RNA/DNA/Protein Purification Kit (Fisher BioReagents, Fairlawn, NJ USA) according to the manufacturer's instructions. This kit allowed for isolation of both proteins and purification of genomic DNA. Briefly, 0.8 x 10^6 hTERT-HM cells were used for cell lysate preparation. Initially, total RNA was purified using RNA wash solution/RNA elution buffer and the flowthrough, containing total protein, was retained. Subsequently, genomic DNA from the flowthrough was purified using genomic DNA wash solution and genomic DNA elution buffer. DNA (A260) and protein (A280) concentrations were determined with a Nanodrop Spectrophotometer.

2.9 Data Analysis

Densitometric analysis was performed on immunoblots using ImageJ software (National Institutes of Health, USA). Densitometric measurements of the protein of interest were normalized to the loading control calponin or GAPDH and presented as the mean ± standard error of the mean (SEM). GraphPad Instat version 3.0 (GraphPad Software, San Diego, CA, USA, www.graphpad.com) was used to perform statistical analysis and graphs were prepared using GraphPad Prism version 5.0 (GraphPad Software). Data from normal gestational profiles and progesterone experiments were subjected to a one-way analysis of variance (ANOVA) or a two-way ANOVA, respectively. Data that was found to have significance from a one- way or two-way

ANOVA was then subjected to Newman-Keuls post-hoc test to determine pair wise significance. Data from unilateral pregnancy and RU486 experiments were subjected to a student t-test. The differences were considered significant if the p-value was less than 0.05.

Chapter Three

Results

3.1 Expression of HspB8 During Normal Pregnancy and Labour

3.1.1 *Immunoblot Analysis of HspB8 Protein*

Immunoblot analysis was performed to characterize HspB8 protein expression in non-pregnant and pregnant rat myometrium throughout the gestational period. HspB8 and calponin protein were detected at their predicted molecular weights, 22 kDa and 34 kDa respectively (Figure 3.1.1A). Following densitometric analysis of immunoblots, a one-way ANOVA revealed that HspB8 protein expression changed significantly over gestation ($p< 0.05$; n=4/day). HspB8 protein expression was particularly elevated at d15, d17 and d19 compared to expression at NP and d6. These results were confirmed by additional immunoblot analysis using a second HspB8 specific antibody from Cell Signaling (2.1; Figure 3.1.1C). The two antibodies utilized were polyclonal antisera; however, the antibody from LifeSpan BioSciences was designed to recognize the N-terminus of HspB8 whereas the antibody from Cell Signaling detected endogenous levels of total HspB8 protein.

3.1.2 *Immunofluorescence Detection of HspB8 Protein*

To determine the spatial localization of HspB8 protein in the myometrium throughout gestation, immunofluorescence detection was completed. Detection of HspB8

Figure 3.1.1 Immunoblot analysis of HspB8 protein expression in pregnant rat myometrium. **(A)** Representative immunoblots of HspB8 protein and calponin are shown. Analysis was performed using a HspB8 specific antibody (LifeSpan BioSciences). **(B)** The relative protein expression of HspB8 was analyzed using densitometric analysis. The data were presented as the mean ± SEM of the relative optical density of HspB8 normalized to the optical density of calponin. Values are from four independent experiments. One-way ANOVA revealed that HspB8 protein expression changed significantly overall. HspB8 protein expression was significantly elevated at d15, d17 and d19 compared to expression at NP and d6 (*, $p < 0.05$; Newman-Keuls, post-hoc test; n=4/day). Days 6, 12, 15, 17, 19, 21, 22, and 23 represent gestational time points. NP, non-pregnant; PP, 1 day postpartum. **(C)** Representative immunoblots of HspB8 protein and calponin are shown. Analysis was performed using a HspB8 specific antibody (Cell Signaling). Results further confirm those received using the other commercially available antibody purchased from LifeSpan Biosciences.

A

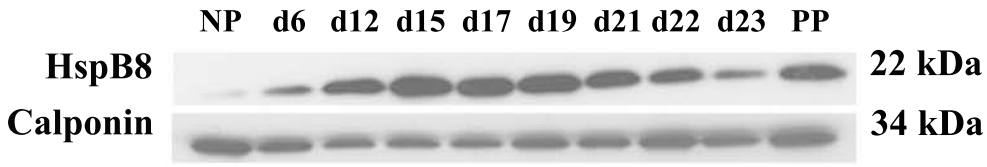
NP d6 d12 d15 d17 d19 d21 d22 d23 PP
HspB8
Calponin
22 kDa
34 kDa

B

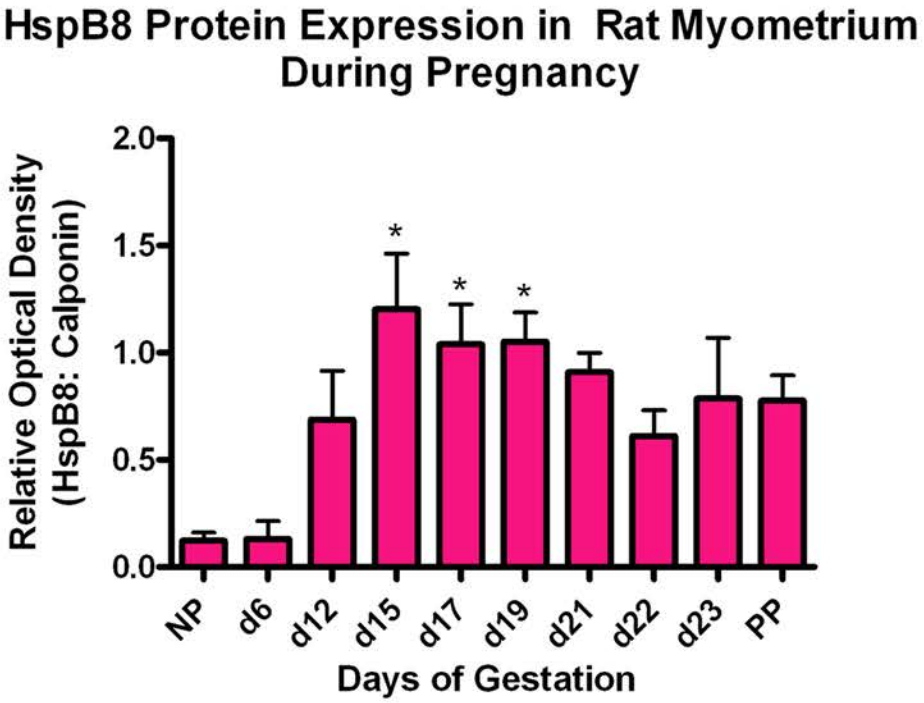
HspB8 Protein Expression in Rat Myometrium During Pregnancy
Relative Optical Density (HspB8: Calponin)
2.0
1.5
1.0
0.5
0.0
*
*
*
NP d6 d12 d15 d17 d19 d21 d22 d23 PP
Days of Gestation

C

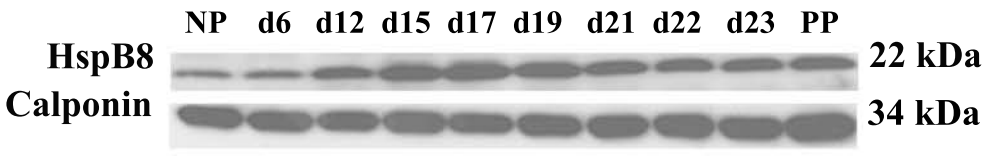
NP d6 d12 d15 d17 d19 d21 d22 d23 PP
HspB8
Calponin
22 kDa
34 kDa

protein in the circular and longitudinal muscle layers revealed that it was primarily localized in the cytoplasm of cells throughout gestation (Figure 3.1.2- 3.1.5). At higher magnification, it was confirmed that HspB8 protein was localized in the cytoplasm and there was an absence of any nuclear staining (Figure 3.1.6). It was also noted that there was particularly intense cytoplasmic staining on d15 and d17 of gestation, indicating concentrated subcellular localization of HspB8 protein.

3.2 Immunofluorescence Detection of HspB8 Protein in Rat Heart Tissue

Although immunoblot analysis demonstrated significant changes in HspB8 protein expression throughout gestation, there was only a slight apparent increase in immunofluorescence detection of HspB8 protein. Thus, as a means to assess the quality of the HspB8 specific antibody for immunofluorescence procedures, immunolocalization of HspB8 protein was examined in rat heart tissue. Depre et al. (2006) reported HspB8 protein expression in heart muscle particularly in the cytoplasm of myocytes [234]. Detection of HspB8 protein was localized to the cytoplasm of rat myocytes (Figure 3.2.1) as previously reported, confirming the specificity of the antisera used.

3.3 Analysis of Proteins Associated with HspB8 during Pregnancy

3.3.1 *Expression of Bag3 protein*

Immunoblot analysis was performed to characterize Bag3 protein expression in non-pregnant and pregnant rat myometrium throughout the gestation period.

Figure 3.1.2 Immunofluorescence detection of HspB8 protein in the circular muscle layer of NP rat myometrium and myometrium from d6 to d17 of gestation. The images demonstrate mainly cytoplasmic localization of the protein and an absence of nuclear staining (n=3/day) using a HspB8-specific antibody (Lifespan BioSciences). Ctrl = control, rabbit IgG. Scale bar = 50 μm.

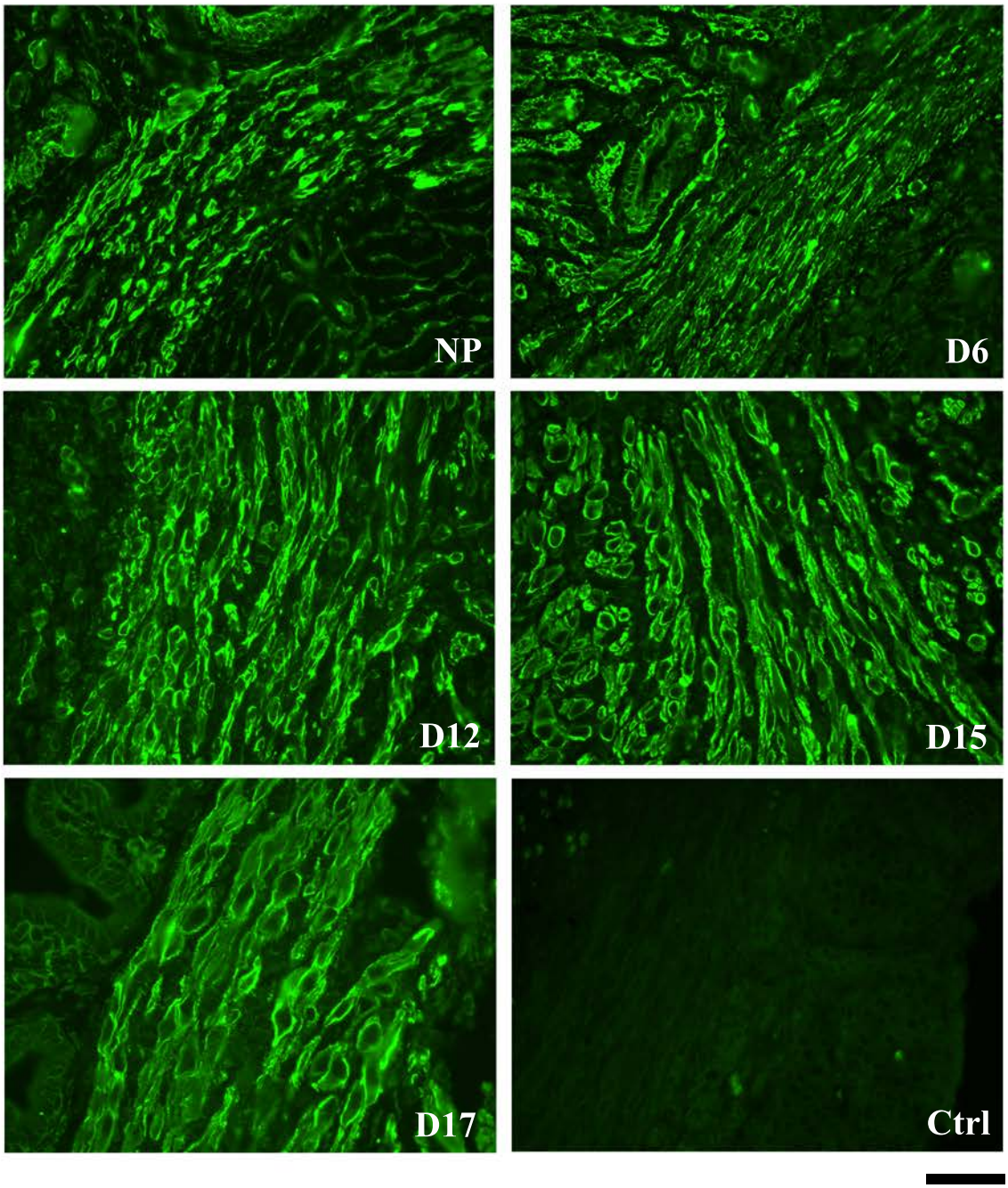
NP
D6
D12
D15
D17
Ctrl

Figure 3.1.3 Immunofluorescence detection of HspB8 protein in the circular muscle layer of rat myometrium at d19 to d23 of gestation and PP. The images demonstrate mainly cytoplasmic localization of the protein and an absence of nuclear staining (n=3/day) using a HspB8 specific antibody (LifeSpan BioSciences). Ctrl = control, rabbit IgG. Scale bar = 50 μm.

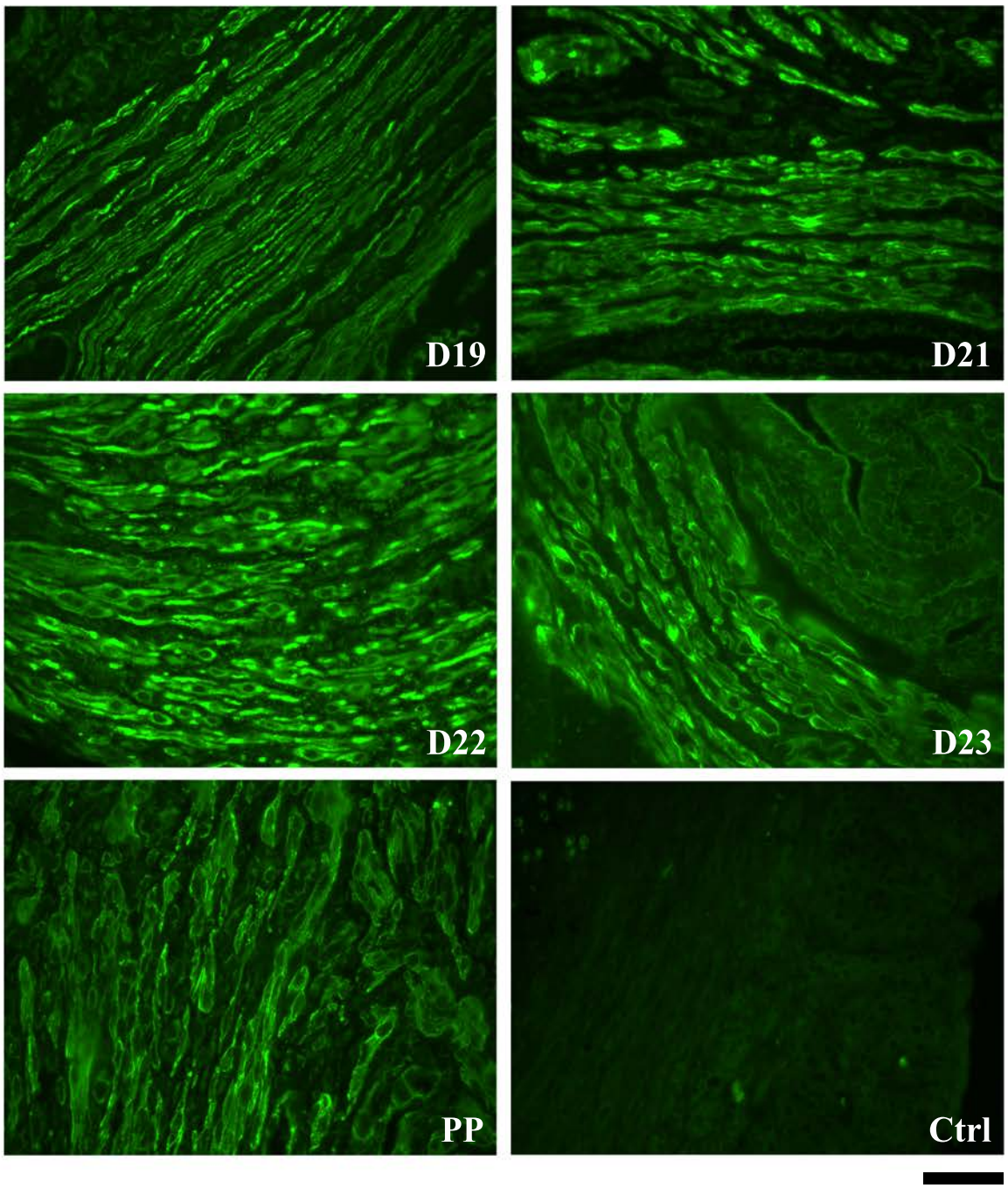
D19
D21
D22
D23
PP
Ctrl

Figure 3.1.4 Immunofluorescence detection of HspB8 protein in the longitudinal muscle layer of NP rat myometrium and d6 to d17 of gestation. Detection of HspB8 protein, using a HspB8 specific antibody (LifeSpan Biosciences), in the longitudinal muscle layer demonstrated that it was primarily and readily localized in the cytoplasm of myometrial cells and there was an absence of nuclear staining (n=3/day). Arrows indicate blood vessels. Ctrl = control, rabbit IgG. Scale bar = 50 μm.

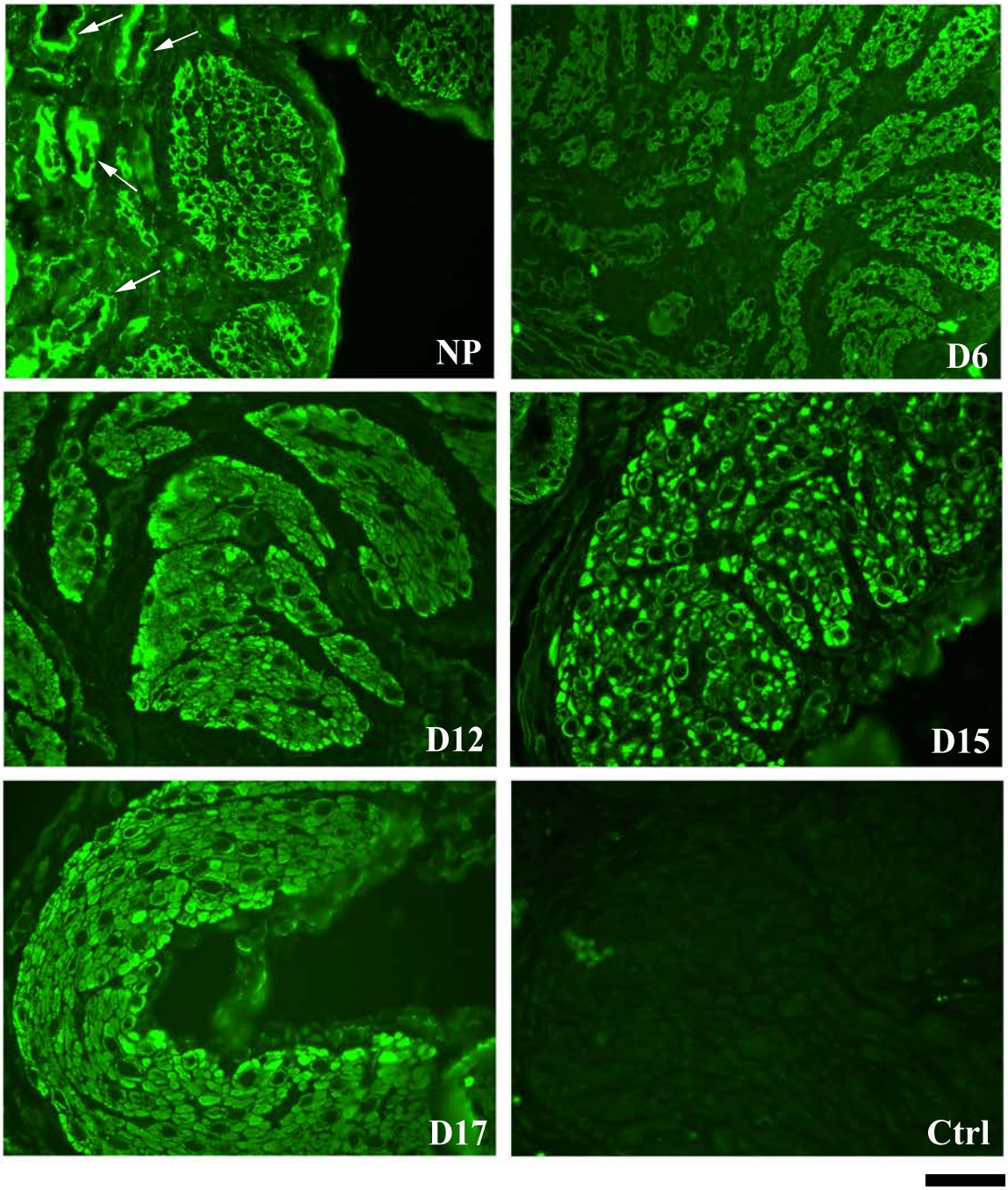
NP
D6
D12
D15
D17
Ctrl

Figure 3.1.5 Immunofluorescence detection of HspB8 protein in the longitudinal muscle layer of rat myometrium at d19 to d23 of gestation and PP. Detection of HspB8 protein, using a HspB8 specific antibody (LifeSpan BioSciences), in the longitudinal muscle layer demonstrated that it was primarily localized in the cytoplasm of myometrial cells and there was an absence of nuclear staining (n=3/day). Ctrl = control, rabbit IgG. Scale bar = 50 μm.

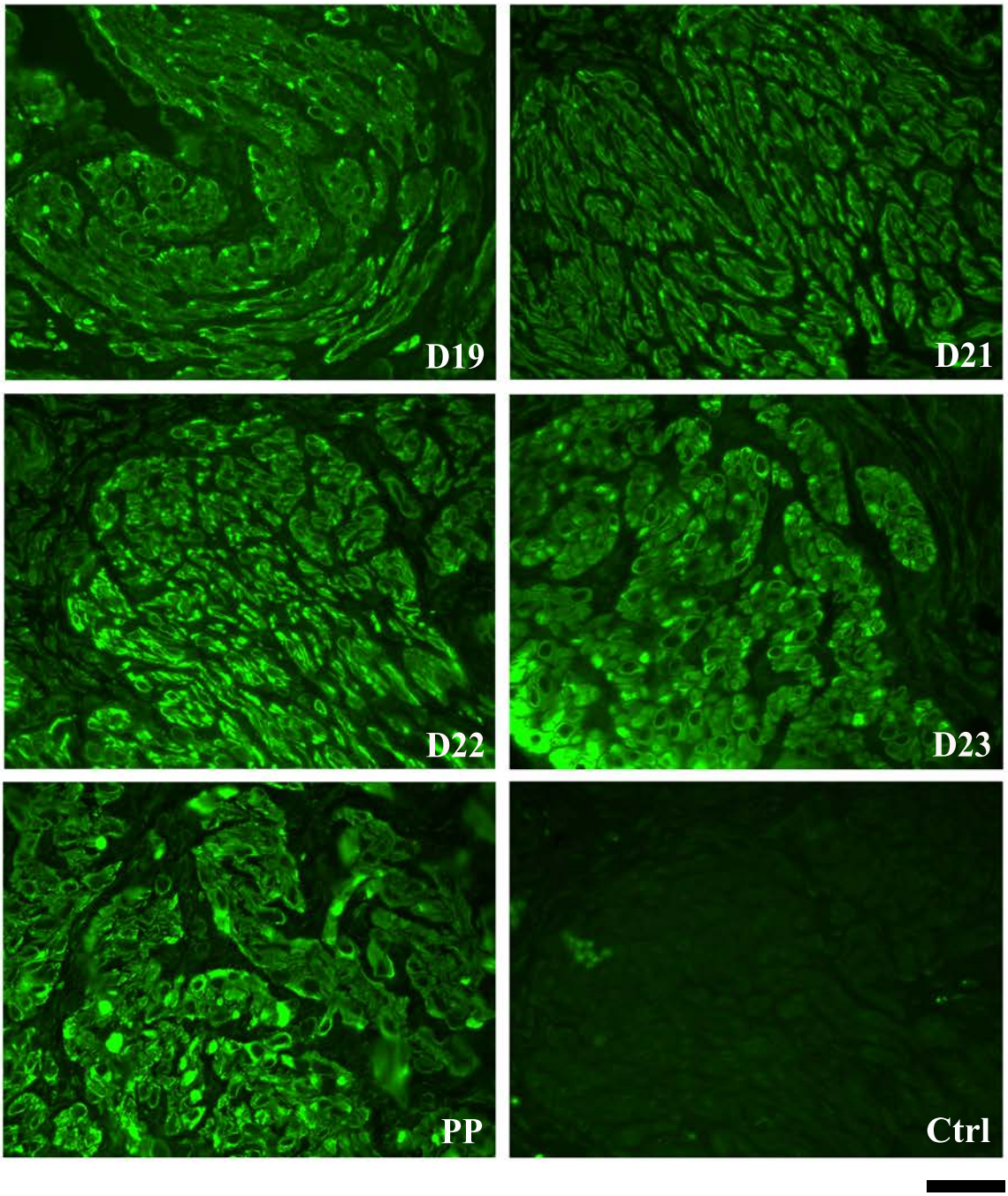
D19
D21
D22
D23
PP
Ctrl

Figure 3.1.6 Immunofluorescence detection of HspB8 protein in the cytoplasm of longitudinal muscle cells of rat myometrium. Sections were probed with a HspB8 specific antibody (LifeSpan BioSciences). The image (d15+ Dapi) demonstrates that there was no nuclear staining (arrows indicate the nucleus); thus, indicating cytoplasmic localization of the protein within myometrial cells (n=3/day). Ctrl = control, rabbit IgG. Scale bar = 50 μm.

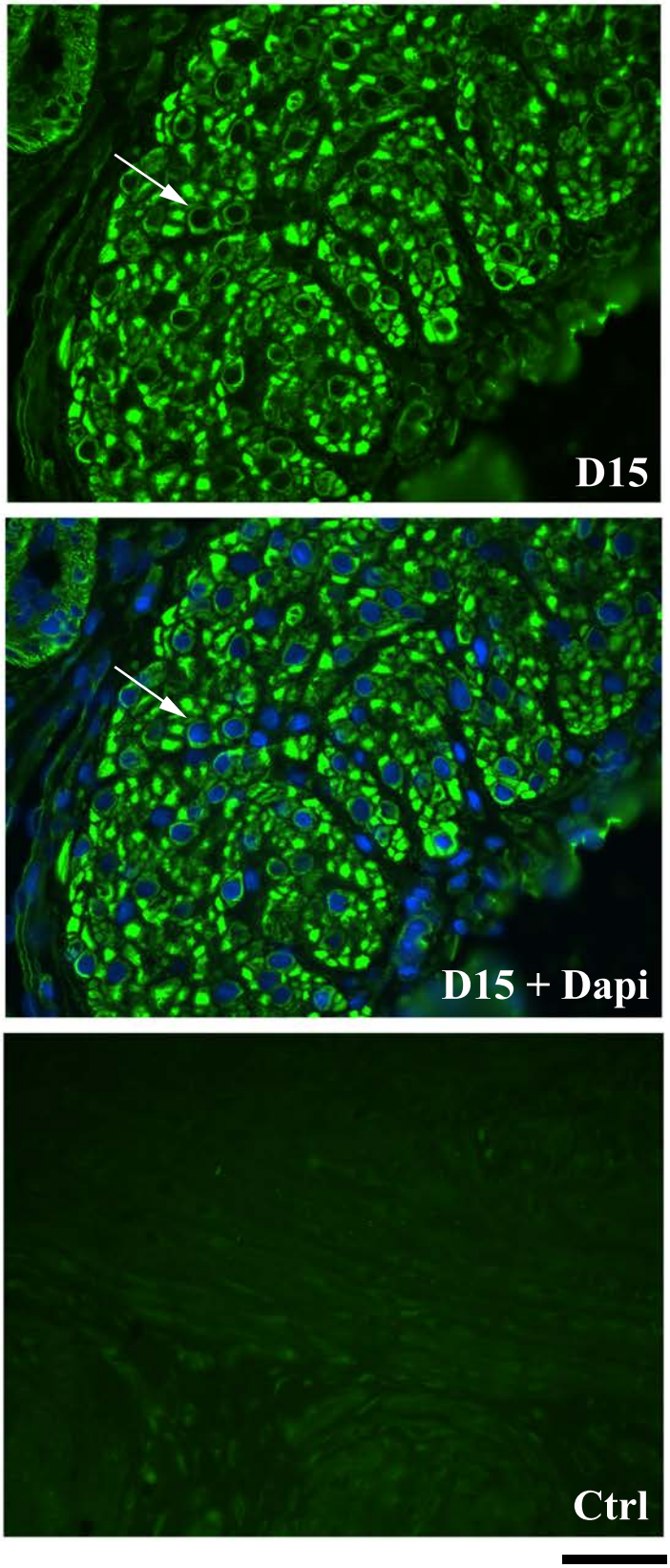
D15
D15 + Dapi
Ctrl

Figure 3.2.1 Immunofluorescence detection of HspB8 protein in rat heart tissue sections. Analysis was conducted using a HspB8 specific antibody (LifeSpan BioSciences). The images demonstrate cytoplasmic localization of the protein within heart myocytes, detection near cell membranes and the absence of any nuclear staining. Based on previous studies, the expected staining for the heart was clear localization in the cytoplasm. Arrows on the control indicate red blood cells. Ctrl = control, rabbit IgG. Scale bar = 50 μm.

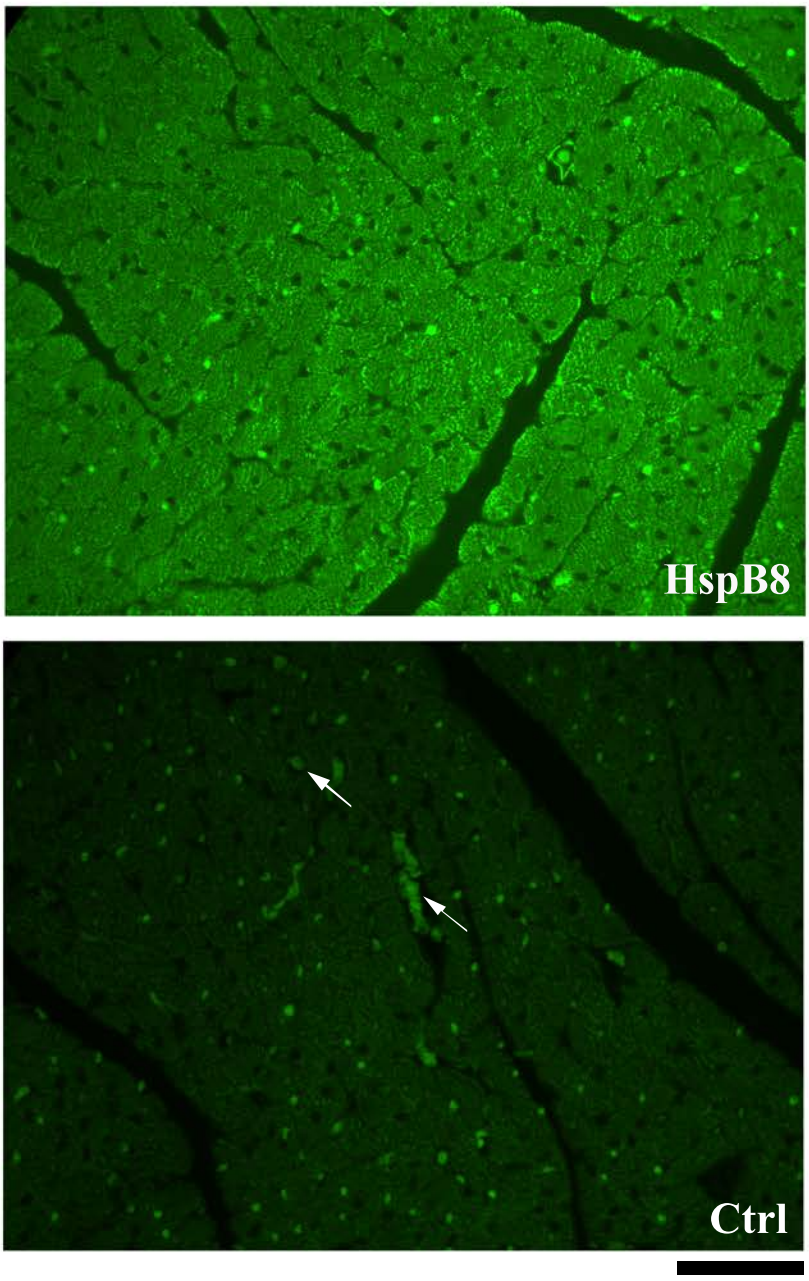
HspB8
Ctrl

Immunoblot analysis was carried out with a Bag3 specific antibody at the time points previously described (Table 2.1; Section 2.2.1). Bag3 and calponin protein were detected at their predicted molecular weights, 74 kDa and 34 kDa respectively (Figure 3.3.1). Following densitometric analysis, one-way ANOVA revealed that Bag3 protein expression changed significantly over gestation ($p< 0.05$; n=4/day). Bag3 protein expression was significantly elevated at d15, compared to expression at NP, and at d17 compared to NP, d6, d23 and PP. Following immunoblot analysis it was noted that additional protein bands were detected at different molecular weights, possibly representing cleavage products of Bag3 (Figure 3.3.2).

3.3.2 *Immunofluorescence Detection of Bag3 Protein*

To determine the spatial localization of Bag3 protein throughout gestation, immunofluorescence detection was completed. Detection of Bag3 protein in the circular and longitudinal muscle layers of rat myometrium indicated that it was homogeneously distributed in the cytoplasm of myometrial cells. Specifically, there was perinuclear localization of Bag3 protein in addition to general cytoplasmic localization, and an absence of nuclear staining (Figure 3.3.3-3.3.6). Immunostaining was more homogeneous and slightly more intense around d15 and d17 in comparison to early time points.

3.3.3 *Expression of Bag1 Protein*

One important function of Bag1 is to mediate protein quality control by targeting selected proteins for proteasome-mediated degradation, likely also an essential process

Figure 3.3.1 Immunoblot analysis of Bag3 protein expression in pregnant rat myometrium. **(A)** Representative immunoblots of Bag3 protein and calponin are shown. **(B)** The relative expression of Bag3 was analyzed using densitometric analysis. The data were presented as the mean ± SEM of the relative optical density of Bag3 normalized to the optical density of calponin. Values are from four independent experiments. One-way ANOVA revealed that Bag3 protein expression changed significantly overall. Bag3 protein expression was significantly elevated at d15 compared to expression at NP (*, $p< 0.05$; Newman-Keuls, post-hoc test; n=4/day). Bag3 protein expression was also significantly elevated at d17 compared to NP, d6, d23 and PP (**, $p< 0.05$). Days 6, 12, 15, 17, 19, 21, 22, and 23 represent gestational time points. NP, non-pregnant; PP, 1 day postpartum.

A

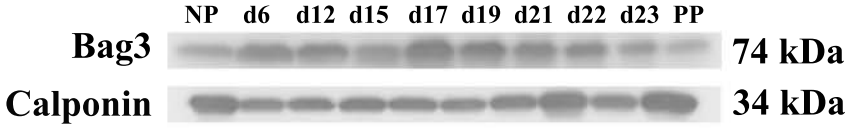
NP d6 d12 d15 d17 d19 d21 d22 d23 PP
Bag3
74 kDa
Calponin
34 kDa

B

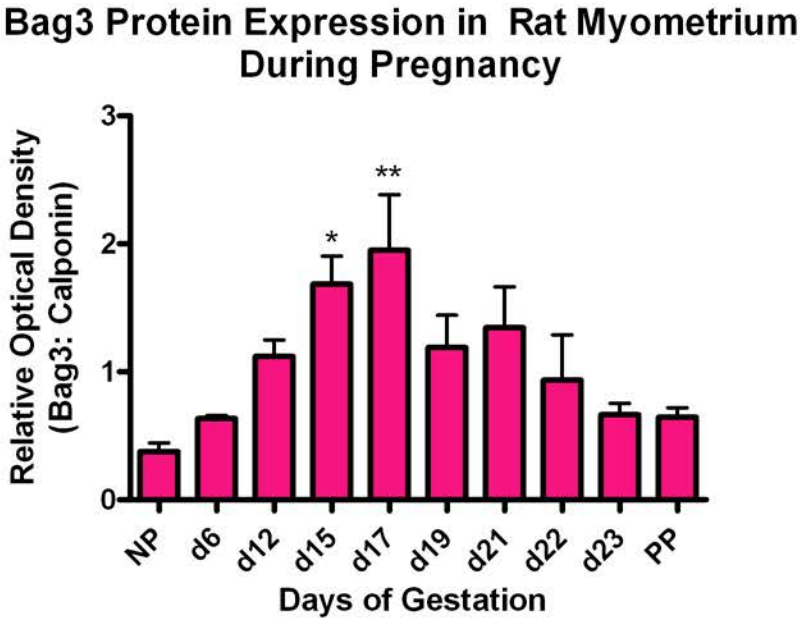
Bag3 Protein Expression in Rat Myometrium During Pregnancy
Relative Optical Density (Bag3: Calponin)
0
1
2
3
*
**
NP
d6
d12
d15
d17
d19
d21
d22
d23
PP
Days of Gestation

Figure 3.3.2 Expression of potential Bag3 cleavage products in rat myometrium during gestation. Representative immunoblot probed with a Bag3 specific antibody. Full-length Bag3 protein has a molecular weight of approximately 74 kDa however, additional bands were also detected at approximately 40 kDa and 25 kDa between NP and ~ d19 of gestation. These bands may represent possible cleavage products of Bag3 protein. Arrows indicate the unknown bands recognized by the Bag3 specific antibody.

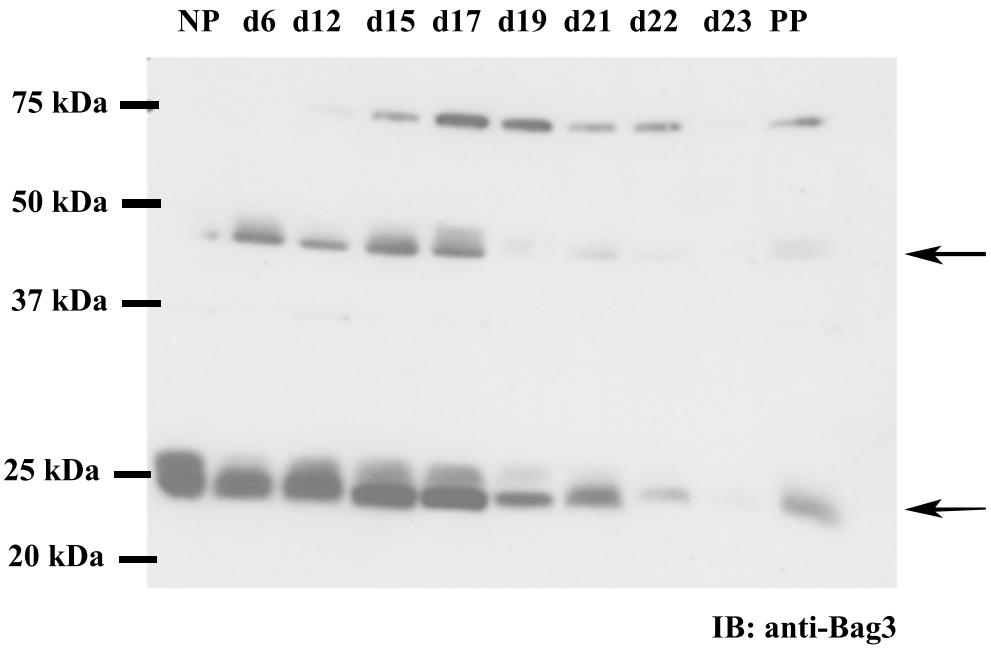
NP d6 d12 d15 d17 d19 d21 d22 d23 PP
75 kDa
50 kDa
37 kDa
25 kDa
20 kDa
IB: anti-Bag3

Figure 3.3.3 Immunofluorescence detection of Bag3 protein in the circular muscle layer of NP rat myometrium and d6 to d17 of gestation. The images demonstrate mainly cytoplasmic localization of the protein, as well as an absence of nuclear staining (n=3/day). Arrows indicate perinuclear localization. Ctrl = control, rabbit IgG. Scale bar = 50 μm.

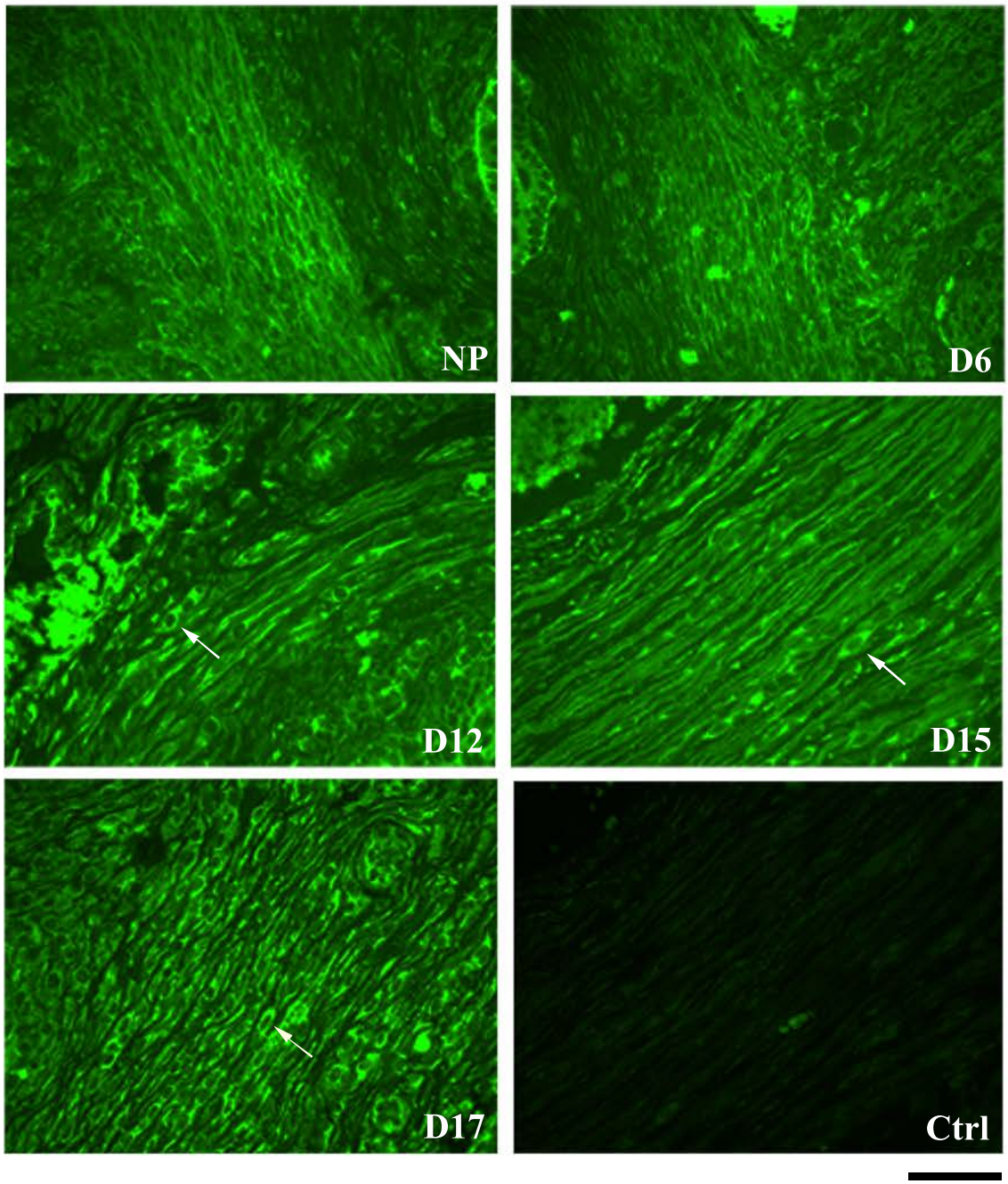
NP
D6
D12
D15
D17
Ctrl

Figure 3.3.4 Immunofluorescence detection of Bag3 protein in the circular muscle layer of rat myometrium at d19 to d23 of gestation and PP. The images demonstrate mainly cytoplasmic localization of the protein, as well as an absence of nuclear staining (n=3/day). Arrows indicate perinuclear localization. Ctrl = control, rabbit IgG. Scale bar = 50 μm.

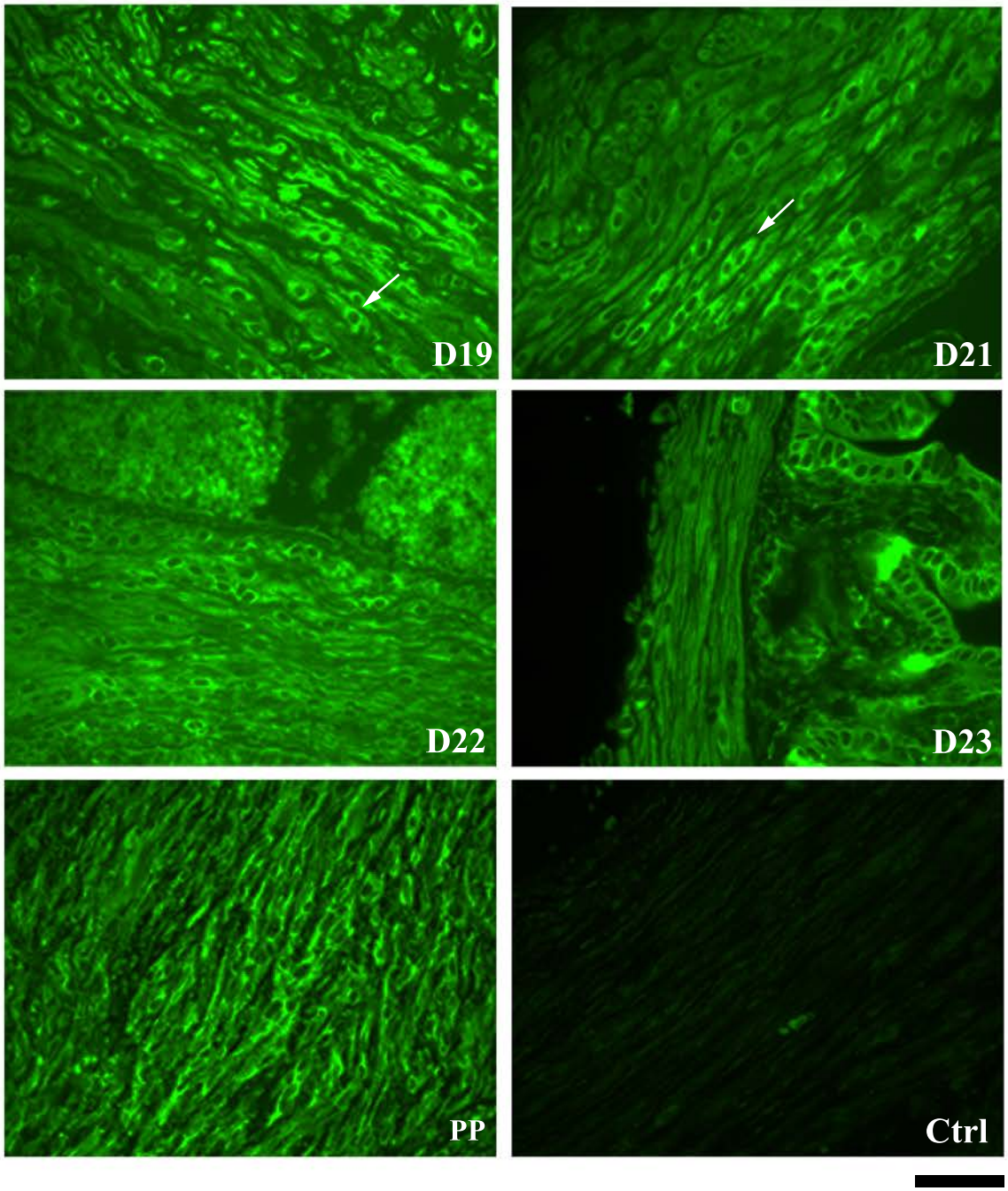
D19
D21
D22
D23
PP
Ctrl

Figure 3.3.5 Immunofluorescence detection of Bag3 protein in the longitudinal muscle layer of NP rat myometrium and myometrium from d6 to d17 of gestation. Detection of Bag3 protein in the longitudinal muscle layer demonstrated that it was primarily and readily localized in the cytoplasm of myometrial cells. There was also an absence of nuclear staining (n=3/day). Ctrl = control, rabbit IgG. Scale bar = 50 μm.

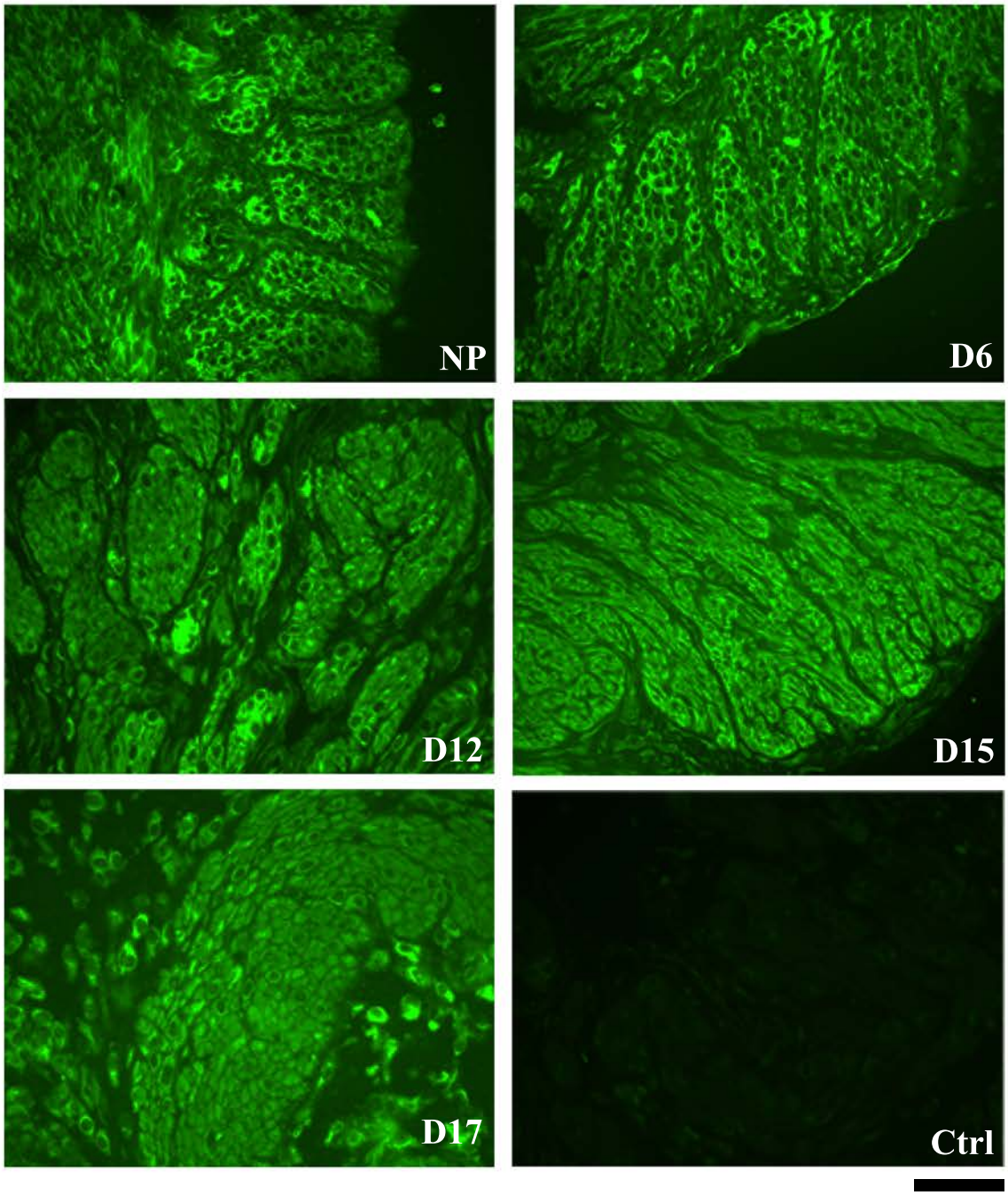
NP
D6
D12
D15
D17
Ctrl

Figure 3.3.6 Immunofluorescence detection of Bag3 protein in the longitudinal muscle layer of rat myometrium at d19 to d23 of gestation and PP. Detection of Bag3 protein in the longitudinal muscle layer demonstrated that it was primarily localized in the cytoplasm of myometrial cells. There was also an absence of nuclear staining (n=3/day). Ctrl = control, rabbit IgG. Scale bar = 50 μm.

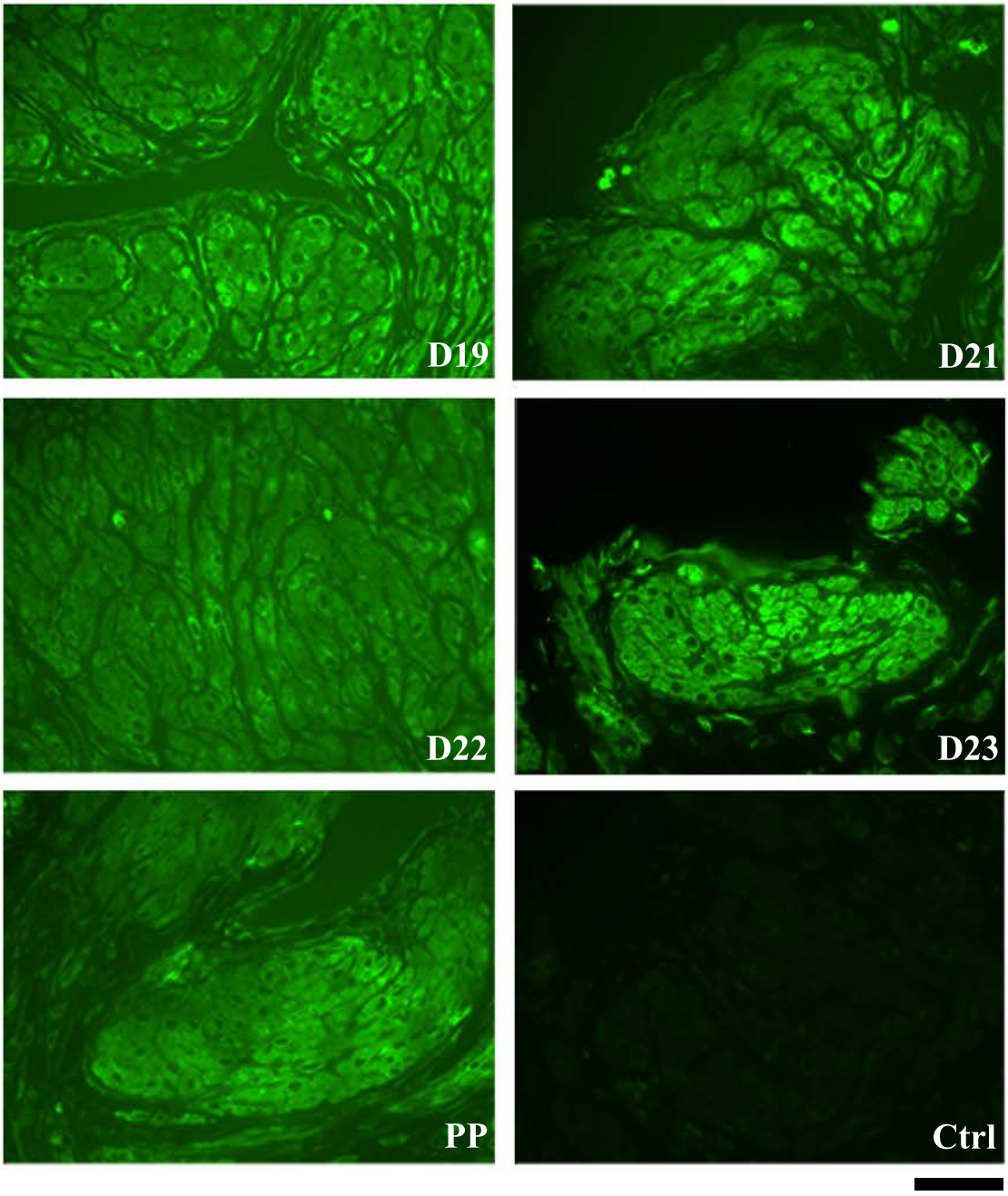
D19
D21
D22
D23
PP
Ctrl

for the maintenance of pregnancy [199]. Immunoblot analysis was performed to characterize Bag1 protein expression in non-pregnant and pregnant rat myometrium throughout the gestational period. Immunoblot analysis was carried out with a Bag1 specific antibody at the time points previously mentioned (Table 2.1; Section 2.2.1). Bag1 and calponin protein were detected at their predicted molecular weights, 38 kDa and 34 kDa respectively (Figure 3.3.7). Following immunoblot analysis it was noted that a doublet protein was visible on immunoblots, representing a possible phosphorylated form of Bag1. Previously published results also suggested the presence of a doublet band of ~38 kDa in peripheral blood mononuclear cells and tonsil as evidence of a phosphorylated form of Bag1 [235]. One-way ANOVA of both bands revealed that Bag1 protein expression changed significantly over gestation ($p < 0.05$; n=4/day). Bag1 protein expression was significantly expressed at NP, d6 and d12 compared to d21, d22 and at d12 compared to d15, d19, d21, d22, d23, PP.

3.3.4 *Expression of Hsp70 and Hsc70 Protein*

It is well known that the Bag proteins are a family of co-chaperones that are capable of interacting with the ATPase domain of Hsc70/Hsp70 through their structural Bag domain [188, 189]. Therefore, to determine the levels of Hsp70 protein throughout normal pregnancy and labour in the rat myometrium, immunoblot analysis was performed. Immunoblot analysis was carried out with an Hsp70 specific antibody throughout gestation (Table 2.1). Hsp70 and calponin protein bands were detected at their predicted molecular weights, 70 kDa and 34 kDa respectively (Figure 3.3.8). Following

Figure 3.3.7 Immunoblot analysis of Bag1 protein expression in pregnant rat myometrium. **(A)** Representative immunoblots of Bag1 protein and calponin are shown. **(B)** The relative expression of Bag1 was analyzed using densitometric analysis. The data were presented as the mean ± SEM of the relative optical density of Bag1 normalized to the optical density of calponin. Values are from four independent experiments. One-way ANOVA revealed that Bag1 protein expression changed significantly overall. Bag1 protein expression was significantly elevated at NP, d6 and d17 compared to d21 and d22 (*, $p< 0.05$; Newman-Keuls, post-hoc test; n=4/day).. Bag1 protein expression was also significantly elevated at d12 compared to d15, d19, d21, d22, d23 and PP (**, $p< 0.05$). Days 6, 12, 15, 17, 19, 21, 22, and 23 represent gestational time points. NP, non-pregnant; PP, 1 day postpartum.

A

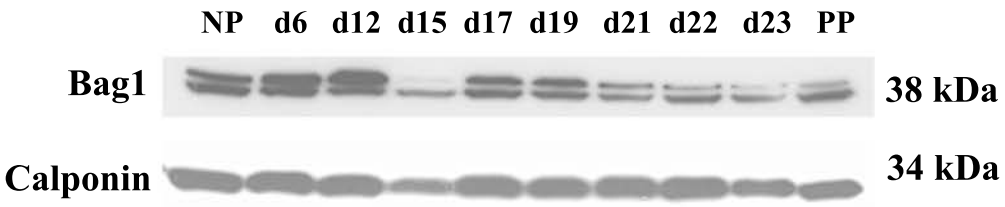
NP d6 d12 d15 d17 d19 d21 d22 d23 PP
Bag1
38 kDa
Calponin
34 kDa

B

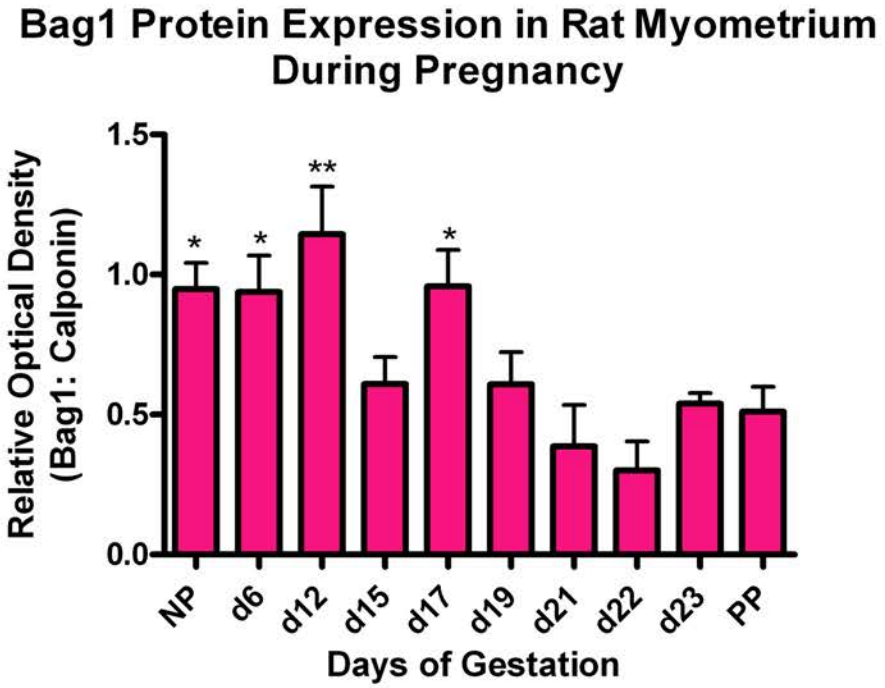
Bag1 Protein Expression in Rat Myometrium During Pregnancy
Relative Optical Density (Bag1: Calponin)
1.5
1.0
0.5
0.0
*
*
**
*
NP
d6
d12
d15
d17
d19
d21
d22
d23
PP
Days of Gestation

Figure 3.3.8 Immunoblot analysis of Hsp70 protein expression in pregnant rat myometrium. **(A)** Representative immunoblots of Hsp70 protein and calponin are shown. **(B)** The relative expression of Hsp70 was analyzed using densitometric analysis. The data were presented as the mean ± SEM of the relative optical density of Hsp70 normalized to the optical density of calponin. Values are from four independent experiments (n=4/day). One-way ANOVA revealed that Hsp70 protein expression changed significantly overall. Hsp70 protein expression was significantly elevated at 19, 21, 22, 23 and PP ccompared to expression at NP and d6 (*, $p< 0.05$; Newman-Keuls, post-hoc test; n=4/day). Furthermore, Hsp70 protein expression on d23 and PP was significantly higher than d12 and d15 (**, $p< 0.05$). Days 6, 12, 15, 17, 19, 21, 22, and 23 represent gestational time points. NP, non-pregnant; PP, 1 day postpartum.

A

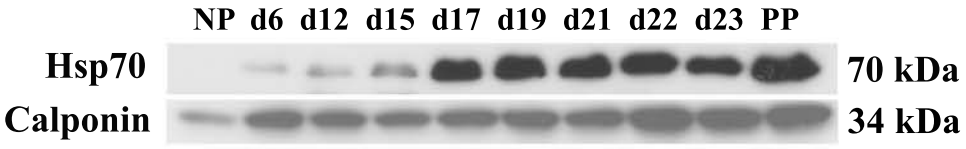
NP d6 d12 d15 d17 d19 d21 d22 d23 PP
Hsp70
70 kDa
Calponin
34 kDa

B

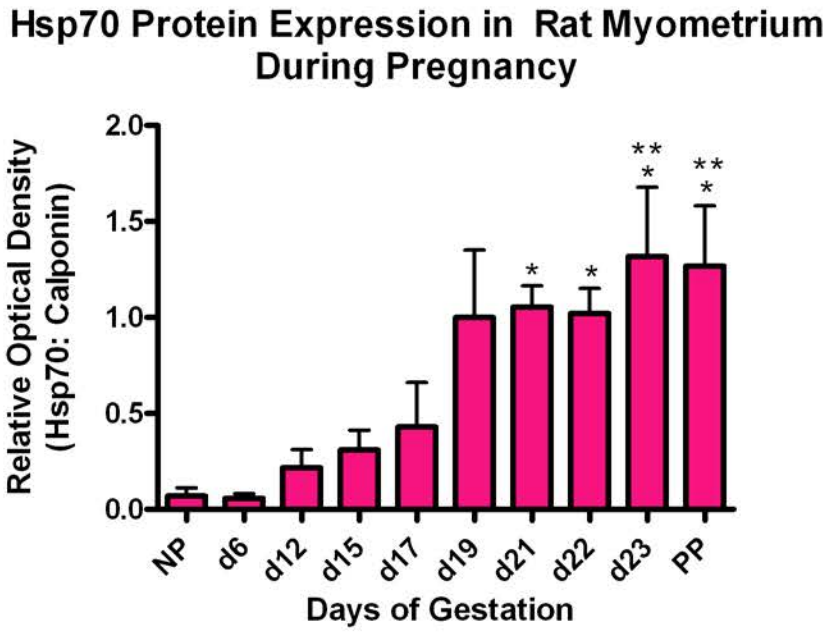
Hsp70 Protein Expression in Rat Myometrium During Pregnancy
Relative Optical Density (Hsp70: Calponin)
2.0
1.5
1.0
0.5
0.0
*
*
**
*
**
*
NP
d6
d12
d15
d17
d19
d21
d22
d23
PP
Days of Gestation

immunoblot and densitometric analysis, one-way ANOVA revealed that Hsp70 protein expression changed significantly over gestation ($p < 0.05$; n=4/day). Protein expression was significantly elevated at d19, d21, d22 and d23 compared to expression at NP and d6. Furthermore, Hsp70 protein expression was significantly higher on d23 and PP compared to d12 and d15.

Immunoblot analysis was also performed to characterize Hsc70 protein expression in non-pregnant and pregnant rat myometrium throughout the gestational period. Immunoblot analysis was carried out with an Hsc70 specific antibody throughout gestation (Table 2.1). Hsc70 and calponin protein bands were detected at their predicted molecular weights, 73 kDa and 34 kDa respectively (Figure 3.3.9). Following immunoblot and densitometric analysis one-way ANOVA revealed that Hsc70 protein expression did not change significantly throughout gestation ($p > 0.05$; n=4/day). Hsc70 protein was constitutively expressed throughout pregnancy.

3.3.5 *Expression of CHIP Protein*

HspB8 has been found to be part of a multi-heteromeric complex, comprised of HspB8, Bag3, Hsc70 and CHIP, which is responsible for the removal of misfolded proteins through macroautophagy activation. Therefore, immunoblot analysis was performed to characterize CHIP protein expression in non-pregnant and pregnant rat myometrium throughout the gestational period. Immunoblot analysis was carried out with a CHIP specific antibody throughout gestation (Table 2.1). CHIP and calponin protein

Figure 3.3.9 Immunoblot analysis of Hsc70 protein expression in pregnant rat myometrium. **(A)** Representative immunoblots of Hsc70 protein and calponin are shown. **(B)** The relative expression of Hsc70 was analyzed using densitometric analysis. The data were presented as the mean ± SEM of the relative optical density of Hsc70 normalized to the optical density of calponin. Values are from four independent experiments. One-way ANOVA revealed that Hsc70 expression did not change significantly overall ($p > 0.05$; n=4/day). Hsc70 protein is constitutively expressed throughout gestation. Days 6, 12, 15, 17, 19, 21, 22, and 23 represent gestational time points. NP, non-pregnant; PP, 1 day postpartum.

A

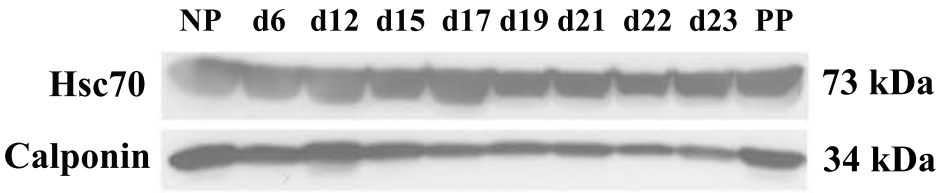
NP d6 d12 d15 d17 d19 d21 d22 d23 PP
Hsc70
73 kDa
Calponin
34 kDa

B

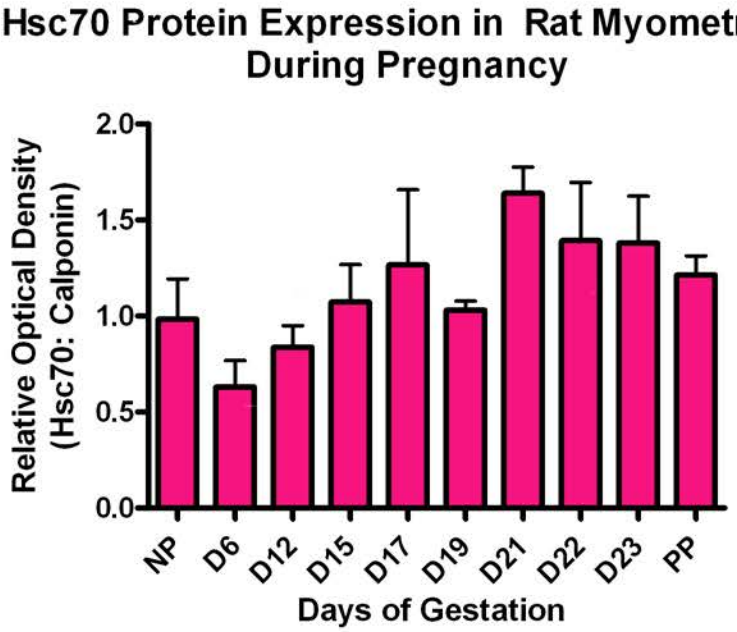
Hsc70 Protein Expression in Rat Myometrium During Pregnancy
Relative Optical Density (Hsc70: Calponin)
2.0
1.5
1.0
0.5
0.0
NP
D6
D12
D15
D17
D19
D21
D22
D23
PP
Days of Gestation

bands were detected at their predicted molecular weights, 39 kDa and 34 kDa respectively (Figure 3.3.10). Following immunoblot and densitometric analysis, one-way ANOVA revealed that CHIP protein expression did not change significantly throughout gestation ($p > 0.05$; n=4/day); CHIP protein was constitutively expressed throughout pregnancy.

3.3.6 *Expression of LC3II Protein*

Thus far, the only known protein found on autophagosomes is LC3II and as a result, it is widely used as a marker for autophagosomes and the process of macroautophagy [218]. As a means to assess autophagosome accumulation, immunoblot analysis was performed to characterize LC3II protein expression in non-pregnant and pregnant rat myometrium throughout gestation. Immunoblot analysis was carried out with a LC3II specific antibody throughout gestation (Table 2.1). LC3II and calponin protein bands were detected at their predicted molecular weights, 16 kDa and 34 kDa respectively (Figure 3.3.11). Following immunoblot and densitometric analysis, one-way ANOVA revealed that LC3II protein expression changed significantly over gestation. LC3II protein expression was significantly elevated at PP compared to expression at NP, d6 and d12 ($p<0.05$; n=4/day).

3.3.7 *Expression of Pser51-eIF2α Protein*

Carra et al. (2009) suggest that HspB8 and Bag3 induce phosphorylation of the α-subunit of the translation initiator factor eIF2 in HEK-293 cells which ultimately results

Figure 3.3.10 Immunoblot analysis of CHIP protein expression in pregnant rat myometrium. **(A)** Representative immunoblots of CHIP protein and calponin are shown. **(B)** The relative expression of CHIP was analyzed using densitometric analysis. The data were presented as the mean ± SEM of the relative optical density of CHIP normalized to the optical density of calponin. Values are from four independent experiments. One-way ANOVA revealed that CHIP expression did not change significantly throughout gestation ($p > 0.05$; n=4/day). CHIP protein is constitutively expressed throughout gestation. Days 6, 12, 15, 17, 19, 21, 22, and 23 represent gestational time points. NP, non-pregnant; PP, 1 day postpartum.

A

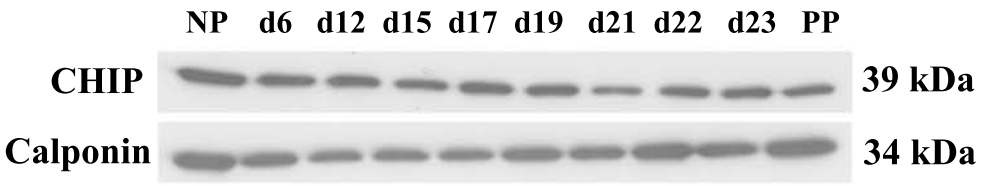
NP d6 d12 d15 d17 d19 d21 d22 d23 PP
CHIP
39 kDa
Calponin
34 kDa

B

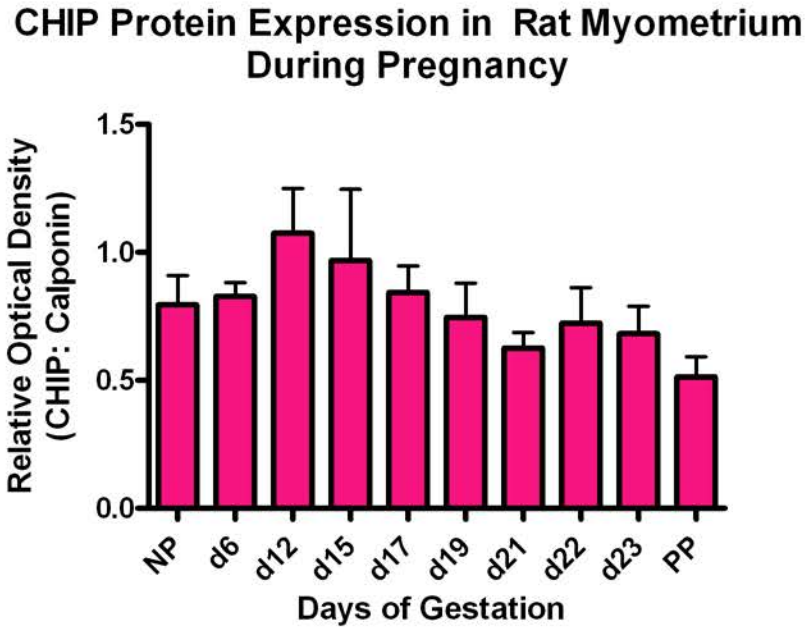
CHIP Protein Expression in Rat Myometrium During Pregnancy
Relative Optical Density (CHIP: Calponin)
1.5
1.0
0.5
0.0
NP
d6
d12
d15
d17
d19
d21
d22
d23
PP
Days of Gestation

Figure 3.3.11 Immunoblot analysis of LC3II protein expression in pregnant rat myometrium. **(A)** Representative immunoblots of LC3II protein and calponin are shown. **(B)** The relative expression of LC3II was analyzed using densitometric analysis. The data were presented as the mean ± SEM of the relative optical density of LC3II normalized to the optical density of calponin. Values are from four independent experiments. One-way ANOVA revealed that LC3II protein expression changed significantly overall. LC3II protein expression was significantly elevated at PP compared to expression at NP, d6 and d12 (*, $p< 0.05$; Newman-Keuls, post-hoc test; n=4/day). Days 6, 12, 15, 17, 19, 21, 22, and 23 represent gestational time points. NP, non-pregnant; PP, 1 day postpartum.

A

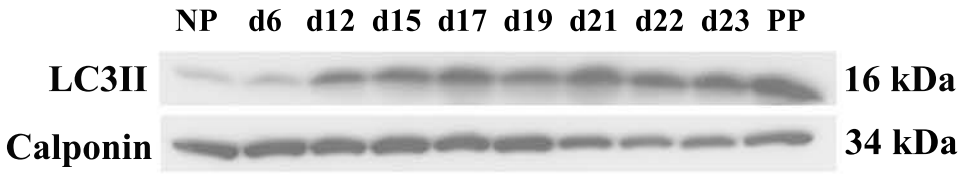
NP d6 d12 d15 d17 d19 d21 d22 d23 PP
LC3II
16 kDa
Calponin
34 kDa

B


LC3II Protein Expression in Rat Myometrium During Pregnancy
Relative Optical Density (LC3II: Calponin)
0
1
2
3
4
*
NP
D6
D12
D15
D17
D19
D21
D22
D23
PP
Days of Gestation

in translational shut-down and activation of the macroautophagy process [186]. To begin assessing whether HspB8 and Bag3 could be inducing phosphorylation of the α-subunit of eIF2 in a temporal-specific manner within the myometrium, immunoblot analysis was performed to characterize Pser51-eIF2α protein expression in non-pregnant and pregnant rat myometrium throughout gestation. Immunoblot analysis was carried out with a Pser51-eIF2α specific antibody throughout gestation (Table 2.1). Pser51-eIF2α and calponin proteins were detected at their predicted molecular weights, 36 kDa and 34 kDa respectively (Figure 3.3.12). Following immunoblot and densitometric analysis, one-way ANOVA revealed that Pser51-eIF2α protein expression did not change significantly throughout gestation ($p > 0.05$; n=4/day). Pser51-eIF2α protein was constitutively expressed throughout pregnancy and post-partum.

3.4 The Effect of Uterine Distension on HspB8 Expression: Unilateral Pregnancy Model

3.4.1 *Expression of HspB8 Protein*

As immunoblot analysis demonstrated an increase in HspB8 protein expression at d15, d17 and d19 of gestation, a period of stretch-induced hypertrophy, the role of uterine distension on regulating HspB8 protein expression was assessed using a unilateral pregnancy model [14]. Immunoblot analysis was performed using protein lysates from the stretched (gravid) and non-stretched (non-gravid) uterine horns at d15, d19 and d23 and an HspB8 specific antibody (Table 2.1). There were no statistically significant

Figure 3.3.12 Immunoblot analysis of Pser51-eIF2α protein expression in pregnant rat myometrium. **(A)** Representative immunoblots of Pser51-eIF2α protein and calponin are shown. **(B)** The relative expression of Pser51-eIF2α was analyzed using densitometric analysis. The data were presented as the mean ± SEM of the relative optical density of Pser51-eIF2α normalized to the optical density of calponin. Values are from four independent experiments. One-way ANOVA revealed that Pser51-eIF2α expression did not change significantly overall ($p > 0.05$; n=4/day). Pser51-eIF2α protein is constitutively expressed throughout gestation. Days 6, 12, 15, 17, 19, 21, 22, and 23 represent gestational time points. NP, non-pregnant; PP, 1 day postpartum.

A

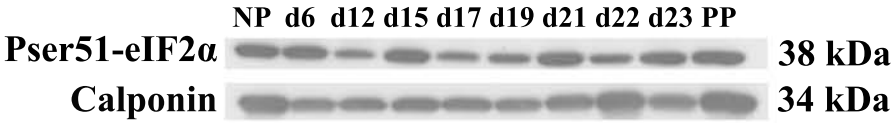
NP d6 d12 d15 d17 d19 d21 d22 d23 PP
Pser51-eIF2α
38 kDa
Calponin
34 kDa

B

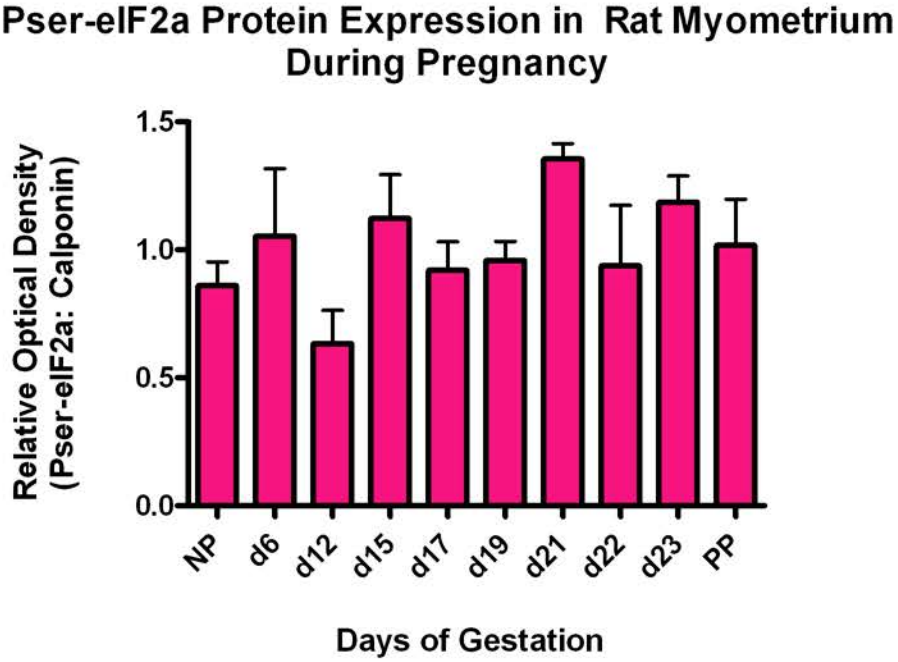
Pser-eIF2a Protein Expression in Rat Myometrium During Pregnancy
Relative Optical Density (Pser-eIF2a: Calponin)
1.5
1.0
0.5
0.0
NP
d6
d12
d15
d17
d19
d21
d22
d23
PP
Days of Gestation

changes in the level of detection of HspB8 protein between the non-gravid and gravid samples at any of the time points examined (Figure 3.4.1).

3.4.2 *Immunofluorescence Detection of HspB8 Protein*

To determine if the spatial localization of HspB8 protein changed due to uterine stretch, immunofluorescence detection was performed. Detection of HspB8 protein in the circular and longitudinal muscle layers at d19 and d23 of gestation demonstrated that HspB8 protein was primarily localized to the cytoplasm of myometrial cells and that there was an absence of nuclear staining in both the non-gravid and gravid uterine samples (Figure 3.4.2- 3.4.3). In addition, there were no marked differences in the level of detection of HspB8 protein between the non-gravid and gravid samples at the two time points analyzed.

3.5 The Effect of Progesterone on HspB8 Expression

3.5.1 *Progesterone-induced Delayed Labour: Expression of HspB8 Protein*

As HspB8 protein expression was elevated during this d15-d19 window of gestation compared to earlier time points (Figure 3.1.1), it was hypothesized that the observed pattern of HspB8 expression was under the influence of progesterone. Thus, administration of exogenous progesterone may further induce HspB8 protein expression.

Figure 3.4.1 HspB8 protein expression is not influenced by uterine stretch. Representative immunoblots of HspB8 protein and calponin detection are shown for three gestational time points, d15 **(A)**, d19 **(B)** and d23 **(C)**. Analysis was performed using a HspB8 specific antibody (Cell Signaling). Densitometric analysis revealed that there were no statistically significant differences in HspB8 protein expression between the non-gravid and gravid samples at the time points examined (paired t-test; $p > 0.05$). Values are from 4 independent experiments (n=4/day) ± SEM.

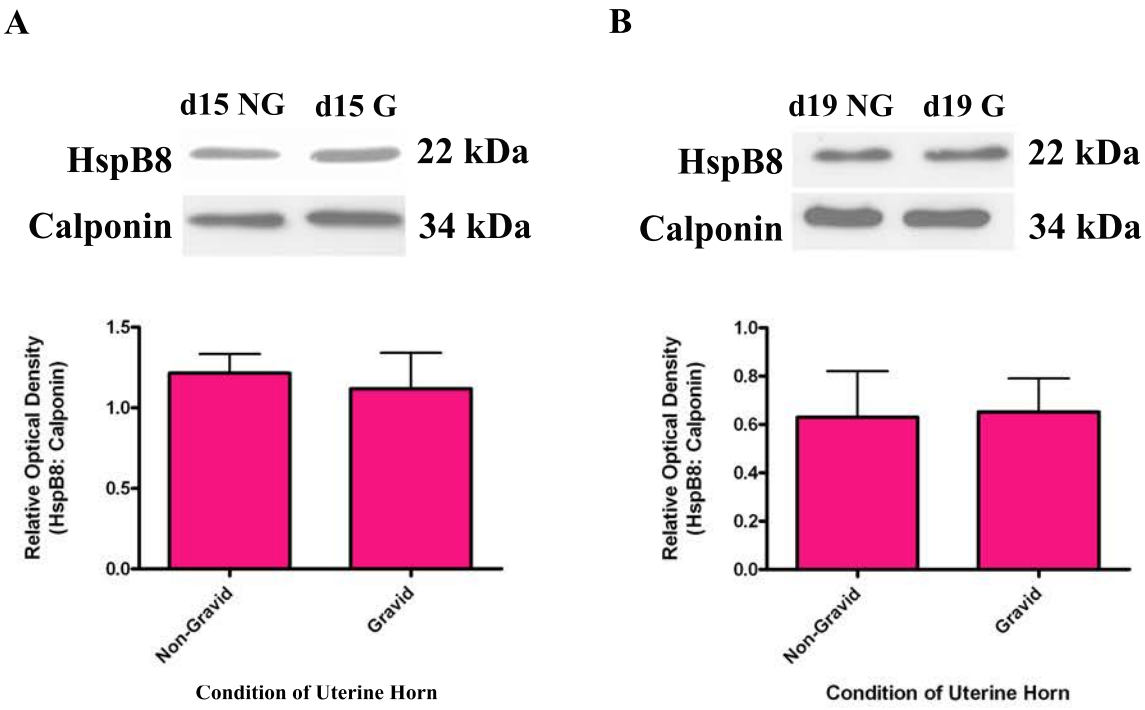
A
d15 NG
d15 G
HspB8
22 kDa
Calponin
34 kDa
Relative Optical Density (HspB8: Calponin)
1.5
1.0
0.5
0.0
Non-Gravid
Gravid
Condition of Uterine Horn
B
d19 NG
d19 G
HspB8
22 kDa
Calponin
34 kDa
Relative Optical Density (HspB8: Calponin)
1.0
0.8
0.6
0.4
0.2
0.0
Non-Gravid
Gravid
Condition of Uterine Horn

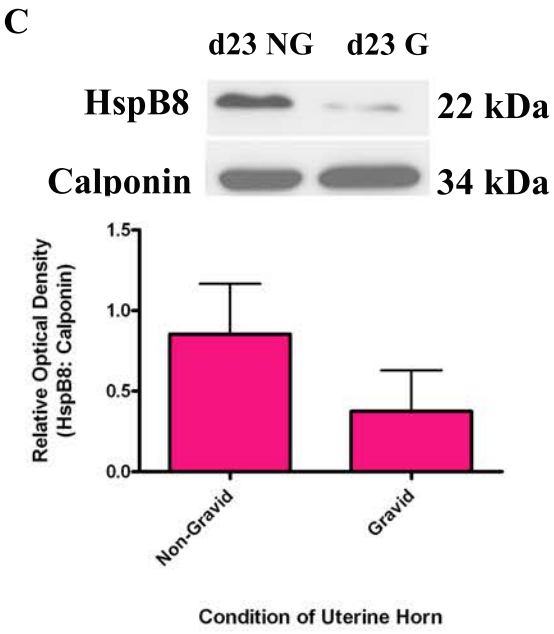
C
d23 NG
d23 G
HspB8
22 kDa
Calponin
34 kDa
Relative Optical Density (HspB8: Calponin)
1.5
1.0
0.5
0.0
Non-Gravid
Gravid
Condition of Uterine Horn

Figure 3.4.2 Immunofluorescence detection of HspB8 protein in the circular muscle layer of rat myometrium in gravid (G) and non-gravid (NG) uterine horns. Sections were probed with a HspB8 specific antibody (LifeSpan BioSciences). Two representative time points of pregnancy are shown, d19 and d23. The images demonstrate cytoplasmic localization of the protein in myometrial cells; however, there was no visible marked change in the level of detection of HspB8 protein between the non-gravid and gravid samples at either time point (n=2/day). Ctrl = control, rabbit IgG. Scale bar = 50 μm.

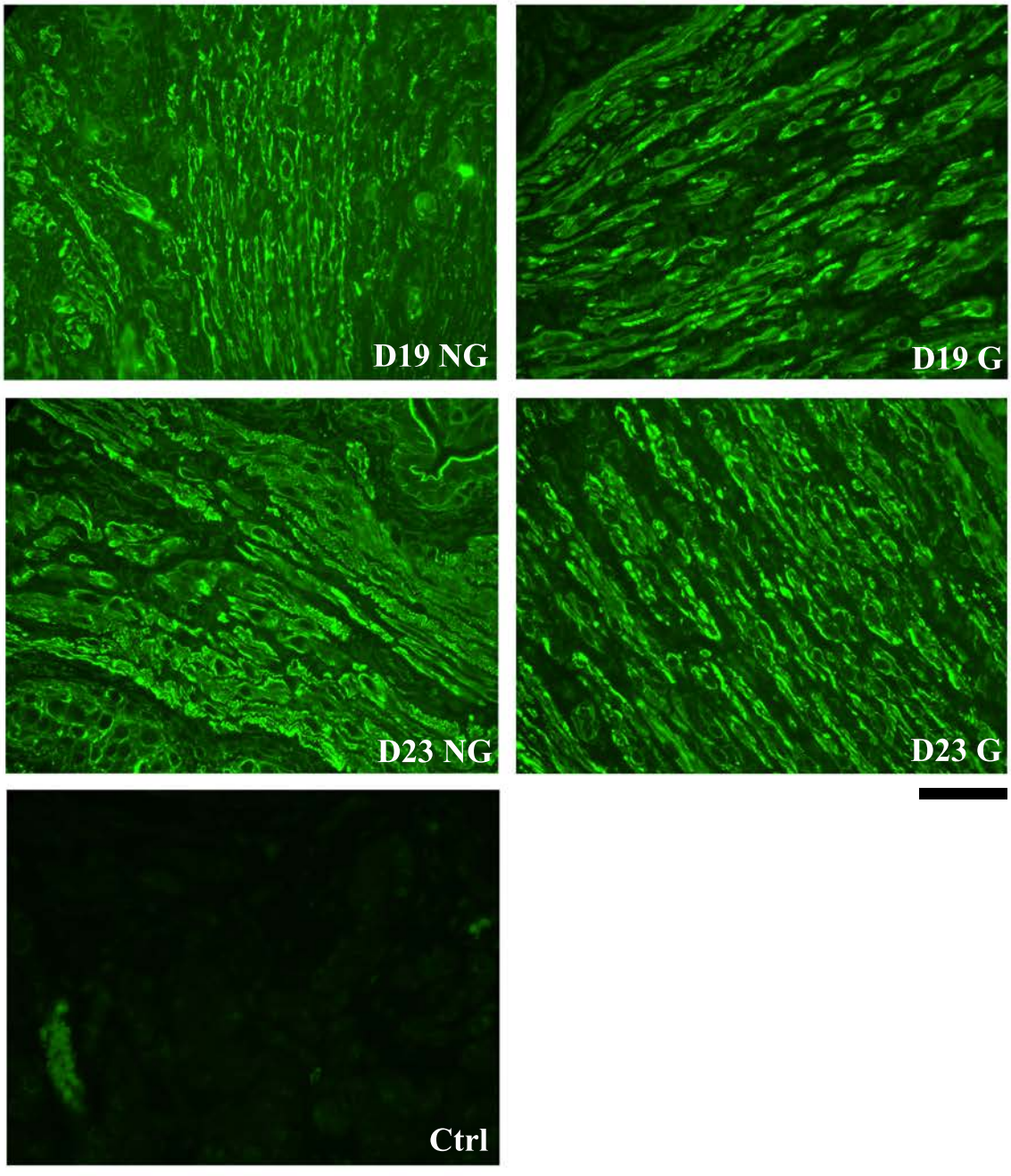
D19 NG
D19 G
D23 NG
D23 G
Ctrl

Figure 3.4.3 Immunofluorescence detection of HspB8 protein in the longitudinal muscle layer of rat myometrium in gravid (G) and non-gravid (NG) uterine horns. Sections were probed with a HspB8 specific antibody (LifeSpan BioSciences). Two representative time points of pregnancy are shown, d19 and d23. The images demonstrate cytoplasmic localization of the protein in myometrial cells; however, there was no visible marked change in the level of detection of HspB8 between the non-gravid and gravid samples at either time point (n=2/day). Ctrl = control, rabbit IgG. Scale bar = 50 μm.

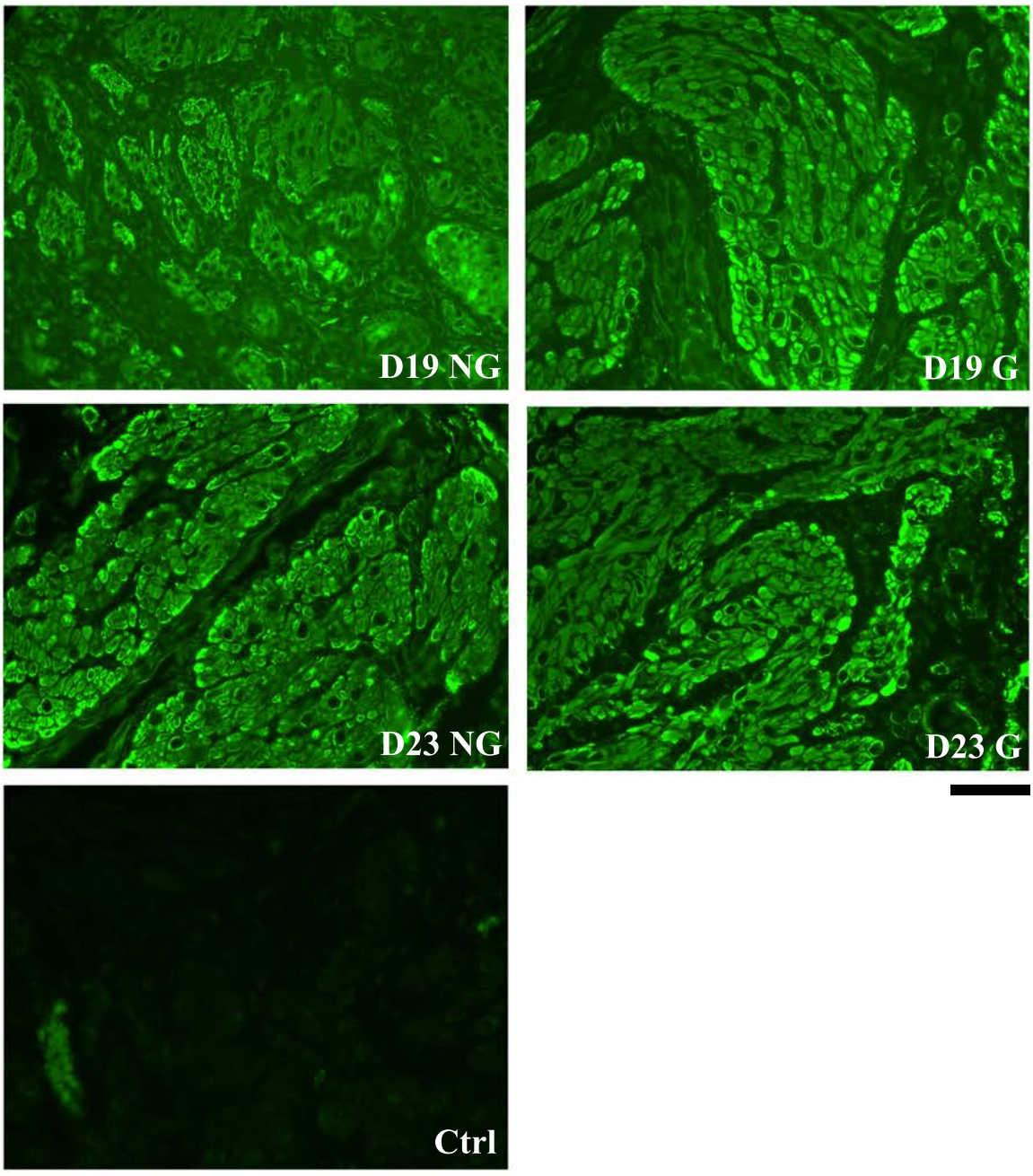
D19 NG
D19 G
D23 NG
D23 G
Ctrl

Animals were administered progesterone beginning on d20 of gestation and did not go into labour on d23 of gestation. Immunoblot analysis of HspB8 protein expression in myometrial tissue collected from vehicle and progesterone-treated rats indicated that progesterone administration significantly affected HspB8 protein expression ($p<0.05$; n=4/day; Table 2.1; Figure 3.5.1A). HspB8 and calponin protein bands were detected at their predicted molecular weights, 22 kDa and 34 kDa respectively. Densitometric analysis of immunoblot data and two-way ANOVA indicated that HspB8 protein expression at d23 in rats administered progesterone was significantly lower compared to expression in rats at d23 administered vehicle. Immunoblot analysis of the two treatment groups was also performed using another commercially available antibody (Cell Signaling) to further confirm the results ($p<0.05$; n=4/day; Table 2.1; Figure 3.5.1C). Overall, immunoblot analysis indicated that progesterone might have an inhibitory effect on HspB8 protein expression.

3.5.2 *RU486-induced Progesterone Withdrawal: Expression of HspB8 Protein*

Upon administration of the progesterone receptor antagonist RU486 to pregnant rats on d18 of gestation, preterm labour is induced within 24 h. Immunoblot analysis of HspB8 protein expression in myometrial tissue collected from vehicle and RU486-treated rats indicated that a functional progesterone withdrawal significantly affected HspB8 protein expression ($p<0.05$; n=4/day; Figure 3.5.2). HspB8 protein expression was significantly increased following administration of RU486. This result further suggests that progesterone may negatively regulate HspB8 gene expression.

Figure 3.5.1 Immunoblot analysis of HspB8 protein expression in a delayed-labour model following administration of progesterone (P4) or corn oil (O; vehicle control) to pregnant rats. **(A)** Representative immunoblots of HspB8 protein and calponin are shown. Analysis was performed using a HspB8 specific antibody (LifeSpan BioSciences). **(B)** The relative protein expression of HspB8 was analyzed using densitometric analysis. The data were presented as the mean ± SEM of the relative optical density of HspB8 normalized to the optical density of calponin. Values are from four independent experiments. Two-way ANOVA revealed that HspB8 protein expression changed significantly between the two treatment groups ($p < 0.05$; n=4/day). All data indicated with symbols are significantly different (paired t-test; $p < 0.05$). HspB8 protein expression at d23-P4 was significantly lower compared to expression at d23-O (*, $p < 0.05$). O, oil; P4, progesterone. Designations 21-O, 22-O, 23-O, 21-P4, 22-P4, 23-P4 represent gestational time points in the two treatment groups. **(C)** Representative immunoblots of HspB8 protein and calponin are shown. Analysis was performed using a HspB8 specific antibody (Cell Signaling). Results further confirm those received using the other commercially available antibody from LifeSpan BioSciences.

A

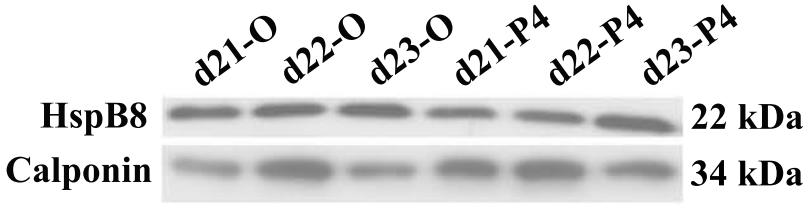
d21-O
d22-O
d23-O
d21-P4
d22-P4
d23-P4
HspB8
22 kDa
Calponin
34 kDa

B


HspB8 Expression in Rat Myometrium
in a Delayed-Labour Model
Relative Optical Density
(HspB8: Calponin)
2.0
1.5
1.0
0.5
0.0
*
d21-O
d22-O
d23-O
d21-P4
d22-P4
d23-P4
Days of Gestation

C

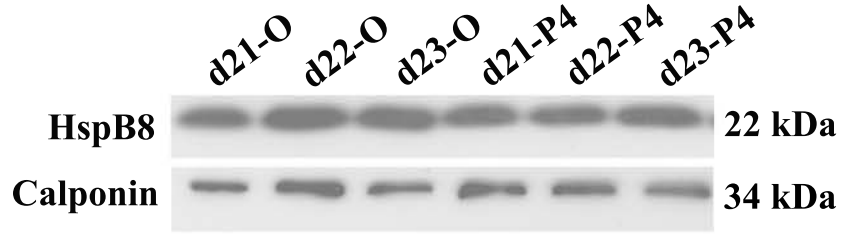
d21-O
d22-O
d23-O
d21-P4
d22-P4
d23-P4
HspB8
22 kDa
Calponin
34 kDa

Figure 3.5.2 Immunoblot analysis of HspB8 protein expression in rat myometrium in a preterm labour model, following administration of RU486 or corn oil (vehicle control) to pregnant rats. Treatment was administered on d18 and samples were collected on d19 of gestation. **(A)** Representative immunoblots of HspB8 protein and calponin are shown. **(B)** The relative expression of HspB8 was analyzed using densitometric analysis. The data were presented as the mean ± SEM of the relative optical density of HspB8 normalized to the optical density of calponin. Values are from four independent experiments. Paired t-test revealed that HspB8 protein expression changed significantly overall (*, $p < 0.05$; n=4/day). O, Oil (vehicle control); T, RU486.

A

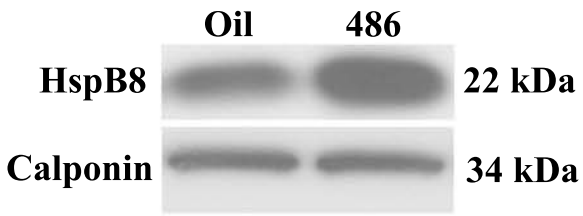

B

HspB8 Expression in Rat Myometrium Following RU-486-Induced Progesterone Withdrawal

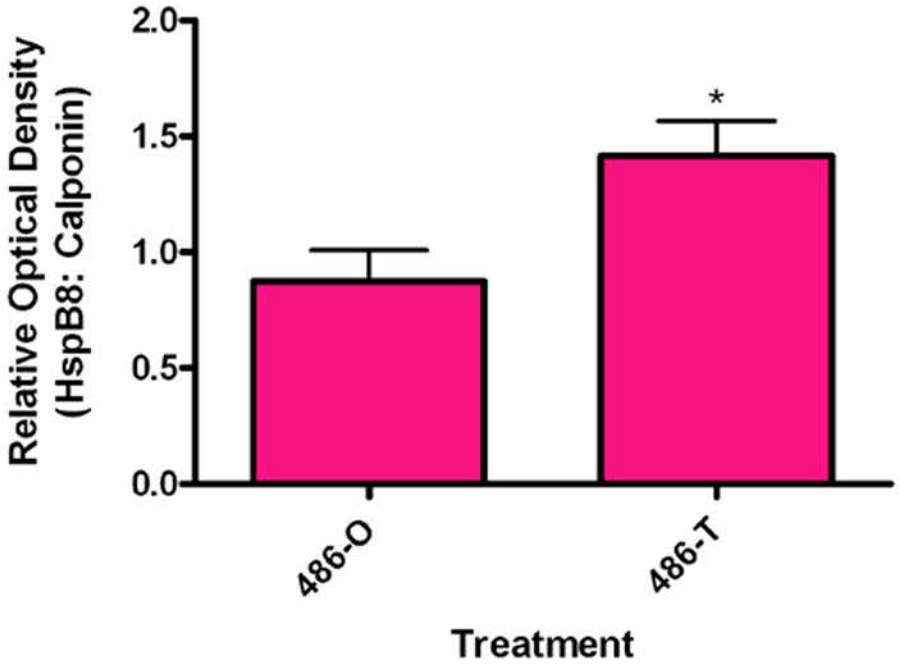

3.5.3 *Immunofluorescence Detection of HspB8 Protein*

To determine if the spatial localization of HspB8 protein changed due to RU486 administration, immunofluorescence detection was conducted. Detection of HspB8 protein in the circular and longitudinal muscle layers demonstrated that HspB8 was primarily localized to the cytoplasm of myometrial cells and that there was an absence of nuclear staining in both treatment groups (RU486 or vehicle alone) (Figure 3.5.3). There was a notable decrease in HspB8 protein in the circular muscle layer of rat myometrium following RU486 administration; however, there was an apparent small increase in the level of HspB8 protein in the longitudinal muscle layer following RU486 administration (n=2/day). This indicates that there may be myometrial layer-specific up-regulation of HspB8 protein expression as a result of functional progesterone withdrawal.

3.5.4 *Expression of Bag3 Protein*

RU486 treated rat myometrial samples were also used to study the effects of progesterone on Bag3 protein expression. Immunoblot analysis of Bag3 protein expression in myometrial tissue collected from vehicle and RU486-treated rats indicated that a functional progesterone withdrawal did not significantly affect Bag3 protein expression ($p>0.05$; n=4/day; Figure 3.5.4). This result suggests that progesterone is not a major regulator of Bag3 protein expression.

Figure 3.5.3 Immunofluorescence detection of HspB8 protein in the longitudinal and circular muscle layers of rat myometrium, using a HspB8 specific antibody (LifeSpan BioSciences), following treatment of pregnant rats with RU486 (486) or corn oil (vehicle control). Treatment was administered on d18 and samples were collected on d19 of gestation. The images demonstrate mainly cytoplasmic localization of HspB8 protein and an absence of nuclear staining. There was a notable decrease in HspB8 protein in the circular muscle layer and an apparent small increase in HspB8 protein in the longitudinal muscle layer, following RU486 administration (n=2/day). Ctrl = control, rabbit IgG. Scale bar = 50 μm.

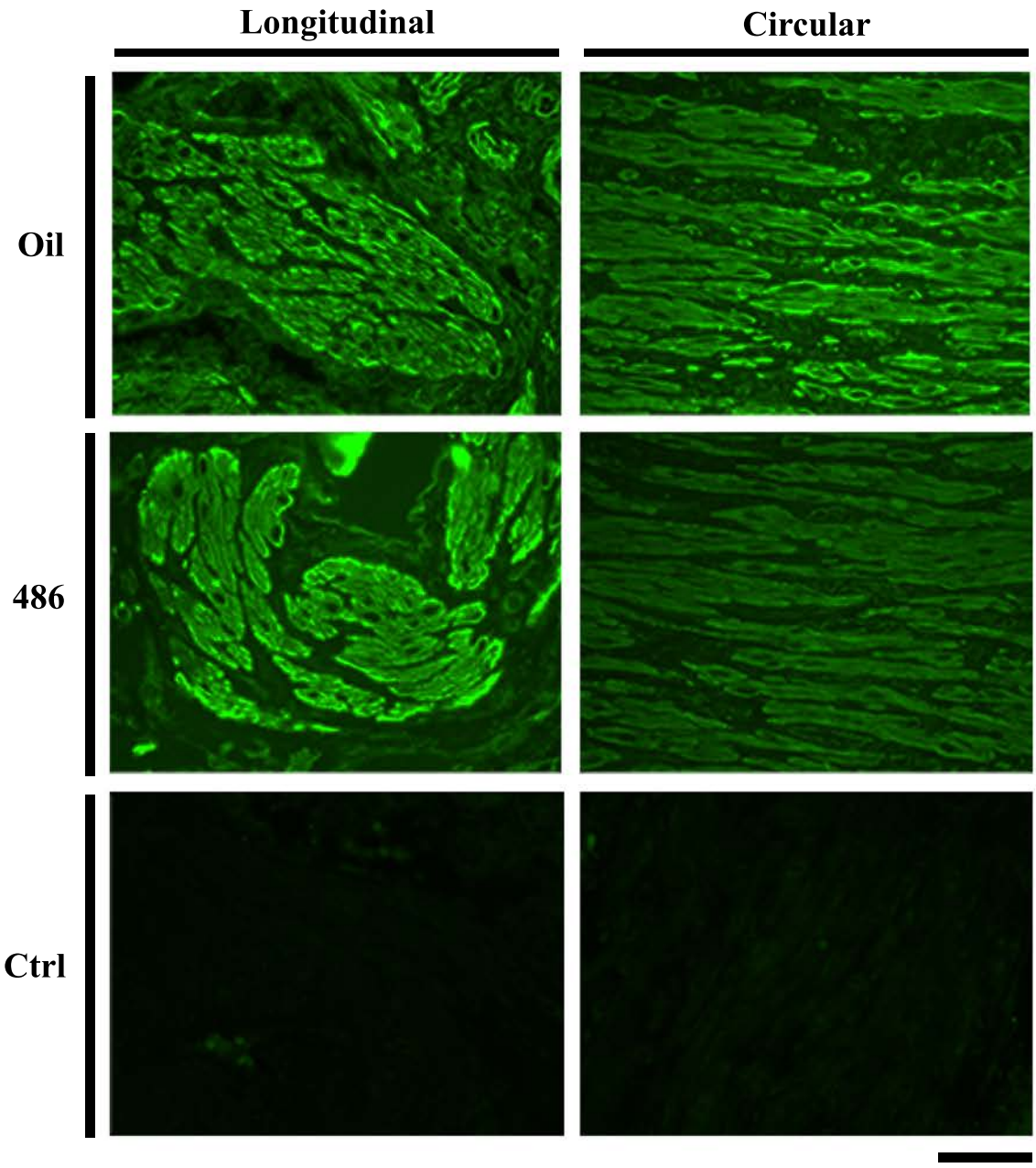
Longitudinal
Circular
Oil
486
Ctrl

Figure 3.5.4 Immunoblot analysis of Bag3 protein in the rat myometrium in a preterm labour model, following administration of RU486 or corn oil (vehicle control) to pregnant rats. Treatment was administered on d18 and samples were collected on d19 of gestation. **(A)** Representative immunoblots of Bag3 protein and calponin are shown. **(B)** The relative expression of Bag3 was analyzed using densitometric analysis. The data were presented as the mean ± SEM of the relative optical density of Bag3 normalized to the optical density of calponin. Values are from four independent experiments. Paired t-test revealed that Bag3 protein expression did not change significantly overall ($p > 0.05$; n=4/day). O, Oil (vehicle control); T, RU486.

A

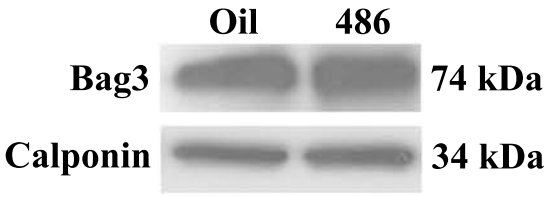
Oil
486
Bag3
74 kDa
Calponin
34 kDa

B

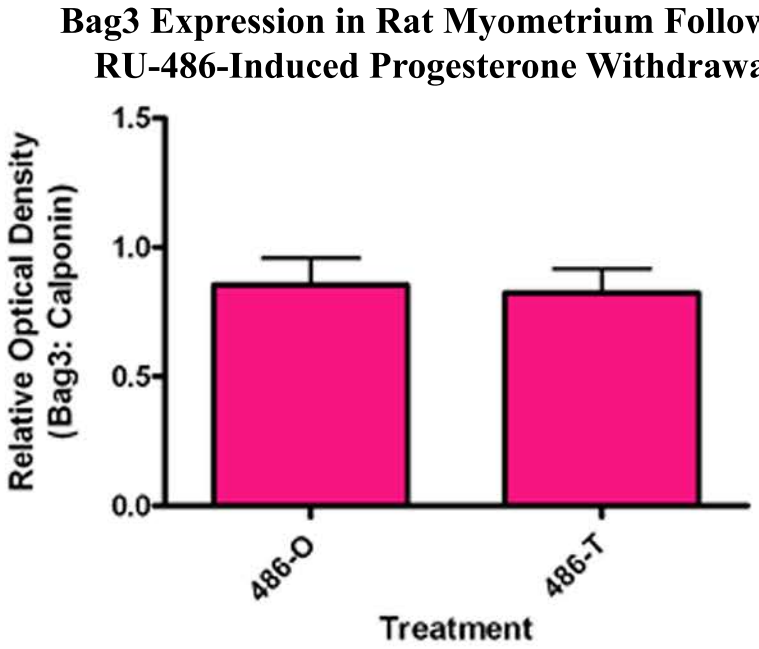
Bag3 Expression in Rat Myometrium Following
RU-486-Induced Progesterone Withdrawal
Relative Optical Density
(Bag3: Calponin)
1.5
1.0
0.5
0.0
486-O
486-T
Treatment

3.5.5 *Expression of LC3II Protein*

RU486 treated myometrial samples were also used to study the effects of progesterone on LC3II protein expression. Immunoblot analysis of LC3II protein expression in myometrial tissue collected from vehicle and RU486-treated rats indicated that a functional progesterone withdrawal results in a small, but statistically significant increase in LC3II protein expression ($p>0.05$; n=4/day; Figure 3.5.5).

3.6 Exogenous Expression of HspB8 in hTERT-HM Cells

3.6.1 *Optimization of Transfection Efficiency of hTERT-HM Cells*

Experiments were conducted in triplicate to optimize the transfection efficiency of hTERT-HM cells with expression vectors using an Amaxa Nucleofector system. pEGFP-C3 expression vector was transiently transfected into hTERT-HM cells using Amaxa basic nucleofector kit for primary smooth muscle cells (Lonza). Transfection of the cells was conducted using the programs A-033, D-033, P-013, P-042, U-025, B-017 or no program (control). Optimization of transfection was repeated with a focus on Lonza nucleofector programs A-033 and U-025 as they had the highest transfection efficiency and the least amount of cell loss in the initial experiment. Consultation with the company Lonza also resulted in the testing of the program B-017 (Figure 3.6.1- 3.6.2). The results indicated that Program A-033 had the highest transfection efficiency and the least amount of cell loss for hTERT-HM cells. Thus, Program A-033 was utilized for all further transfection experiments.

Figure 3.5.5 Immunoblot analysis of LC3II protein expression in rat myometrium in a preterm labour model, following administration of RU486 or corn oil (vehicle control) to pregnant rats. Treatment was administered on d18 and samples were collected on d19 of gestation. **(A)** Representative immunoblots of LC3II protein and calponin are shown. **(B)** The relative expression of LC3II was analyzed using densitometric analysis. The data were presented as the mean ± SEM of the relative optical density of LC3II normalized to the optical density of calponin. Values are from four independent experiments (n=4/day). Paired t-test revealed that LC3II protein expression changed significantly overall (*, $p < 0.05$). O, Oil (vehicle control); T, RU486.

A

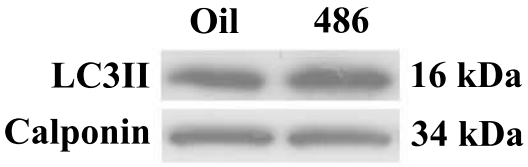
Oil
486
LC3II
16 kDa
Calponin
34 kDa

B

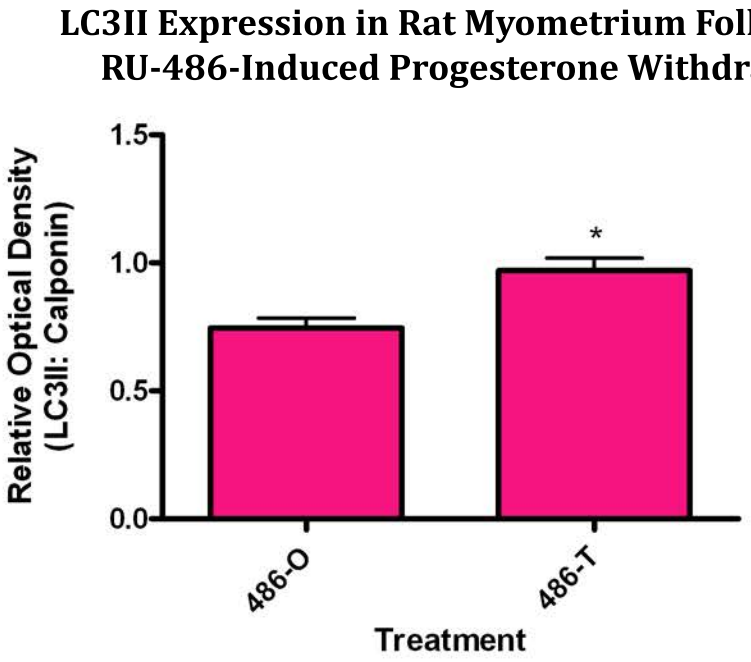
LC3II Expression in Rat Myometrium Following RU-486-Induced Progesterone Withdrawal
Relative Optical Density (LC3II: Calponin)
1.5
1.0
0.5
0.0
*
486-O
486-T
Treatment

Figure 3.6.1 Micrographs of hTERT-HM cells 24 h post-transfection with programs A-033, U-025 and B-017. Images on the left represent phase contrast micrographs 24 h after transfection while immunofluorescence micrographs on the right demonstrate the same cells that have been transiently transfected with pEGFP-C3 expression vector. Scale bar = 100 μm.

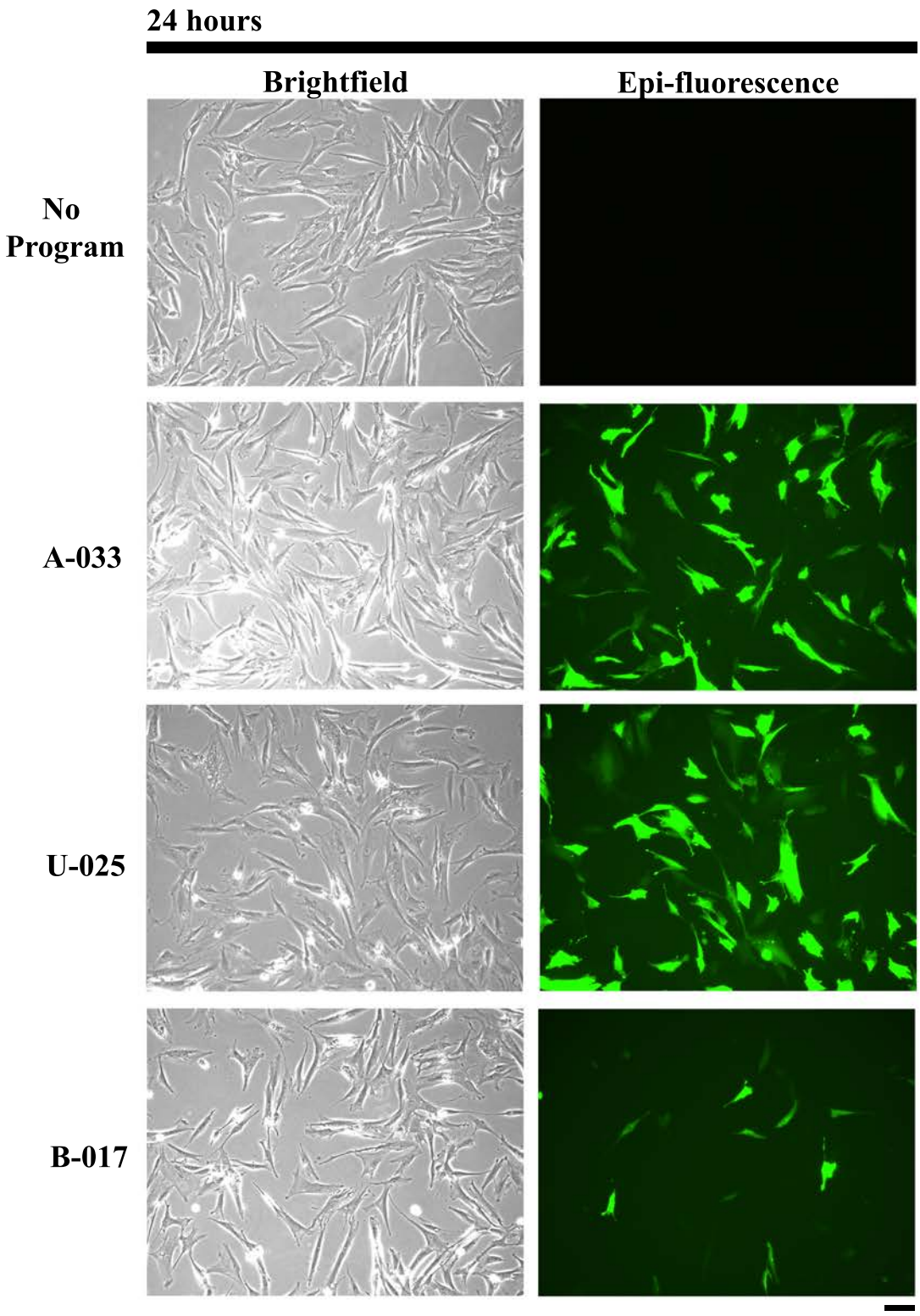
24 hours
Brightfield
Epi-fluorescence
No Program
A-033
U-025
B-017

Figure 3.6.2 Micrographs of hTERT-HM cells 48 h post-transfection with programs A-033, U-025 and B-017. Images on the left represent phase contrast micrographs 48 h after transfection while immunofluorescence micrographs on the right indicate cells that have been transiently transfected with pEGFP-C3 expression vector 48 h after transfection. Scale bar = 100 μm.

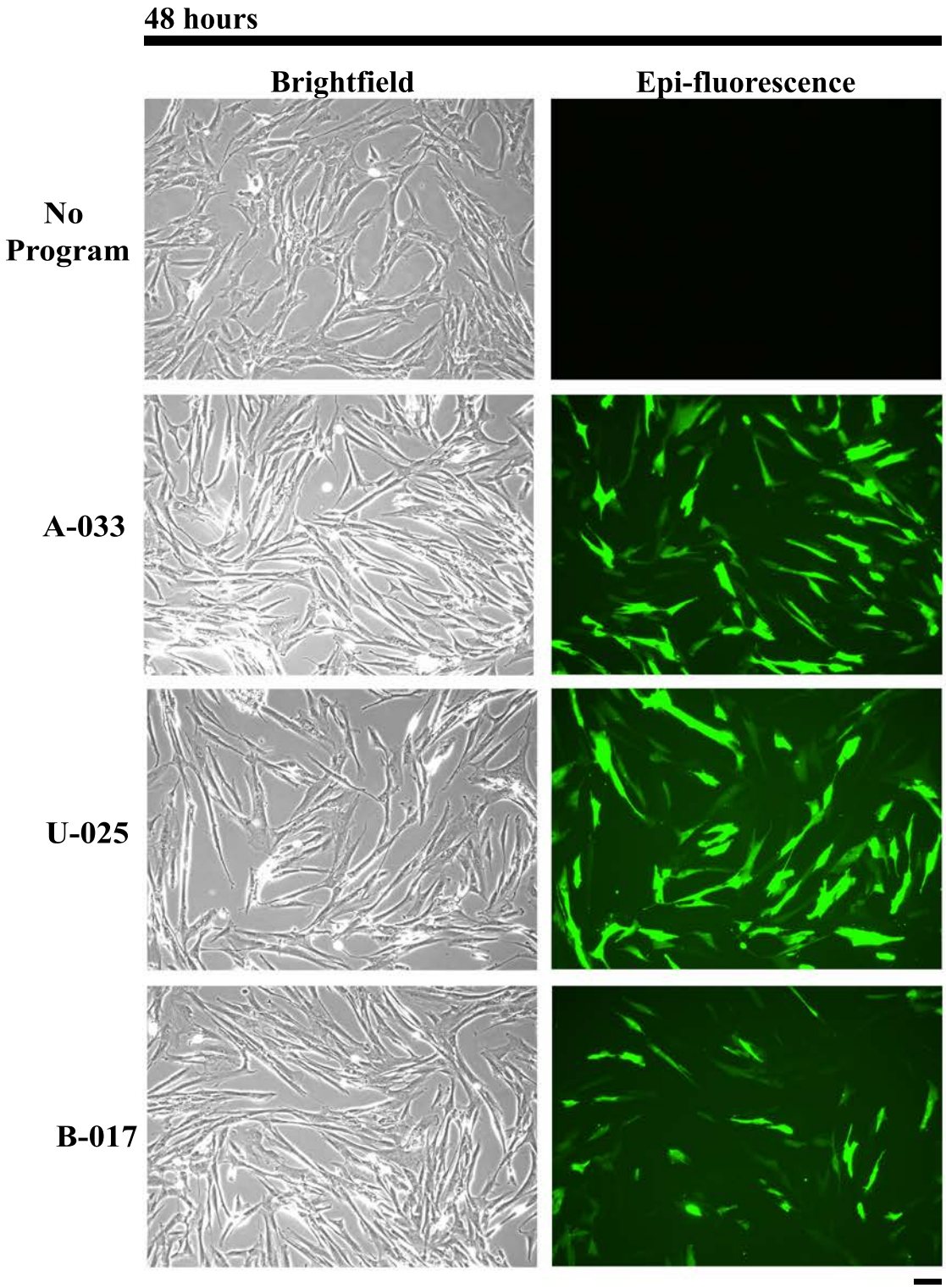
48 hours
Brightfield
Epi-fluorescence
No Program
A-033
U-025
B-017

3.6.2 *Transfection of hTERT-HM Cells with pCImycHspB8 Vector*

Initially hTERT-HM cells were transiently transfected with pEGFP-C3 expression vector or co-transfected with pCImycHspB8 and pEGFP-C3 expression vectors. hTERT-HM cells that were not transfected (No Program) served as a negative control. Seventy two hours post-transfection of hTERT-HM cells with pCImycHspB8 expression vector, protein lysates were collected and immunoblot analysis was performed using a myc-tag specific antibody (Table 2.1). Immunoblot analysis demonstrated that myc-tagged HspB8 protein was present at ~25 kDa (Figure 3.6.3A). Subsequently, immunoblot analysis was performed using an HspB8 specific antibody (Table 2.1). A band was detected at ~22 kDa, representing endogenous expression of HspB8 protein, and at ~25 kDa representing myc-tagged HspB8 protein (Figure 3.6.3B).

3.6.3 *Transfection of hTERT-HM Cells with pCImycBag3 Vector*

Initially hTERT-HM cells were transiently transfected with pEGFP-C3 expression vector or co-transfected with pCImycBag3 and pEGFP-C3 expression vectors. hTERT-HM cells that were not transfected (No Program) served as a negative control. Following transfection of hTERT-HM cells with pCImycBag3 expression vector, protein lysates were collected and immunoblot analysis was performed using a myc-tag specific antibody (Table 2.1). Immunoblot analysis demonstrated that myc-tagged Bag3 protein was detected at the expected ~74 kDa demonstrating exogenous Bag3 expression (Figure 3.6.4A). Subsequently, immunoblot analysis was performed using a Bag3 specific

Figure 3.6.3(A) Immunoblot analysis of myc-HspB8 expression. Following transfection of hTERT-HM cells with pCImycHspB8 expression vector, protein lysates were collected and immunoblot analysis was performed using an a myc-tag specific antibody (Millipore). Lane 1 represents No program (cells were not transfected), Lane 2 represents cells that have been transiently transfected with pEGFP-C3 expression vector and Lane 3 represents cells that have been transiently transfected with pCImycHspB8 expression vector. Following immunoblot analysis a band is detected in lane 3 at ~25 kDa indicating the presence of myc-tagged HspB8, suggesting that the transfection was successful. (**B)** Following immunoblot analysis using a HspB8 specific antibody, a band is detected in lanes 1 2 and 3 at ~22 kDa, representing endogenous expression of HspB8 protein. In lane 3 a band is also detected at ~25 kDa representing myc-tagged HspB8 protein.

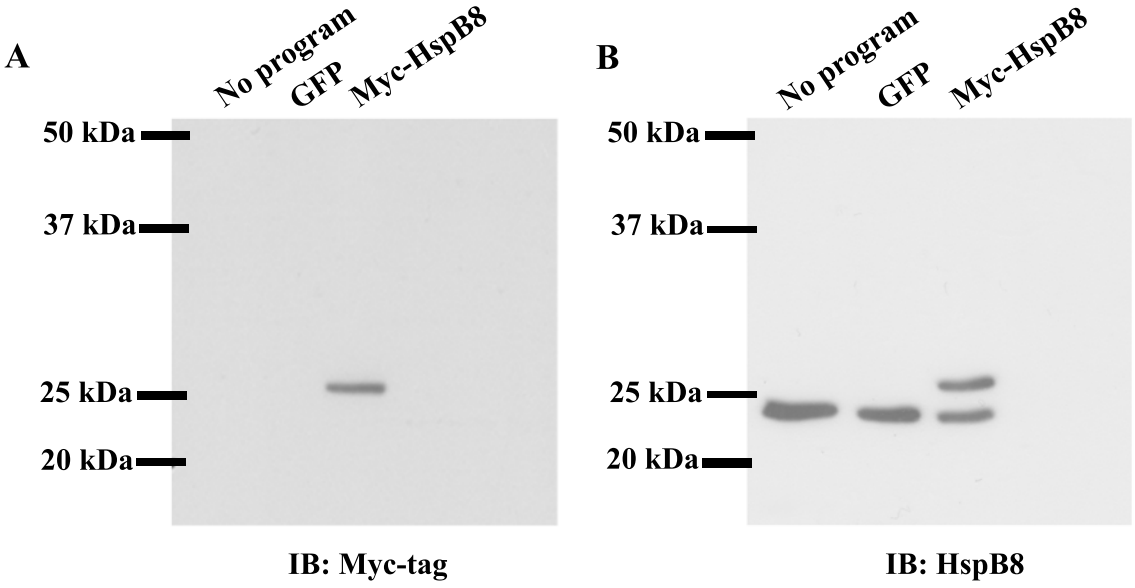
A
No program
GFP
Myc-HspB8
50 kDa
37 kDa
25 kDa
20 kDa
IB: Myc-tag
B
No program
GFP
Myc-HspB8
50 kDa
37 kDa
25 kDa
20 kDa
IB: HspB8

Figure 3.6.4 Immunoblot analysis of myc-Bag3 expression in hTERT-HM cells. Following transient transfection of hTERT-HM cells with pCImycBag3 expression vector, protein lysates were collected and immunoblot analysis was performed using a myc-tag specific antibody (Millipore). Lane 1 represents No program (cells were not transfected), Lane 2 represents cells that have been transiently transfected with pEGFP-C3 expression vector and Lane 3 represents cells that have been transiently transfected with pCImycBag3 expression vector. **(A)** Following immunoblot analysis a band is detected in lane 3 at ~74 kDa indicating the presence of myc-tagged Bag3 protein, suggesting that the transfection was successful. (**B)** Following immunoblot analysis, using a Bag3 specific antibody, a band is detected in lanes 1 2 at ~74 kDa, representing endogenous expression of Bag3 protein. In lane 3 a band is also detected at ~74 kDa, representing both endogenous expression of Bag3 protein and myc-tagged Bag3 protein.

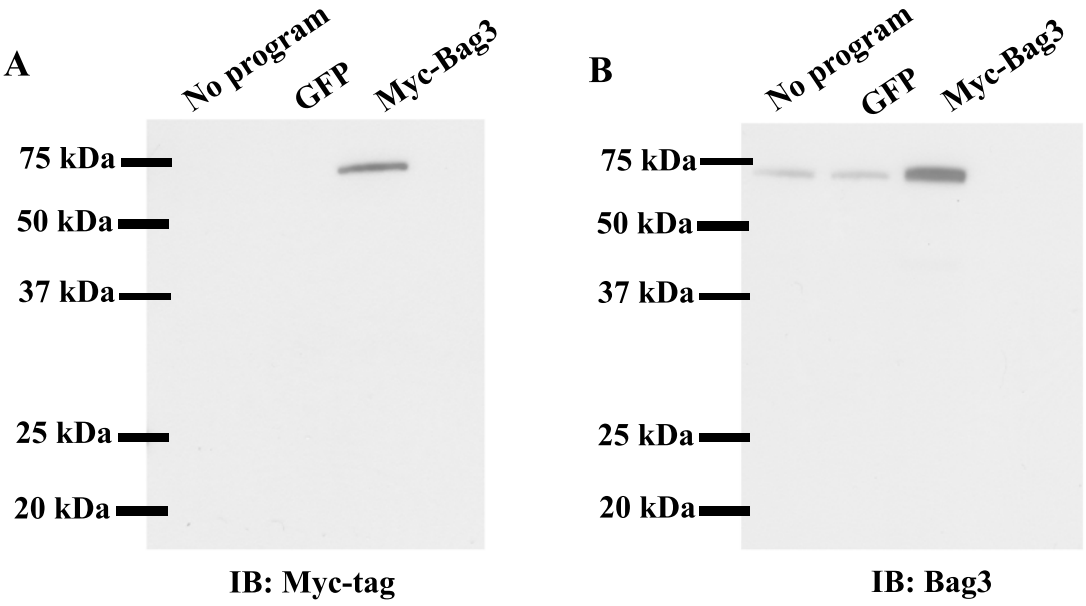
A
No program
GFP
Myc-Bag3
75 kDa
50 kDa
37 kDa
25 kDa
20 kDa
IB: Myc-tag
B
No program
GFP
Myc-Bag3
75 kDa
50 kDa
37 kDa
25 kDa
20 kDa
IB: Bag3

antibody (Table 2.1). A band was detected at ~74 kDa representing endogenous expression of Bag3 protein (Figure 3.6.4B).

3.6.4 *Transfection of hTERT-HM Cells with pCImycHspB8, pCImycBag3 and pEGFP-C3 Vectors*

Initially hTERT-HM cells were transiently transfected with pEGFP-C3 expression vector or co-transfected with pEGFP-C3, pCImycHspB8, and pCImycBag3 expression vectors. hTERT-HM cells that were not transfected (No Program) served as a negative control. Seventy-two hours following transfection of hTERT-HM cells with expression vectors, protein lysates were collected and immunoblot analyses were performed using myc-tag specific antisera (Table 2.1). Immunoblot analysis demonstrated that myc-tagged HspB8 protein and myc-tagged Bag3 protein were present as described in sections 3.6.4 and 3.6.5 (Figure 3.7.5A). Subsequently, immunoblot analysis was performed using an HspB8 specific antibody or a Bag3 specific antibody (Table 2.1). Appropriate proteins were detected (Figure 3.7.5 B, C) as described previously in sections 3.6.4 and 3.6.5.

3.6.5 *Protein/DNA ratios and Flow Cytometric Analysis of Transfected hTERT-HM Cells*

Protein/DNA ratios were calculated using an RNA/DNA/Protein Purification Kit. Following isolation of proteins and purification of genomic DNA no significant increase in the protein to DNA ratio was found to occur following transfection of hTERT-HM cells with expression vectors (Table 3.1). In order to further assess any exogenous protein-induced hypertrophy in hTERT-HM cells, flow cytometric analysis was

Figure 3.6.5 Immunoblot analysis of myc-HspB8 and myc- Bag3 in co-transfected hTERT-HM cells. Following transient transfection of hTERT-HM cells with pCImycHspB8, pCImycBag3 and pEGFP-C3 expression vectors, protein lysates were collected and immunoblot analysis was performed using a myc-tag specific antibody (Millipore). **(A)** Lane 1 represents No program (cells were not transfected), Lane 2 represents cells that have been transiently transfected with pEGFP-C3 expression vector and Lane 3 represents cells that have been transiently co-transfected with pCImycHspB8 and pCImycBag3 expression vectors. Following immunoblot analysis two bands are detected in lane 3 at ~75 kDa and ~25 kDa indicating the presence of myc-tagged Bag3 protein and myc-tagged HspB8 protein respectively, signifying that the transfection was successful. (**B)** Following immunoblot analysis, using a HspB8 specific antibody, a band is detected in lanes 1 2 and 3 at ~22 kDa, representing endogenous expression of HspB8 protein. In lane 3 a band is also detected at ~25 kDa, representing myc-tagged HspB8 protein. **(C)** Following immunoblot analysis, using a Bag3 specific antibody, a band is detected in lanes 1 2 at ~74 kDa, representing endogenous expression of Bag3 protein. In lane 3 a band is also detected at ~74 kDa, representing myc-tagged Bag3 protein.

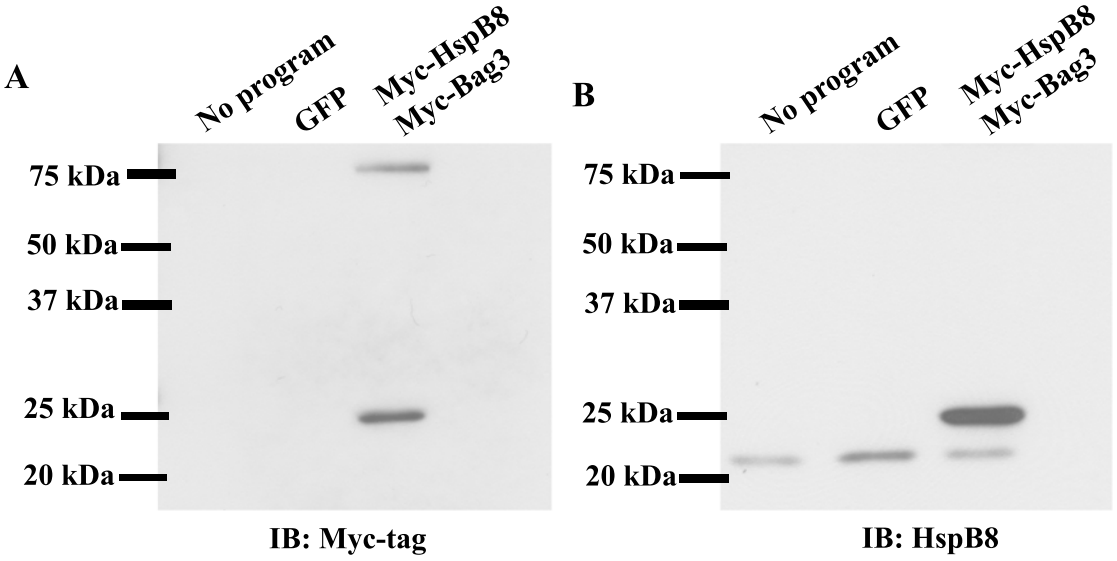
A
No program
GFP
Myc-HspB8
Myc-Bag3
75 kDa
50 kDa
37 kDa
25 kDa
20 kDa
IB: Myc-tag
B
No program
GFP
Myc-HspB8
Myc-Bag3
75 kDa
50 kDa
37 kDa
25 kDa
20 kDa
IB: HspB8

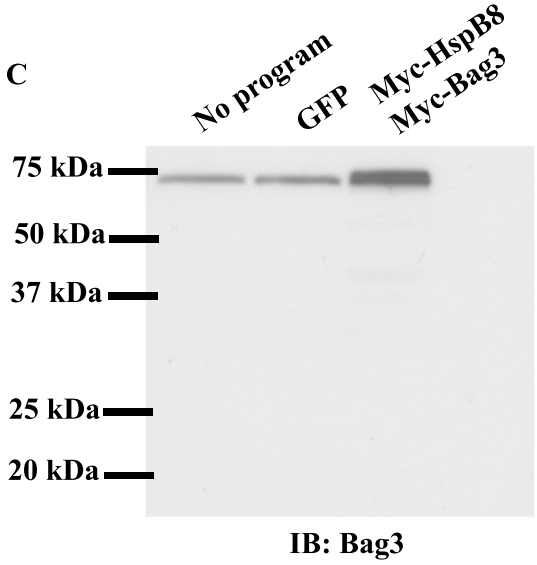
C
No program
GFP
Myc-HspB8
Myc-Bag3
75 kDa
50 kDa
37 kDa
25 kDa
20 kDa
IB: Bag3

Table 3.1 Protein/DNA ratios of transfected hTERT-HM cells.

hTERT-HM, Human Telomerase Reverse Transcriptase- Human Myometrial Cells

Sample ID	[DNA] µg/µl	[Protein] µg/µl	[Protein]/[DNA]	Average (1&2)
No Program 1	0.22335	1.61	7.21	4.68
No Program 2	0.63503	1.36	2.14	
pEGFP-C3 1	0.29311	0.77	2.63	3.29
pEGFP-C3 2	0.22297	0.88	3.95	
pCImycHspB8 1	0.31706	0.83	2.62	2.68
pCImycHspB8 2	0.30825	0.84	2.73	
pCImycBag3 1	0.25737	0.76	2.95	2.74
pCImycBag3 2	0.26203	0.92	3.51	
pCImycHspB8/Bag3 1	0.31982	0.81	2.53	2.57
pCImycHspB8/Bag3 2	0.28701	0.75	2.61	

performed. hTERT-HM cells were transiently transfected with pEGFP-C3 expression vector or co-transfected with pCImycHspB8 and pEGFP-C3 expression vectors as previously described. Following transfections all cells were labeled with far-red fluorescent reactive dye (Cy5) using a LIVE/DEAD® Fixable Dead Cell Stain Kit (Invitrogen, Burlington, ON, Canada). Subsequently, hTERT-HM cells were analyzed using a BD FACSCalibur™ flow cytometer. hTERT-HM cells were gated on the basis of forward scatter (FSC) and side scatter (SSC) and cy5 and GFP positivity, respectively (Figure 3.6.6A-C and D-F). hTERT-HM cells labeled with both Cy5 and GFP were compared to those labeled with only Cy5, using a gating strategy. Double-labeled cells appear in the upper right quadrant of the bivariate correlation plot (Figure 3.6.6 D-F). Forward scatter analysis was then used as an indicator of cell size, as shown in the graph representing an overlay of No Program Control (Cy5), pEGFP-C3 (Cy5), pEGFP-C3 (Cy5/GFP), pCImycHspB8/pEGFP-C3 (Cy5) and pCImycHspB8/ pEGFP-C3 (Cy5/GFP) (Figure 3.6.6G). As there was little variance in the forward scatter, transient transfection of hTERT-HM cells with pCImycHspB8 expression vector was not sufficient to induce cellular hypertrophy. Flow cytometric analysis was then repeated, in a similar manner, for hTERT-HM cells that had been co-transfected with pCImycBag3 and pEGFP-C3 expression vector or pCImycHspB8, pCImycBag3 and pEGFP-C3 expression vectors. hTERT-HM cells were again gated on the basis of forward scatter (FSC) and side scatter (SSC) and cy5 and GFP positivity, respectively (Figure 3.6.7A-C, Figure 3.6.8A-C; Figure 3.6.7D-F, Figure 3.6.8D-F). Subsequently, forward scatter analysis was used as an indicator of cell size, as shown in the graph representing an

Figure 3.6.6 Flow cytometric analysis of hTERT-HM cells transiently transfected with pEGFP-C3 expression vector or co-transfected with pCImycHspB8 and pEGFP-C3 expression vectors. hTERT-HM cells were gated on the basis of forward scatter (FSC) and side scatter (SSC) (**A-C**) and cy5 and GFP positivity (**D-F**). hTERT-HM cells labeled with both Cy5 and GFP were compared to those labeled with only Cy5, using a gating strategy. Double-labeled cells appear in the upper right quadrant of the bivariate correlation plot (**D-F**). FSC analysis was used as an indicator of cell size as shown in the graph, which represents an overlay of No Program Control (Cy5), pEGFPC-3 (Cy5), pEGFP-C3 (Cy5/GFP), pCImycHspB8/pEGFP-C3 (Cy5) and pCImycHspB8/ pEGFP-C3 (Cy5/GFP) (**G**).

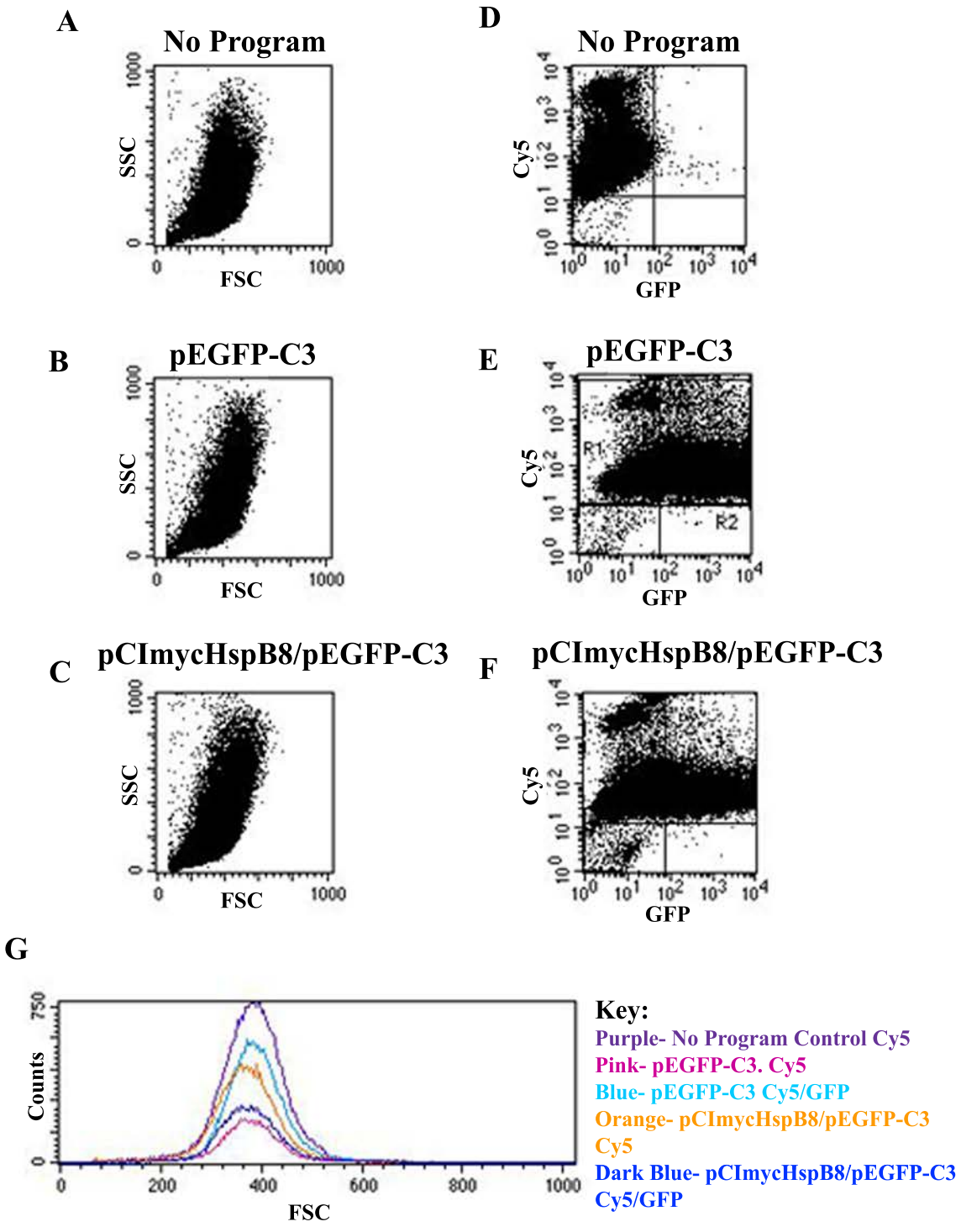
A
No Program
SSC
FSC
D
No Program
Cy5
GFP
B
pEGFP-C3
SSC
FSC
E
pEGFP-C3
R1
R2
Cy5
GFP
C
pCImycHspB8/pEGFP-C3
SSC
FSC
F
pCImycHspB8/pEGFP-C3
Cy5
GFP
G
Counts
FSC
Key:
Purple- No Program Control Cy5
Pink- pEGFP-C3. Cy5
Blue- pEGFP-C3 Cy5/GFP
Orange- pCImycHspB8/pEGFP-C3 Cy5
Dark Blue- pCImycHspB8/pEGFP-C3 Cy5/GFP

Figure 3.6.7 Flow cytometric analysis of hTERT-HM cells transiently transfected with pEGFP-C3 expression vector or co-transfected with pCImycBag3 and pEGFP-C3 expression vectors. hTERT-HM cells were gated on the basis of forward scatter (FSC) and side scatter (SSC) (**A-C**) and cy5 and GFP positivity (**D-F**). hTERT-HM cells labeled with both Cy5 and GFP were compared to those labeled with only Cy5, using a gating strategy. Double-labeled cells appear in the upper right quadrant of the bivariate correlation plot (**D-F**). FSC analysis was used as an indicator of cell size as shown in the graph, which represents an overlay of No Program Control (Cy5), pEGFPC-3 (Cy5), pEGFP-C3 (Cy5/GFP), pCImycBag3/pEGFP-C3 (Cy5) and pCImycBag3/ pEGFP-C3 (Cy5/GFP) (**G**).

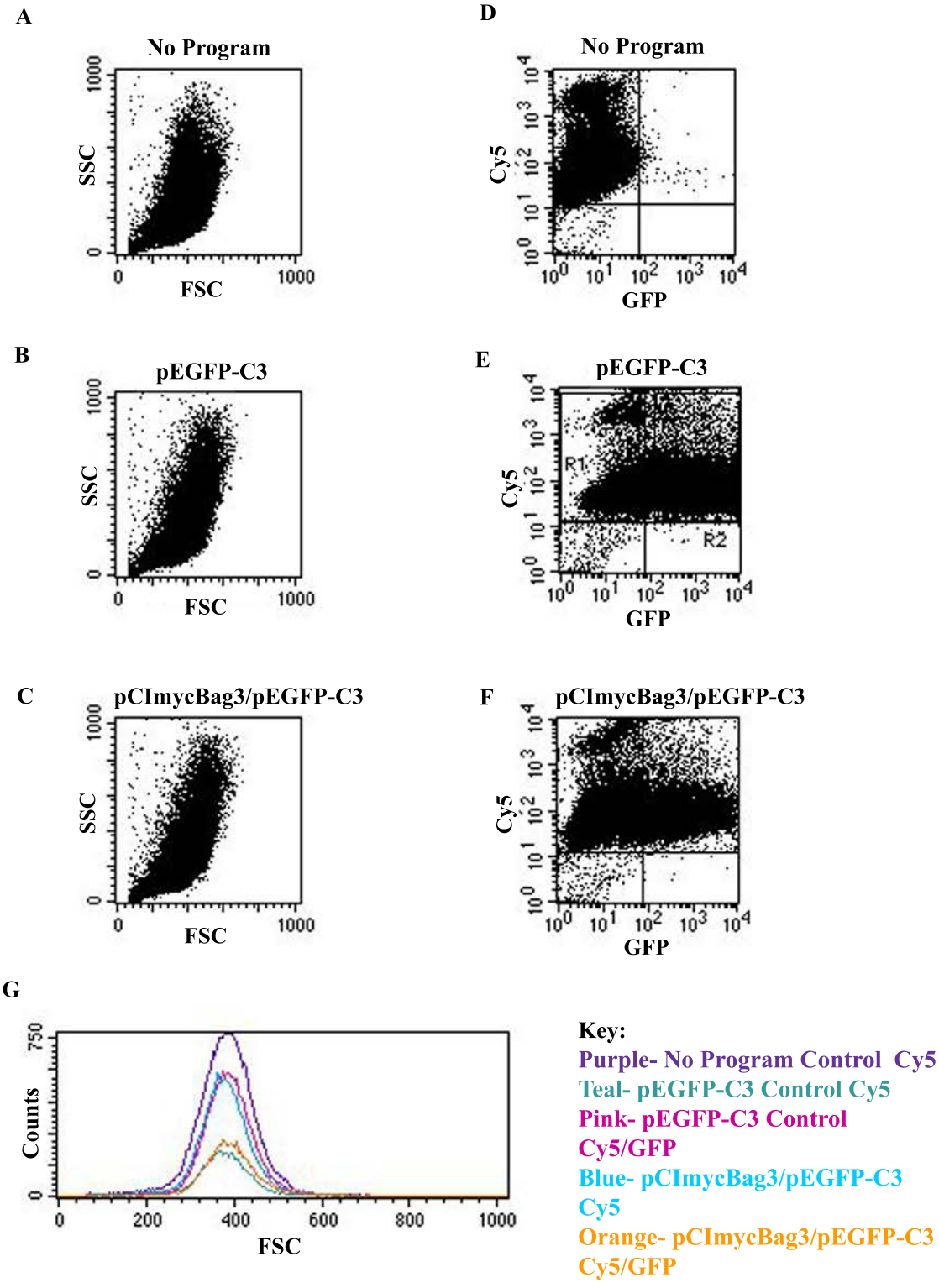
A
No Program
SSC
FSC
0
1000
D
No Program
Cy5
GFP
B
pEGFP-C3
SSC
FSC
E
pEGFP-C3
R1
R2
Cy5
GFP
C
pCImycBag3/pEGFP-C3
SSC
FSC
F
pCImycBag3/pEGFP-C3
Cy5
GFP
G
Counts
750
0
200
400
600
800
1000
FSC
Key:
Purple- No Program Control Cy5
Teal- pEGFP-C3 Control Cy5
Pink- pEGFP-C3 Control Cy5/GFP
Blue- pCImycBag3/pEGFP-C3 Cy5
Orange- pCImycBag3/pEGFP-C3 Cy5/GFP

Figure 3.6.8 Flow cytometric analysis of hTERT-HM cells transiently transfected with pEGFP-C3 expression vector or co-transfected with pCImycHspB8, pCImycBag3 and pEGFP-C3 expression vectors. hTERT-HM cells were gated on the basis of forward scatter (FSC) and side scatter (SSC) (**A-C**) and cy5 and GFP positivity (**D-F**). hTERT-HM cells labeled with both Cy5 and GFP were compared to those labeled with only Cy5, using a gating strategy. Double-labeled cells appear in the upper right quadrant of the bivariate correlation plot (**D-F**). FSC analysis was used as an indicator of cell size as shown in the graph, which represents an overlay of No Program Control (Cy5), pEGFPC-3 (Cy5), pEGFP-C3 (Cy5/GFP), pCImycHspB8/pCImycBag3/pEGFP-C3 (Cy5) and pCImycHspB8/pCImycBag3/pEGFP-C3 (Cy5/GFP) (**G**).

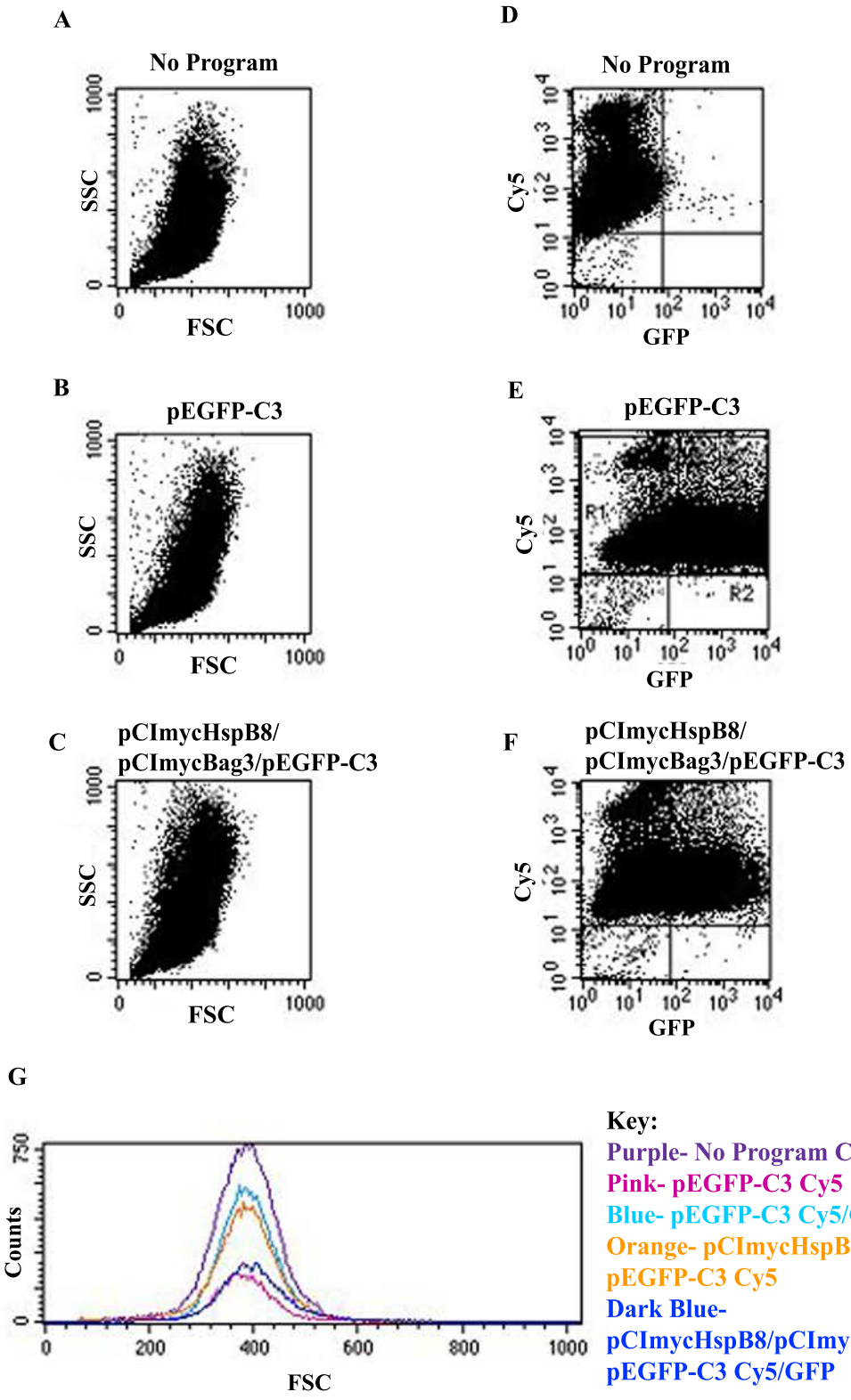
A
No Program
SSC
FSC
B
pEGFP-C3
SSC
FSC
C
pCImycHspB8/
pCImycBag3/pEGFP-C3
SSC
FSC
D
No Program
Cy5
GFP
E
pEGFP-C3
R1
R2
Cy5
GFP
F
pCImycHspB8/
pCImycBag3/pEGFP-C3
Cy5
GFP
G
Counts
FSC
Key:
Purple- No Program Control Cy5
Pink- pEGFP-C3 Cy5
Blue- pEGFP-C3 Cy5/GFP
Orange- pCImycHspB8/pCImycBag3/
pEGFP-C3 Cy5
Dark Blue-
pCImycHspB8/pCImycBag3/
pEGFP-C3 Cy5/GFP

overlay of all hTERT-HM cells being analyzed (Figure 3.6.7G, Figure 3.6.8G). Once again transient transfection of hTERT-HM cells, with pCImycBag3 or pCImycHspB8 and pCImycBag3 expression vectors, was not sufficient to induce cellular hypertrophy.

3.7 Expression of HspB8 in hTERT-HM Cells Following Ang II Treatment

hTERT-HM cells were administered 1000 nM of Ang II for 72 h as described in section 2.6.3. Observation of hTERT-HM cells following 72 h of Ang II administration indicated that there was no visible increase in cell size (Figure 3.7.1- 3.7.2). Immunoblot analysis was then performed to determine if Ang II administration had any effect on HspB8 or Bag3 protein expression. Seventy two hours of Ang II administration to hTERT-HM cells did not significantly increase HspB8 or Bag3 protein expression (Figure 3.7.3). Protein/DNA ratios were calculated using an RNA/DNA/Protein Purification Kit as described in section 2.8. Following isolation of proteins and purification of genomic DNA there was no significant increase in the protein to DNA ratio of hTERT-HM cells following Ang II administration (Table 3.2). To fully assess hypertrophy in hTERT-HM cells following Ang-II administration, flow cytometric analysis was performed following 72 h of Ang II (1000 nM) administration. hTERT-HM cells were gated on the basis of forward scatter (FSC) and side scatter (SSC) and SSC and cy5 positivity (Figure 3.7.4A,B). FSC analysis was used as an indicator of cell size which represents an overlay of hTERT-HM control cells (0 nM Ang II) and hTERT-HM cells administered 1000 nM Ang II (Figure 3.7.4C). There was little variance in the FSC suggesting that Ang II administration was not sufficient to induce cellular hypertrophy of

Figure 3.7.1 Representative images from phase contrast micrographs of hTERT-HM cells following administration of Ang II (1000 nM). Images on the left represent hTERT-HM control cells that were not administered Ang II. Images on the right represent hTERT-HM cells that were administered Ang II for 24, 48 or 72 h. Scale bar = 100 μm. Ang II = Angiotensin II.

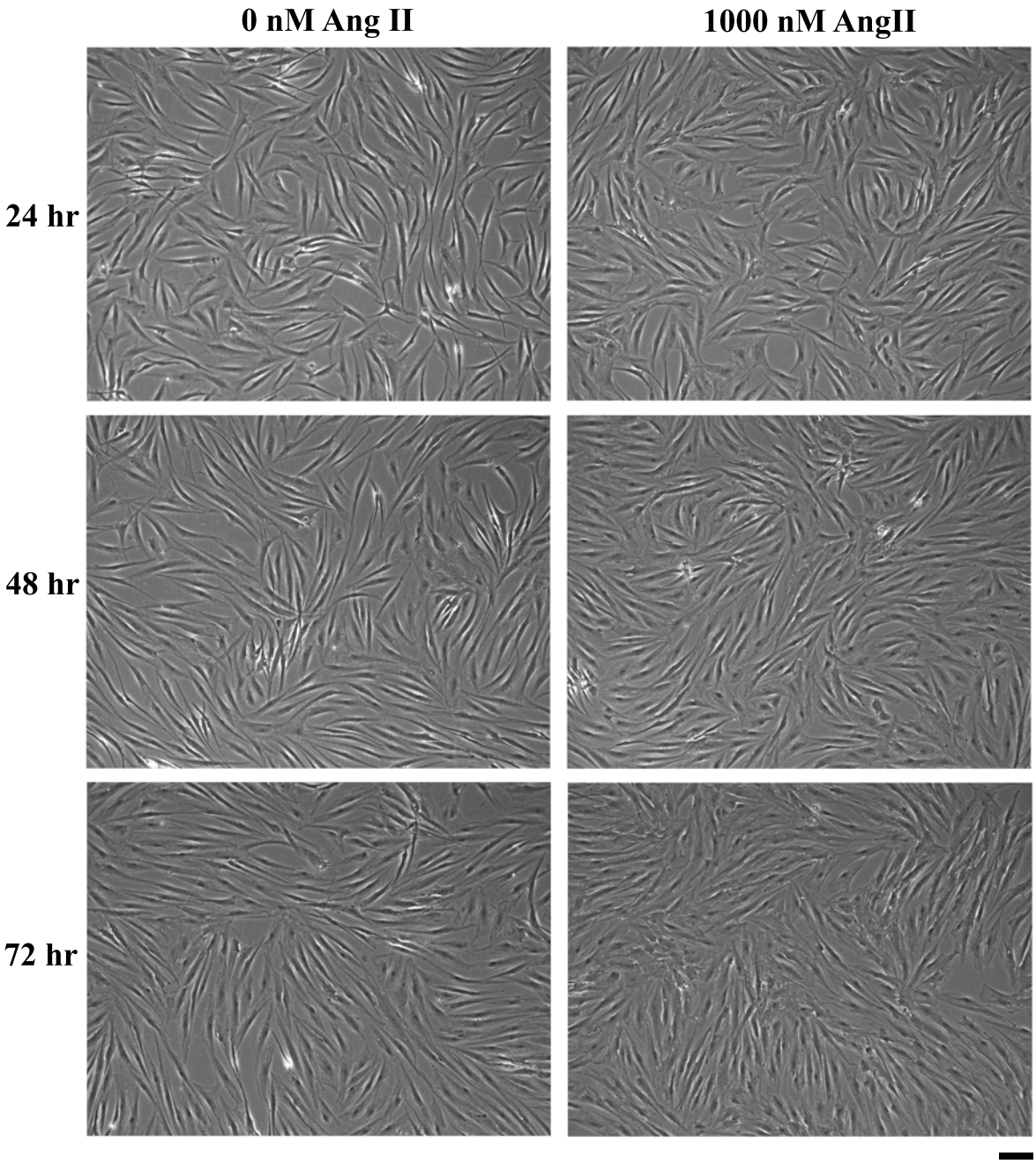
0 nM Ang II
1000 nM AngII
24 hr
48 hr
72 hr

Figure 3.7.2 Magnification of representative images from phase contrast micrographs of hTERT-HM cells following administration of Ang II (1000 nM). The image on the top represents control cells that were not administered Ang II, after 48 h. The image on the bottom represents cells administered 1000 nM Ang II for 48 h. Scale bar = 100 μm. Ang II = Angiotensin II.

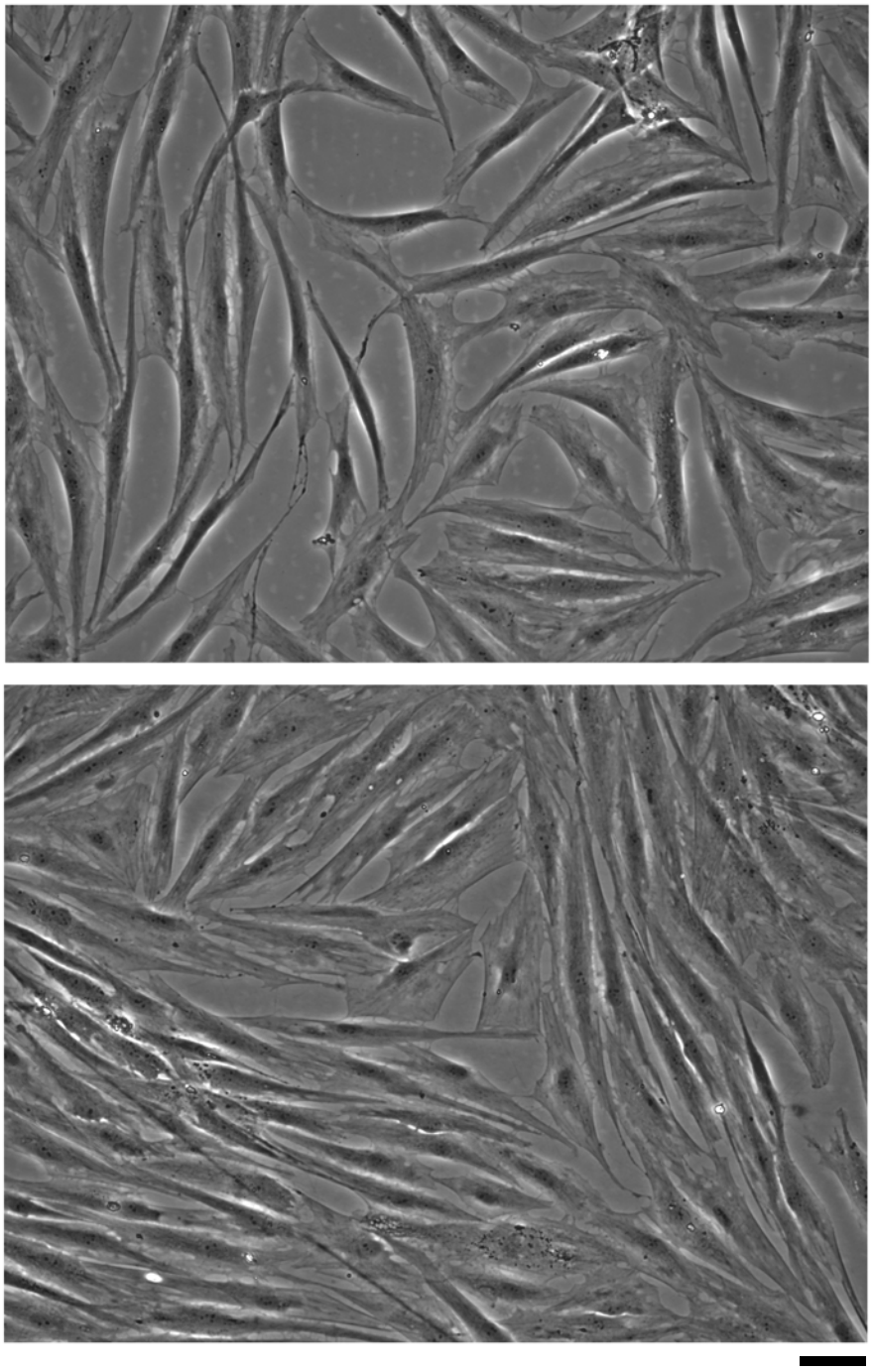
0 nM
Ang II
1000 nM
Ang II

Figure 3.7.3 Immunoblot analysis of HspB8, Bag3 and GAPDH in hTERT-HM cells following Ang II (0 nM versus 1000 nM) administration for 72 h. Representative immunoblots are shown. Analysis was performed using HspB8 and Bag3 specific antibodies (Dr. Jacques Landry). Ang II= Angiotensin II.

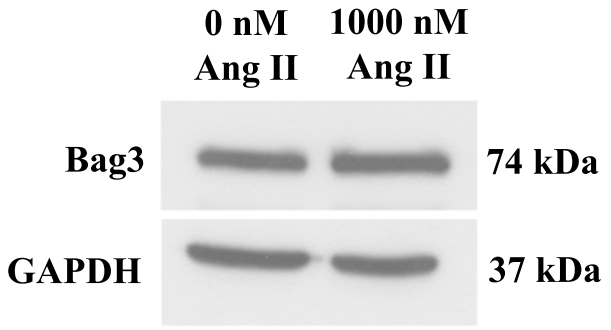
0 nM
Ang II
1000 nM
Ang II
Bag3
74 kDa
GAPDH
37 kDa

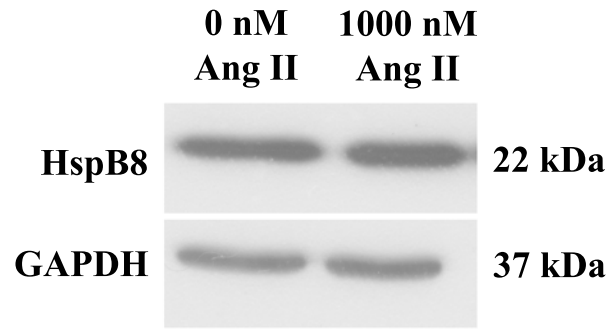
0 nM
Ang II
1000 nM
Ang II
HspB8
22 kDa
GAPDH
37 kDa

Table 3.2 Protein/DNA ratios of hTERT-HM cells following Ang II administration. hTERT-HM, Human Telomerase Reverse Transcriptase- Human Myometrial Cells; Ang II, Angiotensin II

Sample ID	[DNA] µg/µl	[Protein] µg/µl	[Protein]/[DNA]	Average (1&2)
0 nM Ang II 1	0.13083	0.64	4.89	4.62
0 nM Ang II 2	0.17527	0.76	4.34	
1000 nM AngII 1	0.12673	0.71	5.60	4.67
1000 nM AngII 2	0.20078	0.75	3.74	

Figure 3.7.4 Flow cytometric analysis of hTERT-HM cells following 72 h of Ang II (1000 nM) administration. hTERT-HM cells were gated on the basis of forward scatter (FSC) and side scatter (SSC) and SSC and cy5 positivity (A, B). FSC analysis was used as an indicator of cell size as shown in the graph, which represents an overlay of hTERT-HM control cells (0 nM Ang II) and hTERT-HM cells administered 1000 nM Ang II (**C**). Ang II = Angiotensin II.

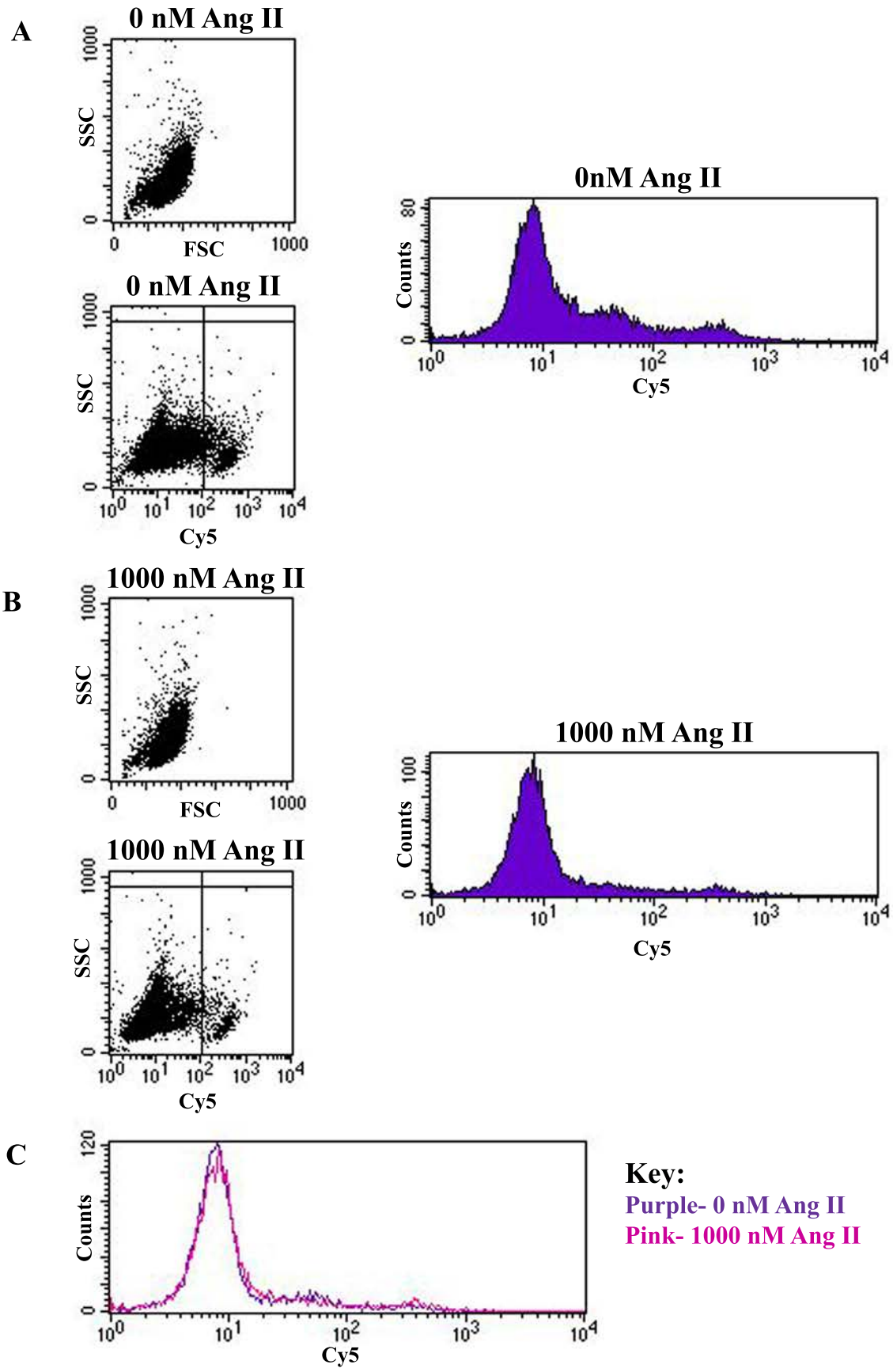
A
0 nM Ang II
SSC
FSC
0 nM Ang II
SSC
Cy5
0nM Ang II
Counts
Cy5
B
1000 nM Ang II
SSC
FSC
1000 nM Ang II
SSC
Cy5
1000 nM Ang II
Counts
Cy5
C
Counts
Cy5
Key:
Purple- 0 nM Ang II
Pink- 1000 nM Ang II

hTERT-HM cells within the timeframe utilized in the experiments.

3.8 Assessment of HspB8 and Bag3 Protein Association in Myometrial Cell and Tissue Lysates by Immunoprecipitation

Utilizing HeLa (human cervical cancer) and COS-1 (African green monkey kidney) cells, Carra et al. (2008) have suggested a new chaperone complex that is comprised of HspB8 and Bag3 proteins [236]. To determine the interaction, if any, between HspB8 and Bag3 in uterine smooth muscle, IP experiments were conducted on hTERT-HM protein lysates, as well as myometrial tissue homogenates from NP, d15, and d23 of rat pregnancy. IP of HspB8 protein, myc-tagged HspB8 protein and Bag3 protein in hTERT-HM cells was followed by immunoblot analysis using HspB8, Bag3, and myc-specific antibodies (Table 2.1). HspB8 protein was detected at ~22 kDa in all three pull downs (Figure 3.8.1A). It is important to note that IP of myc-tagged HspB8 protein resulted in detection of HspB8 protein at a slightly higher molecular weight due to the added myc tag. Conversely, after IP of HspB8, myc-HspB8 and Bag3 proteins and subsequent immunoblot analysis with a Bag3 specific antibody, Bag3 protein was detected at ~74 kDa in all three pull downs (Figure 3.8.1B). These results suggested that HspB8 and Bag3 are interacting with one another to form a complex in hTERT-HM cells.

To confirm whether HspB8 and Bag3 were interacting *in vivo,* IP experiments were conducted on myometrial tissue homogenates from the following time points: NP, d15 and d23 of rat pregnancy. IP of HspB8 or Bag3 in tissue lysates was followed by immunoblot analysis using HspB8 and Bag3 specific antibodies (Table 2.1). After IP and

Figure 3.8.1 Immunoprecipitation (IP) and immunoblot analyses (IB) of HspB8, myc-tagged HspB8 and Bag3 proteins in hTERT-HM cells. **(A)** Lane 1, input, represents a hTERT-HM lysate ($1/10^{th}$), lane 2 represents IP of HspB8 protein, lane 3 represents IP of myc-tagged HspB8 protein, lane 4 represents IP of Bag3 protein and lane 5 represents IP with Rabbit IgG (control). Figure A indicates that following IP there was detection of HspB8 protein at ~22 kDa or myc-tagged HspB8 protein at ~25 kDa. **(B)** Conversely, Figure B indicates that following IP there was detection of Bag3 at ~74 kDa. These results demonstrate that HspB8 and Bag3 form a complex in hTERT-HM cells.

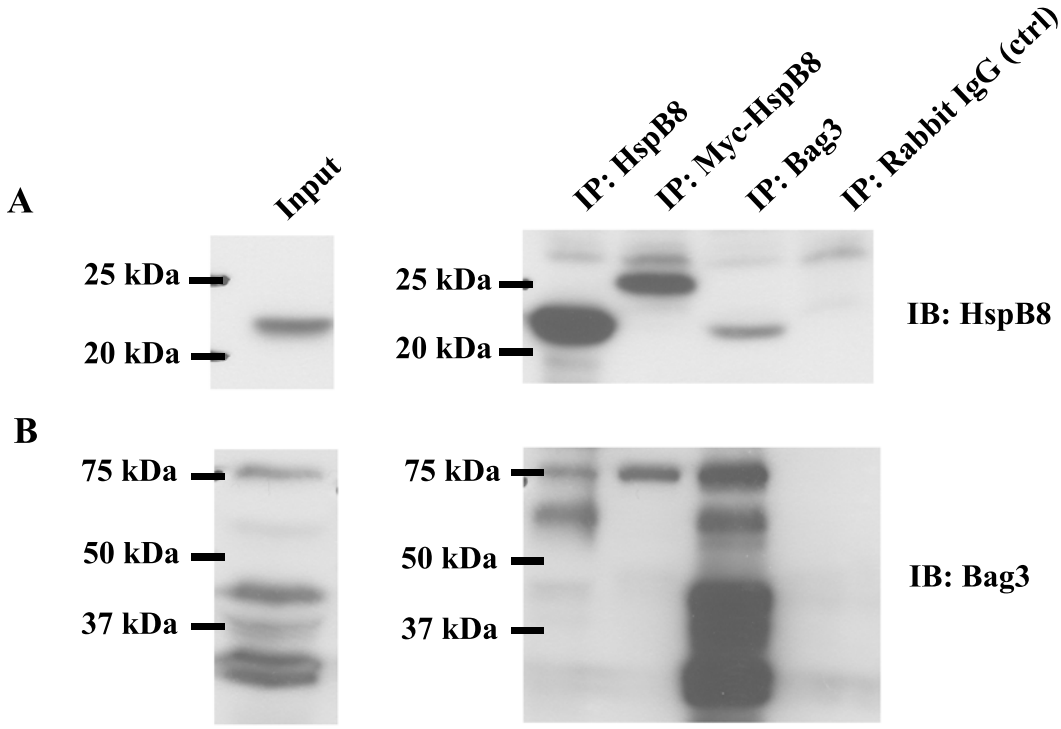
A
Input
IP: HspB8
IP: Myc-HspB8
IP: Bag3
IP: Rabbit IgG (ctrl)
25 kDa
20 kDa
25 kDa
20 kDa
IB: HspB8
B
75 kDa
50 kDa
37 kDa
75 kDa
50 kDa
37 kDa
IB: Bag3

subsequent immunoblot analysis, Bag3 protein was detected at ~74 kDa in all HspB8 and Bag3 pull downs (Figure 3.8.2A). After IP and immunoblot analysis, HspB8 protein was also detected at ~22 kDa in all HspB8 and Bag3 pull downs (Figure 3.8.2B). Together these results demonstrated that HspB8 and Bag3 were associating with one another *in vitro* and *in vivo*.

Figure 3.8.2 Immunoprecipitation (IP) and immunoblot analysis (IB) of HspB8 and Bag3 proteins in rat myometrial tissue lysates (NP, d15, d23). Following IP there was detection of HspB8 protein at ~22 kDa and Bag3 protein at ~74 kDa at all three gestational time points (n=3/day). These results demonstrate that HspB8 and Bag3 form a complex in rat myometrium during pregnancy.

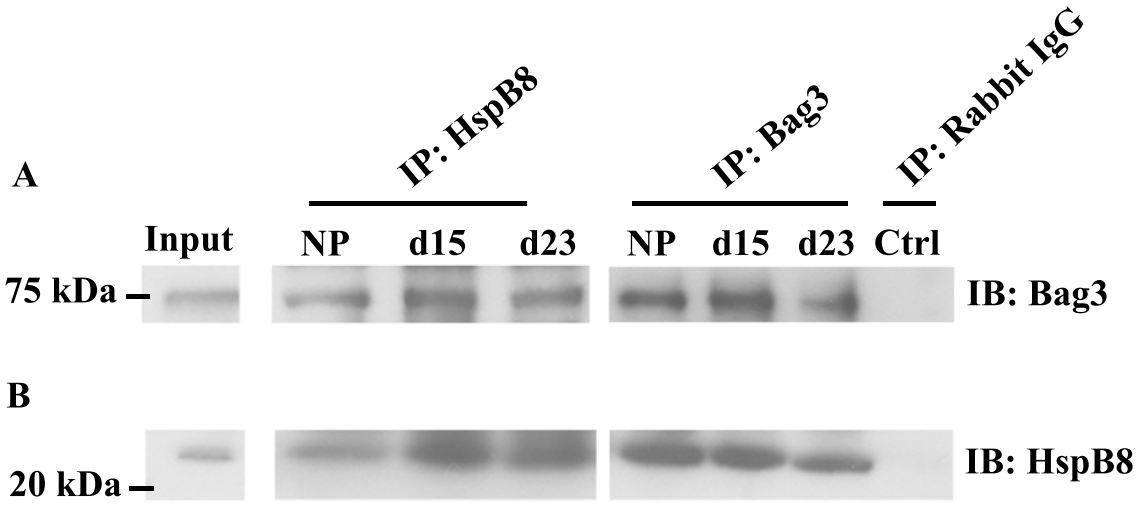
A
IP: HspB8
IP: Bag3
IP: Rabbit IgG
Input
NP
d15
d23
NP
d15
d23
Ctrl
75 kDa
IB: Bag3
B
20 kDa
IB: HspB8

Chapter Four

Discussion

4.1 Analysis of HspB8 and Bag3 Protein Expression in Myometrium during Pregnancy and Labour

Our lab previously reported that HspB8 mRNA levels were initially low and then expression began to increase significantly between d17 and PP (with the exception of d22) [237]. We therefore hypothesized that HspB8 protein expression would be elevated towards mid-pregnancy. In this study, HspB8 protein expression was significantly elevated at d15, d17 and d19 compared to NP and d6 time points.

Significantly increased HspB8 protein expression beginning at d15 of gestation was in contrast to the observed significant increase in HspB8 mRNA expression beginning at d17. As mRNA is normally translated to form protein a greater correlation of mRNA and HspB8 expression was expected. It is possible that there was sufficient mRNA available for protein translation during early pregnancy and that the increased HspB8 mRNA expression at d17 and later reflects a need for increased HspB8 translation. Furthermore, the variation in gestational timing when tissues were collected (± 12 hours) may serve as a small contributing factor to the poor correlation in mRNA and protein expression. As both HspB8 mRNA and protein expression began to increase after mid-gestation, our results indicate that HspB8 may play an important role during this time in pregnancy.

Immunoblot analysis was also performed to determine the expression pattern for Bag3 protein in pregnant rat myometrium. Bag3 protein expression was significantly elevated at d15, compared to expression at NP, and at d17 compared NP, d6, d23 and PP. During immunoblot analysis, it was noted that in addition to the band representing full-length Bag3 protein (~74 kDa), other bands (~40kDa/~25kDa) were detected representing possible cleavage products of Bag3. A smaller form of Bag3 (~40 kDa), in neural synaptosomes homogenates, has been analyzed by IP and mass spectrometry [210]. Furthermore, published reports indicate that Bag3 is cleaved during apoptosis. Bag3 is efficiently cleaved by caspase-3, to a smaller extent by caspases-1 and -8, and relatively inefficiently by caspase-9 [238]. More specifically, caspase-3 is able to cleave Bag3 into 2 smaller fragments in pancreatic cancer cells resulting in products of ~40 kDa and ~25 kDa similar to results presented in this thesis [238, 239]. As it is known that caspase-3 is up-regulated between the proliferative and synthetic phase of myometrial differentiation [41], the ~40 kDa and ~25 kDa bands recognized by the Bag3 antibody may be cleavage products of Bag3.

The up-regulation of HspB8 and Bag3 at mid-gestation coincides with the differentiation of the myometrium from a state of hyperplasia to hypertrophy (Figure 4.1A). As they show similar patterns of expression this suggests that they may interact or play similar roles during pregnancy.

Figure 4.1 Representative patterns of HspB8 and Bag3 protein expression during the phases of myometrial differentiation. **(A)** HspB8 protein expression (black curve) was found to be significantly elevated at d15, d17 and d19 compared to NP and d6. Bag3 protein expression (red curve) was significantly elevated at d15, compared to expression at NP, and at d17 compared to NP, d6, d23 and PP. The up-regulation of HspB8 and Bag3 proteins coincides with differentiation of the myometrium from a state of hyperplasia to hypertrophy **(B)** Hsp70 protein expression (yellow curve) was significantly elevated at d19, d21, d22 and d23 compared to NP and d6. Hsc70 protein and CHIP (dark blue curve) are constitutively expressed. LC3II protein expression (teal curve) was found to be significantly elevated at PP compared to expression at NP, d6 and d12.

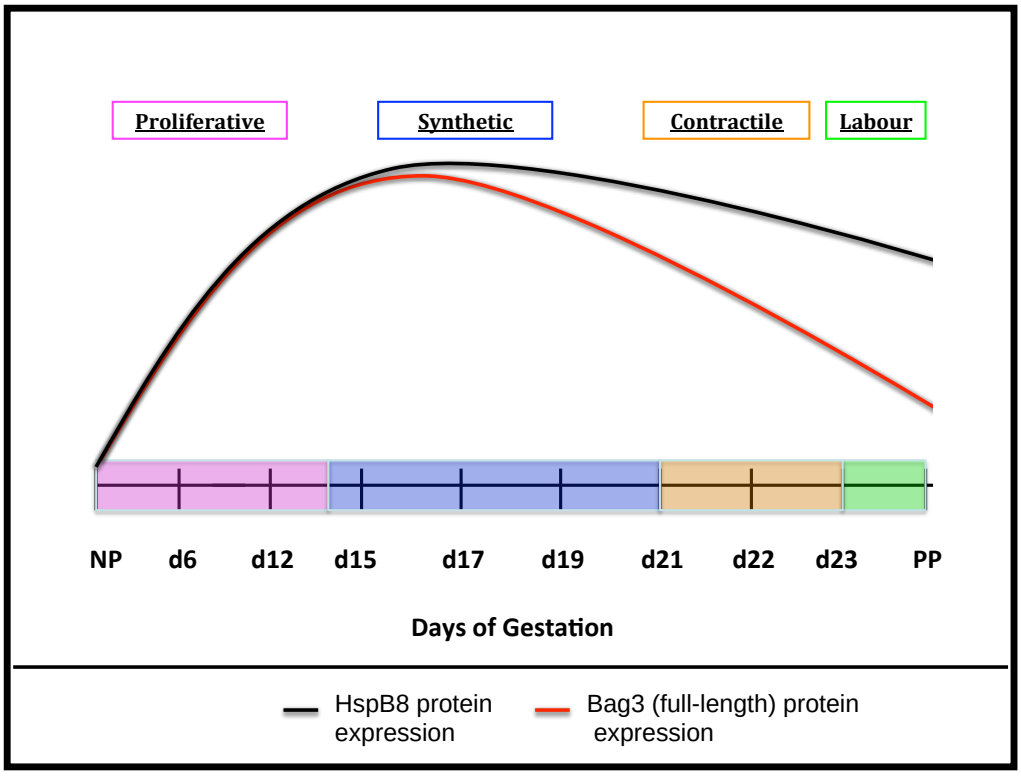
Proliferative
Synthetic
Contractile
Labour
NP
d6
d12
d15
d17
d19
d21
d22
d23
PP
Days of Gestation
HspB8 protein expression
Bag3 (full-length) protein expression

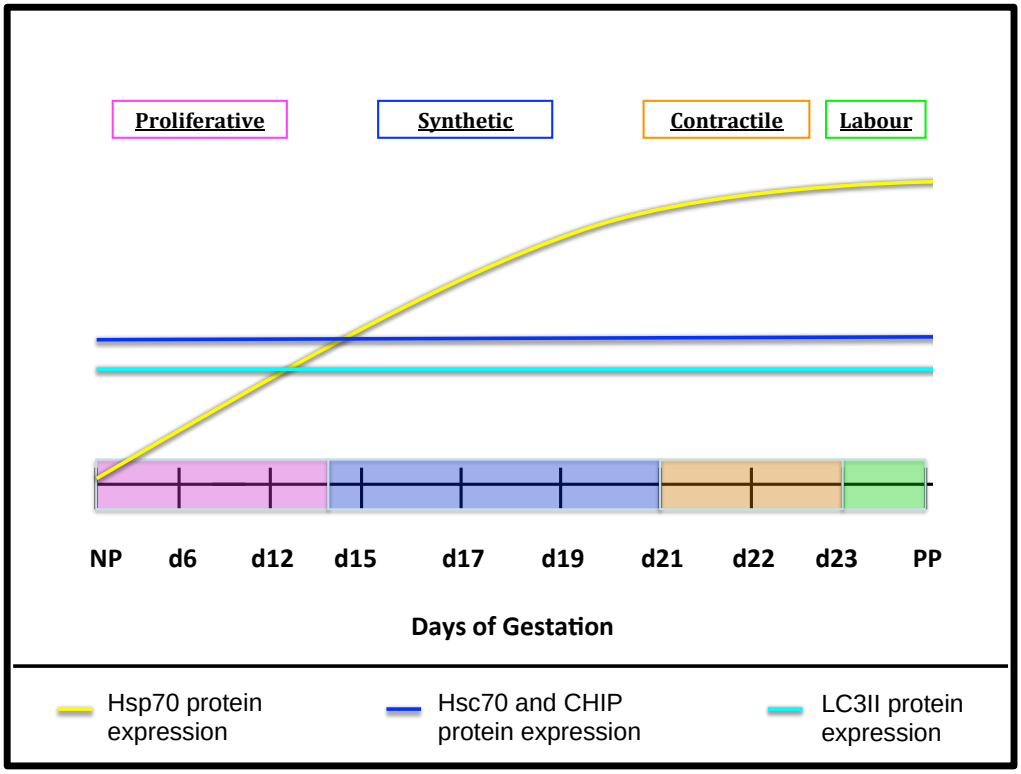
Proliferative
Synthetic
Contractile
Labour
NP
d6
d12
d15
d17
d19
d21
d22
d23
PP
Days of Gestation
Hsp70 protein expression
Hsc70 and CHIP protein expression
LC3II protein expression

4.2 Intracellular Localization of HspB8 and Bag3 Proteins in the Myometrium during Pregnancy

This is the first report of the intracellular localization of HspB8 and Bag3 in the myometrium. The spatiotemporal expression of HspB8 and Bag3 in pregnant rat myometrium was determined *in situ* using rat uterine tissue samples and immunofluorescence microscopy. HspB8 was predominantly localized to the cytoplasm of cells and there was an absence of nuclear staining. This is consistent with previous research on extracts of estrogen receptor-positive breast cancer cells using size-exclusion chromatography, indicating that HspB8 was detected primarily in the cell cytoplasm [240]. HspB8 was also detected near cell membranes in the rat myometrium. This specific cellular localization has also been shown in a human neuroblastoma cell line, SK-N-SH [241]. There was intense cytoplasmic staining, particularly on d15, indicating concentrated subcellular localization of HspB8 protein. HspB8 has been found to colocalize with aggregates formed by misfolded or partially denatured proteins. For instance, HspB8 can be trapped within inclusions formed by proteins with polyglutamine tails (Htt43Q) in order to prevent the formation of large aggregates [178]. HspB8 has also been found in aggregates formed by αB-crystallin mutants, which are involved in myofibrillar myopathy [242]. Thus, HspB8 may be responsible for preventing aggregation or promoting degradation of misfolded proteins, which may result in concentrated subcellular localization.

The intracellular localization of Bag3 protein was also examined. There was an absence of nuclear staining, as well as some perinuclear localization of Bag3 along with

the general cytoplasmic localization in myometrial cells. Previous research on HeLa cells indicates that when the cells were exposed to cadmium, zinc or to 42°C, the localization of Bag3 changed to a reticular, perinuclear localization on a cytosolic background. More specifically, co-immunofluorescence experiments demonstrated calreticulin, a protein resident in the rough endoplasmic reticulum (ER), co-localized with Bag3 protein in cadmium-treated HeLa cells [243]. Reticular, perinuclear localization of Bag3 may have a role(s) in the myometrium throughout gestation. The ER is known to be a major point of integration of damage-sensing or pro-apoptotic stimuli [244]. Even though Bag3 lacks an ER localization signal, it is probable that Bag3 is required in the ER to complex with other proteins, as interactions with different proteins play an important role in determining the function of Bag3 [245]. Bag3 is capable of interacting with Bcl2, for instance, which can result in increased anti-apoptotic activity and a decrease in the apoptosis induced via Bax or Fas in HeLa cells [246]. Alternatively, Bag3 may form a large multichaperone complex consisting of HspB8-Bag3-Hsp70/Hsc70-CHIP, as a means to regulate the degradation of misfolded proteins through the stimulation of the macroautophagy pathway [183, 184, 200, 202, 208].

Localization of both HspB8 and Bag3 proteins in the cytoplasm of the myometrium is consistent with their aggregations in this compartment and with reports showing an interaction between the two proteins [183].

4.3 Role of HspB8 and Bag3 as Regulators of Apoptosis

There are three major processes that help to maintain homeostasis of the myometrium throughout gestation: proliferation, differentiation and apoptosis. Apoptosis, also known as programmed cell death, is responsible for eliminating dysfunctional cells during development or normal tissue homeostasis. The process of apoptosis can be activated via two different pathways: the extrinsic and the intrinsic pathway. Both pathways result in activation of a caspase cascade and the effector, caspase-3. Caspase-3 activation is associated with cleavage of cellular substrates that ultimately results in cell death, but it also reduces myocyte contractility in smooth muscle [247, 248]. Caspase-3 in the myometrium is also hypothesized to act as an anti-contractile agent that is activated around d14, between the phases of myometrial hyperplasia and hypertrophy, to help maintain uterine quiescence [41]. At this time, Shynlova et al. (2006) found that there was also a notable increase in the expression of two anti-apoptotic regulating proteins, Bcl2 and Bcl2l1, and as a result there were no physiological manifestations of apoptosis in the myometrial cells [18].

In this study, the up-regulation of HspB8, at d15, d17 and d19, coincides with the increase in expression of caspase-3, as the myometrium differentiates from a state of hyperplasia to hypertrophy (Figure 4.1) [41]. HspB8 acts as a regulator of apoptosis and therefore it is possible that HspB8 may play such a role during this transition period [249-252]. Depre et al. (2006) found that HspB8 was able to protect the myocardium against apoptosis by binding to PKB and AMPK, resulting in stimulation of survival mechanisms

in both the cytosol and nucleus [234]. This included inhibition of pro-apoptotic effectors, such as Bad, FOXO and glycogen synthase kinase-3β. Similarly, treatment of human breast cancer cell line MCF-7 with 17β-estradiol elevates HspB8 protein expression, and protects breast cancer cells from apoptosis [249]. HspB8 is also overexpressed in stomach tumors, proliferating human keratinocytes, and rat pheochromocytoma (PC12) cells, once again demonstrating anti-apoptotic properties [253].

Bag3 also serves as an anti-apoptotic effector. In several published reports *Bag3* silencing or overexpression caused enhanced or inhibited spontaneous or drug-induced apoptosis, respectively [188, 192, 254-261]. For example, in 293 cells transfected with a Bag3-hyperexpressing construct, apoptosis induced by the glutathione-depriving agent diethylmaleate (DEM) + 2-methyoxymethylestradiol (2-ME) was 60 % lower when compared to control cultures. Similarly, in human myeloid U937 cells, a decrease in Bag3 protein levels by a phosphorothioate antisense oligodeoxynucleotide increased cell apoptotic response to DEM by 40 % [262].

In total, HspB8 as well as Bag3 may play important anti-apoptotic roles by promoting cell survival in the rat myometrium near the window of d12-d15 gestation. Ultimately, more research must be conducted in this area to further confirm the role of HspB8 and Bag3 as anti-apoptotic proteins in smooth muscle, particularly in the transition from hyperplasia to hypertrophy. Furthermore, there have been some contrasting data suggesting HspB8 may have a role in promoting apoptosis. In one experiment performed by Gober et al. (2003) treatment of the tumour cell lines SK-MEL-

2 (melanoma) and PC-3 (prostate cancer) with the demethylating agent 5-aza-2'-deoxycytidine to induce HspB8 expression, transient transfection with HspB8 expression vectors, or retrovirus-mediated delivery of HspB8 resulted in caspase- and $p38^{MAPK}$-dependent apoptosis [250].

4.4 Role of HspB8 and Bag3 as Regulators of Macroautophagy

Following IP experiments, immunoblot analysis indicated that HspB8 and Bag3 interacted with one another *in vitro* in hTERT-HM cells and *in vivo* in rat myometrium during pregnancy. Given that complexing of sHsps is essential for their function, it is plausible that the interaction between HspB8 and Bag3 may be important throughout pregnancy [123]. sHsps have been found to play key roles in proteostasis, which involves modulation of concentration, structure, interactions and cellular localization of proteins. Recently, it was reported that muscle tissue relies on an effective proteostasis network in which macroautophagy is a critical component [208]. The up-regulation of HspB8 and Bag3 just after mid-gestation, as shown by immunoblot analysis, coincides with the differentiation of the myometrium from a state of hyperplasia to hypertrophy. This transition is associated with significant protein turnover and thus alternative to a role in regulating apoptosis. HspB8, Bag3 and a regulatory pathway such as macroautophagy may be required to help maintain protein homeostasis in the myometrium during pregnancy.

The basal level of macroautophagy is a critical regulator of cellular homeostasis as it is responsible for the removal of damaged/old organelles (particularly mitochondria), protein aggregates, and the turnover of long-lived proteins [93, 107]. Bag3, like all Bag family members, is capable of interacting with Hsp70/Hsc70 via its Bag domain, which subsequently interacts with a well-known Hsp70/Hsc70 binding co-factor- the ubiquitin ligase CHIP. Several recent studies showed that the multichaperone complex, HspB8-Bag3-Hsp70/Hsc70-CHIP, was able to regulate the degradation of misfolded proteins, such as polyQ-expanded huntingtin and mutant SOD1, through the stimulation of the macroautophagy pathway [183, 184, 200, 202, 208]. Detection of Hsp70, Hsc70 and CHIP proteins, by immunoblot analysis, indicates that some of the key players involved in the stimulation of the macroautophagy pathway are present in uterine musculature throughout gestation (Figure 4.1B). Thus far, the only known marker for autophagosome formation in the macroautophagy pathway is LC3II and therefore detection of LC3II protein, by immunoblot analysis, in the myometrium throughout gestation supports the notion that macroautophagy may serve as an important homeostatic process during this period to help maintain pregnancy [216, 217]. The autophagosome, however, is an intermediate structure in the dynamic process of macroautophagy and thus, the presence of LC3II in the myometrium does not definitively indicate whether this is due to macroautophagy induction or suppression of the pathway downstream of the autophagosome [218].

As overexpression of HspB8 and Bag3 stimulates phosphorylation of eIF2α, resulting in activation of the macroautophagy machinery, Pser51-eIF2α protein expression was analyzed in rat myometrium throughout gestation [185]. Pser51-eIF2α expression did not increase significantly throughout gestation. This suggests that the up-regulation of HspB8 and Bag3 during mid-gestation, in rat myometrium, is not likely responsible for translational shutdown and subsequent stimulation of the macroautophagy machinery through eIF2α.

4.5 The Effect of Distension on HspB8 Protein Expression

Uterine stretch, as a result of growing pups, is an important inducer of gene expression in uterine muscle. As increased expression of HspB8 protein in the myometrium coincided with a time of increasing distension it was important to determine whether uterine distension had any regulatory effect on HspB8 expression. Virgin female rats underwent unilateral tubal ligation, through a flank incision, and as a result the rat was only able to implant the conceptus in one horn. This procedure isolates the influence of stretch while maintaining a consistent endocrinological environment, except for any local factors secreted by the placenta or fetus [51]. Tissue samples from three different time points in pregnancy, d15, d19 and d23, were examined to determine if uterine distension had an effect on HspB8 protein expression. Unexpectedly, immunoblot analysis revealed that expression of HspB8 protein was not differentially influenced by stretch. Furthermore, immunofluorescence detection demonstrated that there was mainly cytoplasmic localization of HspB8 in myometrial cells, as well as detection near cell

membranes, but there were no marked changes in the expression of HspB8 protein in the gravid uterine horn when compared to the non-gravid horn. Therefore, uterine stretch does not appear to play a regulatory role in the expression of HspB8 protein. This is in contrast to work by White & MacPhee that demonstrated another Hsp, HspB1 was regulated by uterine stretch. In unilaterally pregnant rats, HspB1 mRNA and pSer15-HspB1 protein expression were significantly elevated in distended gravid uterine horns at both d19 and d23 (labour) or gestation compared to non-gravid horns. Both HspB1 mRNA and pSer15-HspB1 protein expression were also markedly increased in ovariectomized, NP rat myometrium distended for 24 h with laminaria tents compared to empty horns [223].

4.6 The Effect of Progesterone on HspB8 Protein Expression and RU486 on HspB8, Bag3 and LC3II Protein Expression

The circulating levels of progesterone in rat maternal serum peak specifically between d15-d19 after which there is a dramatic decline until labour [49]. The peak levels coincide with the noted increase in Bag3 and HspB8 protein levels, suggesting that progesterone may play a role in regulating Bag3 and HspB8 protein expression in rat myometrium. Administration of progesterone to pregnant rats (beginning on d20) did not change HspB8 protein expression until d23, at which point expression significantly decreased. It is unknown whether or not this decrease in HspB8 protein expression is due to the effects of prolonged progesterone levels or an increased stress that is incurred as a result of prolonging labour. In order to further analyze the role of progesterone on HspB8

protein expression in rat myometrium RU486, a progesterone receptor antagonist, was administered to pregnant rats on d18 of gestation. This treatment resulted in preterm delivery of the pups within 24 h as previously reported [263]. Progesterone receptor antagonism resulted in a significant increase in HspB8 protein expression, as well as a change in the spatial localization of this protein within myometrial cells. Following treatment of RU486 there was a marked decrease in the detection of HspB8 in the circular muscle layer; however, there was a marked increase in detection in the longitudinal muscle layer. This indicates that there may be myometrial layer-specific regulation of HspB8 expression as a result of functional withdrawal of progesterone. As Bag3 protein expression followed a similar pattern to HspB8 it was important to see if Bag3 expression was regulated by progesterone. In RU486-administration experiments there was no change in Bag3 protein expression suggesting that progesterone was not a major regulator of Bag3 expression.

As HspB8 protein regulation by progesterone appears to be complex, it was important to analyze LC3II protein expression following RU486 treatment to determine if RU486 had additional effects on myometrial function. Progesterone receptor antagonism by RU486 induced preterm labour and resulted in a significant increase in LC3II protein expression, indicating that there was a potential increase in the requirement for macroautophagy machinery to maintain protein homeostasis. Therefore, it is unclear whether the change in HspB8 protein expression observed upon RU486 administration and preterm birth is a result of the functional withdrawal of progesterone or the

requirements for preterm delivery. It is probable that the side effects of preterm labour, such as increased macroautophagy, may have indirectly led to our observed results. Thus, the role of progesterone in regulating HspB8 protein expression in the myometrium still remains to be fully clarified.

4.7 Myometrial Cell Model of Hypertrophy

Adenoviral-mediated overexpression of HspB8 in neonatal rat cardiac myocytes results in cell hypertrophy within 48 h of expression, as shown by an increase in the protein/DNA ratio by 37% [172]. Therefore, the hTERT-HM cell line was used to help assess the importance of HspB8 and other chaperone machine components in myometrial hypertrophy. In order to determine whether HspB8 and/or Bag3 was capable of inducing myometrial hypertrophy, pCImycHspB8 and/or pCImycBag3 expression vectors were transiently transfected into hTERT-HM cells. Exogenous HspB8 or Bag3 protein expression was verified by immunoblot analysis using a myc-tag specific antibody. Cells did not appear to increase in cell size when viewed with a Leica DMIRE2 inverted microscope equipped with phase contrast optics. Thus, potential hypertrophy of transfected hTERT-HM cells was further assessed by flow cytometry and determination of protein/DNA ratios. There was no change in cell size between transfected cells and control cells and there was no significant increase in protein/DNA ratios between the two cell populations. These results suggest that overexpression of HspB8 and/or Bag3 alone are not sufficient to induce hTERT-HM cell hypertrophy and may require additional protein partners or cell-ECM interactions.

Concentrations of Ang II have been found to increase 4.5-fold over the non-pregnant level in pregnant sheep [264]. In humans the Ang II level was reported to be 700 nM in maternal circulation during pregnancy [265]. Thus, Cui et al. (2010) examined whether Ang II could induce myometrial protein synthesis in a uterine smooth muscle tumor derived cell line (ULTR) [266]. They reported that Ang II was able to induce cellular hypertrophy, as determined by ^{3}H-leucine incorporation [266]. To determine if Ang II could also induce cellular hypertrophy in hTERT-HM cells, protein/DNA ratios were calculated and flow cytometry was performed. There was no change in cell size or significant increase in protein/DNA ratios between the two treatment groups. Following Ang II administration to hTERT-HM cells, HspB8 and Bag3 protein expression was also assessed by immunoblot analysis. Ang II administration had no effect on their protein expression. Thus, Ang II is not sufficient for inducing myometrial hypertrophy in hTERT-HM cells at the concentration and conditions tested.

4.8 Future Research

The results of this investigation provide valuable insights into the formation of a heteromeric complex between HspB8 and Bag3 in uterine musculature. The patterns of expression of HspB8 and Bag3 in the myometrium indicate that they could have important roles during initiation of myometrial hypertrophy and add to the body of knowledge indicating sHsps are uniquely expressed with myometrial programming during pregnancy. However, the exact role of HspB8 in uterine muscle remains enigmatic and therefore there are many important research avenues left to pursue.

First of all, the hTERT-HM cell line could be helpful in investigating the role of HspB8 as a pro- or anti-apoptotic protein throughout gestation. HspB8 could be overexpressed using the pCImycHspB8 expression vector used throughout this study and subsequently apoptotic activity could be quantified by monitoring caspase 3 activity or cell survival by the TUNEL method. This would help determine whether HspB8 has a protective function in the cell as an anti-apoptotic protein. As Bag3 has also displayed anti-apoptotic activity in published reports, similar experiments and assays with the pCIMycBag3 expression vector could also be conducted to help confirm whether Bag3 plays an anti-apoptotic role in the myometrium.

HspB8 and Bag3 have been found to complex with one another in rat myometrium throughout pregnancy. Thus, it would also be important to determine whether they are part of a multiheteromeric complex comprised of HspB8, Bag3, Hsc70 and CHIP during myometrial programming, particularly during the synthetic phase. Co-IP experiments with protein specific antisera and affinity purified IgG (negative control) could be conducted to determine any temporal-specific association of Bag3 or HspB8 with Hsc70 or CHIP. Subsequently, the multichaperone complex (Bag3-HspB8-Hsp70/Hsc70) is thought to mediate macroautophagy in cooperation with the macroautophagy receptor protein p62/SQSTM1. Accordingly, it would be important to assess the requirement for macroautophagy in the myometrium throughout pregnancy. In order to determine the requirement for macroautophagy the “autophagic flux” or the dynamic process of autophagosome synthesis in hTERT-HM cells could be studied. The

amount of LC3II increases upon induction of autophagy, however, after prolonged autophagy activation it decreases. Therefore, reduction of GFP-labelled LC3II expression could be quantitated by flow cytometry in hTERT-HM cells, which inversely correlates with autophagic flux [267]. In order to characterize the role of HspB8 and/or Bag3 in the myometrium it would be helpful to overexpress HspB8 and/or Bag3 and determine their effect on autophagic flux in smooth muscle cells. To fully understand the process of macroautophagy it would also be important to look at the inhibition of autophagic activity and its effect on hTERT-HM cells. Commonly used PI3-kinase inhibitors such as wortmannin, LY294002 or 3-MA could be used to inhibit macroautophagy *in vitro* in order to assess the effects on HspB8 and Bag3, as well as their interaction [97, 268, 269].

Despite published reports, HspB8 overexpression in hTERT-HM cells is not sufficient to induce cellular hypertrophy. First, it would be important to develop a cell model to induce hypertrophy. The use of the ULTR cell line may be warranted. Once induced hypertrophy is fully verified it will be helpful to examine HspB8, Hsc70, Hsp70, Bag3 and CHIP gene expression, both temporally and spatially, during this process. The next essential step would be to use siRNA-specific knockdown of individual mRNA species, such as HspB8, Bag3, Hsc/Hsp70 and CHIP, prior to induction of cellular hypertrophy, to determine the necessity of these proteins for hypertrophic growth.

As previous research has indicated HspB8 may complex with HspB1 [162], further verification of this interaction could be important in determining the function of HspB8 in the myometrium throughout gestation. Once again, co-IP experiments with

protein specific antisera and affinity purified IgG (negative control) could be conducted to determine any temporal-specific association of these proteins. Additionally, a further investigation could be a co-immunolocalization experiment to analyze whether both HspB8 and HspB1 co-localize in the myometrium. Co-localization could lead to further confirmation of the potential interaction between these proteins, perhaps leading to the potential function of this heterodimeric complex.

HspB8 is highly expressed in mitochondria. For example, Lenne & Douce (1994) reported localization of HspB8 to mitochondria in pea plants [270]. Drosophilia melanogaster (Dm) Hsp22 was found by Morrow et al. (2000, 2004) to be a mitochondrial protein that was localized to the mitochondrial matrix, particularly in oligomeric complexes and its high level of expression in aging suggests that is may have a protective role during times of oxidative stress [271, 272]. Co-immunofluorescence detection with mitochondrial markers and an HspB8 specific antibody could be conducted to confirm any mitochondrial specific localization within myometrial cells. Human myometrial cell lines could also be used for this analysis, as the various organelles, such as the mitochondria, are more visible in cells.

Finally, throughout immunofluorescence detection it was noted that there was a significant amount of HspB8 expression in the endometrium. This was a novel finding, so in the future the expression of HspB8 could be studied throughout pregnancy in the endometrium. Perhaps the role of HspB8 in the endometrium would also help reveal its function in the uterus throughout pregnancy.

All of the future experiments mentioned may help to confirm the exact role of HspB8 and Bag3 throughout pregnancy and labour and may provide insight into reducing the incidence of preterm birth.

References

1. Challis, J.R.G., et al., *Endocrine and paracrine regulation of birth at term and preterm.* Endocr Rev, 2000. **21**(5): p. 514-50.
2. Challis, J.R., et al., *Prostaglandins and mechanisms of preterm birth.* Reproduction, 2002. **124**(1): p. 1-17.
3. Beck, S., et al., *The worldwide incidence of preterm birth: a systematic review of maternal mortality and morbidity.* Bull World Health Organ, 2010. **88**(1): p. 31-8.
4. Martin, J.A., et al., *Births: final data for 2007.* Natl Vital Stat Rep, 2010. **58**(24): p. 1-85.
5. Smith, R., *Parturition.* N Engl J Med, 2007. **356**(3): p. 271-83.
6. Spong, C.Y., *Prediction and prevention of recurrent spontaneous preterm birth.* Obstet Gynecol, 2007. **110**(2 Pt 1): p. 405-15.
7. Garfield, R.E. and W.L. Maner, *Physiology and electrical activity of uterine contractions.* Semin Cell Dev Biol, 2007. **18**(3): p. 289-95.
8. March of Dimes, P., Save the Children, WHO, *Born Too Soon: The Global Action Report on Preterm Birth*, ed. M.K. CP Howson, JE Lawn. 2012, Geneva: World Health Organization.
9. Stock, S. and J. Norman, *Preterm and term labour in multiple pregnancies.* Semin Fetal Neonatal Med, 2010. **15**(6): p. 336-41.
10. Russell, R.B., et al., *Cost of hospitalization for preterm and low birth weight infants in the United States.* Pediatrics, 2007. **120**(1): p. e1-9.
11. Goldenberg, R.L., et al., *Epidemiology and causes of preterm birth.* Lancet, 2008. **371**(9606): p. 75-84.
12. Shynlova, O., et al., *Integration of endocrine and mechanical signals in the regulation of myometrial functions during pregnancy and labour.* Eur J Obstet Gynecol Reprod Biol, 2009. **144 Suppl 1**: p. S2-10.
13. Hansen, J.T., F.H. Netter, and D.R. Lambert, *Netter's clinical anatomy*. 2005: Icon Learning Systems.
14. Shynlova, O., et al., *Uterine stretch regulates temporal and spatial expression of fibronectin protein and its alpha 5 integrin receptor in myometrium of unilaterally pregnant rats.* Biol Reprod, 2007. **77**(5): p. 880-8.
15. Monga M, S.B., *Biology and physiology of the reproductive tract and control of myometrial contraction.* 5 ed. 2004, Maternal-Fetal Medicine: Principles and Practice: Pennsylvania: Saunders.
16. Silverthorn, D.U. and B.R. Johnson, *Human Physiology: An Integrated Approach*. 2010: Pearson/Benjamin Cummings.
17. Aguilar, H.N. and B.F. Mitchell, *Physiological pathways and molecular mechanisms regulating uterine contractility.* Hum Reprod Update, 2010. **16**(6): p. 725-44.

18. Shynlova, O., et al., *Myometrial apoptosis: activation of the caspase cascade in the pregnant rat myometrium at midgestation.* Biol Reprod, 2006. **74**(5): p. 839-49.
19. Lye, S.J., et al., *Role of mechanical signals in the onset of term and preterm labor.* Front Horm Res, 2001. **27**: p. 165-78.
20. Shynlova, O., et al., *Insulin-like growth factors and their binding proteins define specific phases of myometrial differentiation during pregnancy in the rat.* Biol Reprod, 2007. **76**(4): p. 571-8.
21. Jaffer, S., O. Shynlova, and S. Lye, *Mammalian target of rapamycin is activated in association with myometrial proliferation during pregnancy.* Endocrinology, 2009. **150**(10): p. 4672-80.
22. Russell, R.C., C. Fang, and K.L. Guan, *An emerging role for TOR signaling in mammalian tissue and stem cell physiology.* Development, 2011. **138**(16): p. 3343-56.
23. Gielen, S.C., et al., *Steroid-modulated proliferation of human endometrial carcinoma cell lines: any role for insulin-like growth factor signaling?* J Soc Gynecol Investig, 2005. **12**(1): p. 58-64.
24. Klotz, D.M., et al., *Requirement of estrogen receptor-alpha in insulin-like growth factor-1 (IGF-1)-induced uterine responses and in vivo evidence for IGF-1/estrogen receptor cross-talk.* J Biol Chem, 2002. **277**(10): p. 8531-7.
25. Wullschleger, S., R. Loewith, and M.N. Hall, *TOR signaling in growth and metabolism.* Cell, 2006. **124**(3): p. 471-84.
26. Zhang, Z., et al., *The role of adapter protein Shc in estrogen non-genomic action.* Steroids, 2004. **69**(8-9): p. 523-9.
27. Brazil, D.P. and B.A. Hemmings, *Ten years of protein kinase B signalling: a hard Akt to follow.* Trends Biochem Sci, 2001. **26**(11): p. 657-64.
28. Verdu, J., et al., *Cell-autonomous regulation of cell and organ growth in Drosophila by Akt/PKB.* Nat Cell Biol, 1999. **1**(8): p. 500-6.
29. Shioi, T., et al., *Akt/protein kinase B promotes organ growth in transgenic mice.* Mol Cell Biol, 2002. **22**(8): p. 2799-809.
30. Inoki, K., et al., *TSC2 is phosphorylated and inhibited by Akt and suppresses mTOR signalling.* Nat Cell Biol, 2002. **4**(9): p. 648-57.
31. Potter, C.J., L.G. Pedraza, and T. Xu, *Akt regulates growth by directly phosphorylating Tsc2.* Nat Cell Biol, 2002. **4**(9): p. 658-65.
32. Miron, M., P. Lasko, and N. Sonenberg, *Signaling from Akt to FRAP/TOR targets both 4E-BP and S6K in Drosophila melanogaster.* Mol Cell Biol, 2003. **23**(24): p. 9117-26.
33. Ma, X.M. and J. Blenis, *Molecular mechanisms of mTOR-mediated translational control.* Nat Rev Mol Cell Biol, 2009. **10**(5): p. 307-18.
34. Holz, M.K., et al., *mTOR and S6K1 mediate assembly of the translation preinitiation complex through dynamic protein interchange and ordered phosphorylation events.* Cell, 2005. **123**(4): p. 569-80.

35. Fingar, D.C., et al., *Mammalian cell size is controlled by mTOR and its downstream targets S6K1 and 4EBP1/eIF4E.* Genes Dev, 2002. **16**(12): p. 1472-87.
36. Lee, C.H., K. Inoki, and K.L. Guan, *mTOR pathway as a target in tissue hypertrophy.* Annu Rev Pharmacol Toxicol, 2007. **47**: p. 443-67.
37. Proud, C.G., *mTOR-mediated regulation of translation factors by amino acids.* Biochem Biophys Res Commun, 2004. **313**(2): p. 429-36.
38. Shynlova, O., et al., *Progesterone and gravidity differentially regulate expression of extracellular matrix components in the pregnant rat myometrium.* Biol Reprod, 2004. **70**(4): p. 986-92.
39. Harkness, M.L. and R.D. Harkness, *The collagen content of the reproductive tract of the rat during pregnancy and lactation.* J Physiol, 1954. **123**(3): p. 492-500.
40. Reynolds, S.R.M., *Physiology of the uterus*. 1965: Hafner Pub. Co.
41. Shynlova, O., A. Dorogin, and S.J. Lye, *Stretch-induced uterine myocyte differentiation during rat pregnancy: involvement of caspase activation.* Biol Reprod, 2010. **82**(6): p. 1248-55.
42. Stewart, A.G., D. Fernandes, and P.R. Tomlinson, *The effect of glucocorticoids on proliferation of human cultured airway smooth muscle.* Br J Pharmacol, 1995. **116**(8): p. 3219-26.
43. Shynlova, O., M. Chow, and S.J. Lye, *Expression and organization of basement membranes and focal adhesion proteins in pregnant myometrium is regulated by uterine stretch.* Reprod Sci, 2009. **16**(10): p. 960-9.
44. Geiger, B., et al., *Transmembrane crosstalk between the extracellular matrix--cytoskeleton crosstalk.* Nat Rev Mol Cell Biol, 2001. **2**(11): p. 793-805.
45. Williams, S.J., B.G. White, and D.J. MacPhee, *Expression of alpha5 integrin (Itga5) is elevated in the rat myometrium during late pregnancy and labor: implications for development of a mechanical syncytium.* Biol Reprod, 2005. **72**(5): p. 1114-24.
46. Macphee, D.J. and S.J. Lye, *Focal adhesion signaling in the rat myometrium is abruptly terminated with the onset of labor.* Endocrinology, 2000. **141**(1): p. 274-83.
47. Shynlova, O., et al., *Expression and localization of alpha-smooth muscle and gamma-actins in the pregnant rat myometrium.* Biol Reprod, 2005. **73**(4): p. 773-80.
48. Graham, J.D. and C.L. Clarke, *Physiological action of progesterone in target tissues.* Endocr Rev, 1997. **18**(4): p. 502-19.
49. Lye, S.J., et al., *Increased expression of connexin-43 in the rat myometrium during labor is associated with an increase in the plasma estrogen:progesterone ratio.* Endocrinology, 1993. **132**(6): p. 2380-6.
50. Ou, C.W., et al., *Increased expression of the rat myometrial oxytocin receptor messenger ribonucleic acid during labor requires both mechanical and hormonal signals.* Biol Reprod, 1998. **59**(5): p. 1055-61.

51. Ou, C.W., A. Orsino, and S.J. Lye, *Expression of connexin-43 and connexin-26 in the rat myometrium during pregnancy and labor is differentially regulated by mechanical and hormonal signals.* Endocrinology, 1997. **138**(12): p. 5398-407.
52. Sobue, K., K. Takahashi, and I. Wakabayashi, *Caldesmon150 regulates the tropomyosin-enhanced actin-myosin interaction in gizzard smooth muscle.* Biochem Biophys Res Commun, 1985. **132**(2): p. 645-51.
53. Li, Y., et al., *ERK1/2-mediated phosphorylation of myometrial caldesmon during pregnancy and labor.* Am J Physiol Regul Integr Comp Physiol, 2003. **284**(1): p. R192-9.
54. Marston, S.B. and W. Lehman, *Caldesmon is a Ca2+-regulatory component of native smooth-muscle thin filaments.* Biochem J, 1985. **231**(3): p. 517-22.
55. Morgan, K.G. and S.S. Gangopadhyay, *Invited review: cross-bridge regulation by thin filament-associated proteins.* J Appl Physiol, 2001. **91**(2): p. 953-62.
56. Novy, M.J., M.J. Cook, and L. Manaugh, *Indomethacin block of normal onset of parturition in primates.* Am J Obstet Gynecol, 1974. **118**(3): p. 412-6.
57. Jouppila, P., et al., *The placental and fetal response to the intra-amniotic injection of prostaglandin F2alpha in midtrimester abortions.* Br J Obstet Gynaecol, 1976. **83**(4): p. 303-6.
58. Al-Matubsi, H.Y., et al., *Expression and localization of the contractile prostaglandin F receptor in pregnant rat myometrium in late gestation, labor, and postpartum.* Biol Reprod, 2001. **65**(4): p. 1029-37.
59. Kasai, Y., et al., *Stretch-induced enhancement of contractions in uterine smooth muscle of rats.* J Physiol, 1995. **486 (Pt 2)**: p. 373-84.
60. Park, J.H., et al., *A potential role of connexin 43 in epidermal growth factor-induced proliferation of mouse embryonic stem cells: involvement of Ca2+/PKC, p44/42 and p38 MAPKs pathways.* Cell Prolif, 2008. **41**(5): p. 786-802.
61. Beyer, E.C., *Gap junctions.* Int Rev Cytol, 1993. **137C**: p. 1-37.
62. Vodstrcil, L.A., et al., *Decreased expression of the rat myometrial relaxin receptor (RXFP1) in late pregnancy is partially mediated by the presence of the conceptus.* Biol Reprod, 2010. **83**(5): p. 818-24.
63. Terzidou, V., et al., *Mechanical stretch up-regulates the human oxytocin receptor in primary human uterine myocytes.* J Clin Endocrinol Metab, 2005. **90**(1): p. 237-46.
64. Magness, R.R., et al., *Endothelial vasodilator production by uterine and systemic arteries. V. Effects of ovariectomy, the ovarian cycle, and pregnancy on prostacyclin synthase expression.* Prostaglandins Other Lipid Mediat, 2000. **60**(4-6): p. 103-18.
65. Korita, D., et al., *Cyclic mechanical stretch augments prostacyclin production in cultured human uterine myometrial cells from pregnant women: possible involvement of up-regulation of prostacyclin synthase expression.* J Clin Endocrinol Metab, 2002. **87**(11): p. 5209-19.

66. Li, Y., et al., *Focal adhesion signaling is required for myometrial ERK activation and contractile phenotype switch before labor.* J Cell Biochem, 2007. **100**(1): p. 129-40.
67. Harkness, R.D. and B.E. Moralee, *The time-course and route of loss of collagen from the rat's uterus during post-partum involution.* J Physiol, 1956. **132**(3): p. 502-8.
68. Jones, R.L., et al., *Identification of chemokines important for leukocyte recruitment to the human endometrium at the times of embryo implantation and menstruation.* J Clin Endocrinol Metab, 2004. **89**(12): p. 6155-67.
69. Phaneuf, S., et al., *Oxytocin-stimulated phosphoinositide hydrolysis in human myometrial cells: involvement of pertussis toxin-sensitive and -insensitive G-proteins.* J Endocrinol, 1993. **136**(3): p. 497-509.
70. Taylor, S.J., et al., *Activation of the beta 1 isozyme of phospholipase C by alpha subunits of the Gq class of G proteins.* Nature, 1991. **350**(6318): p. 516-8.
71. Streb, H., et al., *Release of Ca2+ from a nonmitochondrial intracellular store in pancreatic acinar cells by inositol-1,4,5-trisphosphate.* Nature, 1983. **306**(5938): p. 67-9.
72. Gill, D.L., *Calcium signalling: receptor kinships revealed.* Nature, 1989. **342**(6245): p. 16-8.
73. Anwer, K., M. Monga, and B.M. Sanborn, *Epidermal growth factor increases phosphoinositide turnover and intracellular free calcium in an immortalized human myometrial cell line independent of the arachidonic acid metabolic pathway.* Am J Obstet Gynecol, 1996. **174**(2): p. 676-81.
74. Taggart, M.J. and K.G. Morgan, *Regulation of the uterine contractile apparatus and cytoskeleton.* Semin Cell Dev Biol, 2007. **18**(3): p. 296-304.
75. Wray, S., *Uterine contraction and physiological mechanisms of modulation.* Am J Physiol, 1993. **264**(1 Pt 1): p. C1-18.
76. Sanborn, B.M., *Relationship of ion channel activity to control of myometrial calcium.* J Soc Gynecol Investig, 2000. **7**(1): p. 4-11.
77. Cheung, W.Y., *Calmodulin.* Sci Am, 1982. **246**(6): p. 62-70.
78. Ikebe, M., D.J. Hartshorne, and M. Elzinga, *Identification, phosphorylation, and dephosphorylation of a second site for myosin light chain kinase on the 20,000-dalton light chain of smooth muscle myosin.* J Biol Chem, 1986. **261**(1): p. 36-9.
79. Ikebe, M., D.J. Hartshorne, and M. Elzinga, *Phosphorylation of the 20,000-dalton light chain of smooth muscle myosin by the calcium-activated, phospholipid-dependent protein kinase. Phosphorylation sites and effects of phosphorylation.* J Biol Chem, 1987. **262**(20): p. 9569-73.
80. Ikebe, M., J. Koretz, and D.J. Hartshorne, *Effects of phosphorylation of light chain residues threonine 18 and serine 19 on the properties and conformation of smooth muscle myosin.* J Biol Chem, 1988. **263**(13): p. 6432-7.
81. Garfield, R.E., S. Sims, and E.E. Daniel, *Gap junctions: their presence and necessity in myometrium during parturition.* Science, 1977. **198**(4320): p. 958-60.

82. Beyer, E.C., et al., *Antisera directed against connexin43 peptides react with a 43-kD protein localized to gap junctions in myocardium and other tissues.* J Cell Biol, 1989. **108**(2): p. 595-605.
83. Risek, B., et al., *Modulation of gap junction transcript and protein expression during pregnancy in the rat.* J Cell Biol, 1990. **110**(2): p. 269-82.
84. Komatsu, M., et al., *Loss of autophagy in the central nervous system causes neurodegeneration in mice.* Nature, 2006. **441**(7095): p. 880-4.
85. Mizushima, N. and D.J. Klionsky, *Protein turnover via autophagy: implications for metabolism.* Annu Rev Nutr, 2007. **27**: p. 19-40.
86. Klionsky, D.J., *The molecular machinery of autophagy: unanswered questions.* J Cell Sci, 2005. **118**(Pt 1): p. 7-18.
87. Massey, A.C., C. Zhang, and A.M. Cuervo, *Chaperone-mediated autophagy in aging and disease.* Curr Top Dev Biol, 2006. **73**: p. 205-35.
88. Crotzer, V.L. and J.S. Blum, *Autophagy and its role in MHC-mediated antigen presentation.* J Immunol, 2009. **182**(6): p. 3335-41.
89. Hailey, D.W., et al., *Mitochondria supply membranes for autophagosome biogenesis during starvation.* Cell, 2010. **141**(4): p. 656-67.
90. Mizushima, N., T. Yoshimori, and Y. Ohsumi, *The role of Atg proteins in autophagosome formation.* Annu Rev Cell Dev Biol, 2011. **27**: p. 107-32.
91. Ravikumar, B., et al., *Plasma membrane contributes to the formation of pre-autophagosomal structures.* Nat Cell Biol, 2010. **12**(8): p. 747-57.
92. Tooze, S.A. and T. Yoshimori, *The origin of the autophagosomal membrane.* Nat Cell Biol, 2010. **12**(9): p. 831-5.
93. Ravikumar, B., et al., *Regulation of mammalian autophagy in physiology and pathophysiology.* Physiol Rev, 2010. **90**(4): p. 1383-435.
94. Hosokawa, N., et al., *Nutrient-dependent mTORC1 association with the ULK1-Atg13-FIP200 complex required for autophagy.* Mol Biol Cell, 2009. **20**(7): p. 1981-91.
95. Sarkar, S., et al., *Rapamycin and mTOR-independent autophagy inducers ameliorate toxicity of polyglutamine-expanded huntingtin and related proteinopathies.* Cell Death Differ, 2009. **16**(1): p. 46-56.
96. Mehrpour, M., et al., *Overview of macroautophagy regulation in mammalian cells.* Cell Res, 2010. **20**(7): p. 748-62.
97. Itakura, E., et al., *Beclin 1 forms two distinct phosphatidylinositol 3-kinase complexes with mammalian Atg14 and UVRAG.* Mol Biol Cell, 2008. **19**(12): p. 5360-72.
98. Sun, Q., et al., *Identification of Barkor as a mammalian autophagy-specific factor for Beclin 1 and class III phosphatidylinositol 3-kinase.* Proc Natl Acad Sci U S A, 2008. **105**(49): p. 19211-6.
99. Mizushima, N., et al., *Dissection of autophagosome formation using Apg5-deficient mouse embryonic stem cells.* J Cell Biol, 2001. **152**(4): p. 657-68.

100. Mizushima, N., et al., *Mouse Apg16L, a novel WD-repeat protein, targets to the autophagic isolation membrane with the Apg12-Apg5 conjugate.* J Cell Sci, 2003. **116**(Pt 9): p. 1679-88.
101. Fujita, N., et al., *The Atg16L complex specifies the site of LC3 lipidation for membrane biogenesis in autophagy.* Mol Biol Cell, 2008. **19**(5): p. 2092-100.
102. Eskelinen, E.L., *Maturation of autophagic vacuoles in Mammalian cells.* Autophagy, 2005. **1**(1): p. 1-10.
103. Dunn, W.A., Jr., *Autophagy and related mechanisms of lysosome-mediated protein degradation.* Trends Cell Biol, 1994. **4**(4): p. 139-43.
104. Jager, S., et al., *Role for Rab7 in maturation of late autophagic vacuoles.* J Cell Sci, 2004. **117**(Pt 20): p. 4837-48.
105. Kimura, S., T. Noda, and T. Yoshimori, *Dissection of the autophagosome maturation process by a novel reporter protein, tandem fluorescent-tagged LC3.* Autophagy, 2007. **3**(5): p. 452-60.
106. Tanaka, Y., et al., *Accumulation of autophagic vacuoles and cardiomyopathy in LAMP-2-deficient mice.* Nature, 2000. **406**(6798): p. 902-6.
107. Yang, Z. and D.J. Klionsky, *Mammalian autophagy: core molecular machinery and signaling regulation.* Curr Opin Cell Biol, 2010. **22**(2): p. 124-31.
108. Marzella, L., J. Ahlberg, and H. Glaumann, *Autophagy, heterophagy, microautophagy and crinophagy as the means for intracellular degradation.* Virchows Arch B Cell Pathol Incl Mol Pathol, 1981. **36**(2-3): p. 219-34.
109. Uttenweiler, A., H. Schwarz, and A. Mayer, *Microautophagic vacuole invagination requires calmodulin in a Ca2+-independent function.* J Biol Chem, 2005. **280**(39): p. 33289-97.
110. Arias, E. and A.M. Cuervo, *Chaperone-mediated autophagy in protein quality control.* Curr Opin Cell Biol, 2011. **23**(2): p. 184-9.
111. Chiang, H.L., et al., *A role for a 70-kilodalton heat shock protein in lysosomal degradation of intracellular proteins.* Science, 1989. **246**(4928): p. 382-5.
112. Cuervo, A.M. and J.F. Dice, *A receptor for the selective uptake and degradation of proteins by lysosomes.* Science, 1996. **273**(5274): p. 501-3.
113. Bandyopadhyay, U., et al., *The chaperone-mediated autophagy receptor organizes in dynamic protein complexes at the lysosomal membrane.* Mol Cell Biol, 2008. **28**(18): p. 5747-63.
114. Caspers, G.J., J.A. Leunissen, and W.W. de Jong, *The expanding small heat-shock protein family, and structure predictions of the conserved "alpha-crystallin domain".* J Mol Evol, 1995. **40**(3): p. 238-48.
115. Kim, K.K., R. Kim, and S.H. Kim, *Crystal structure of a small heat-shock protein.* Nature, 1998. **394**(6693): p. 595-9.
116. Jakob, U., et al., *Small heat shock proteins are molecular chaperones.* J Biol Chem, 1993. **268**(3): p. 1517-20.
117. Mosser, D.D. and R.I. Morimoto, *Molecular chaperones and the stress of oncogenesis.* Oncogene, 2004. **23**(16): p. 2907-18.

118. Kappe, G., et al., *The human genome encodes 10 alpha-crystallin-related small heat shock proteins: HspB1-10.* Cell Stress Chaperones, 2003. **8**(1): p. 53-61.
119. MacRae, T.H., *Structure and function of small heat shock/alpha-crystallin proteins: established concepts and emerging ideas.* Cell Mol Life Sci, 2000. **57**(6): p. 899-913.
120. van Montfort, R.L., et al., *Crystal structure and assembly of a eukaryotic small heat shock protein.* Nat Struct Biol, 2001. **8**(12): p. 1025-30.
121. Lambert, H., et al., *HSP27 multimerization mediated by phosphorylation-sensitive intermolecular interactions at the amino terminus.* J Biol Chem, 1999. **274**(14): p. 9378-85.
122. Clark, J.I. and P.J. Muchowski, *Small heat-shock proteins and their potential role in human disease.* Curr Opin Struct Biol, 2000. **10**(1): p. 52-9.
123. Rogalla, T., et al., *Regulation of Hsp27 oligomerization, chaperone function, and protective activity against oxidative stress/tumor necrosis factor alpha by phosphorylation.* J Biol Chem, 1999. **274**(27): p. 18947-56.
124. Van Montfort, R., C. Slingsby, and E. Vierling, *Structure and function of the small heat shock protein/alpha-crystallin family of molecular chaperones.* Adv Protein Chem, 2001. **59**: p. 105-56.
125. Gusev, N.B., N.V. Bogatcheva, and S.B. Marston, *Structure and properties of small heat shock proteins (sHsp) and their interaction with cytoskeleton proteins.* Biochemistry (Mosc), 2002. **67**(5): p. 511-9.
126. Laskowska, E., E. Matuszewska, and D. Kuczynska-Wisnik, *Small heat shock proteins and protein-misfolding diseases.* Curr Pharm Biotechnol, 2010. **11**(2): p. 146-57.
127. Salinthone, S., M. Tyagi, and W.T. Gerthoffer, *Small heat shock proteins in smooth muscle.* Pharmacol Ther, 2008. **119**(1): p. 44-54.
128. Fu, X. and Z. Chang, *Identification of bis-ANS binding sites in Mycobacterium tuberculosis small heat shock protein Hsp16.3: evidences for a two-step substrate-binding mechanism.* Biochem Biophys Res Commun, 2006. **349**(1): p. 167-71.
129. Shearstone, J.R. and F. Baneyx, *Biochemical characterization of the small heat shock protein IbpB from Escherichia coli.* J Biol Chem, 1999. **274**(15): p. 9937-45.
130. Lee, G.J., et al., *A small heat shock protein stably binds heat-denatured model substrates and can maintain a substrate in a folding-competent state.* EMBO J, 1997. **16**(3): p. 659-71.
131. Chang, Z., et al., *Mycobacterium tuberculosis 16-kDa antigen (Hsp16.3) functions as an oligomeric structure in vitro to suppress thermal aggregation.* J Biol Chem, 1996. **271**(12): p. 7218-23.
132. Chowdary, T.K., et al., *Mammalian Hsp22 is a heat-inducible small heat-shock protein with chaperone-like activity.* Biochem J, 2004. **381**(Pt 2): p. 379-87.
133. Behlke, J., et al., *Supramolecular structure of the recombinant murine small heat shock protein hsp25.* FEBS Lett, 1991. **288**(1-2): p. 119-22.

134. Ehrnsperger, M., et al., *The dynamics of Hsp25 quaternary structure. Structure and function of different oligomeric species.* J Biol Chem, 1999. **274**(21): p. 14867-74.
135. Bova, M.P., et al., *Subunit exchange of small heat shock proteins. Analysis of oligomer formation of alphaA-crystallin and Hsp27 by fluorescence resonance energy transfer and site-directed truncations.* J Biol Chem, 2000. **275**(2): p. 1035-42.
136. Haslbeck, M., et al., *Hsp26: a temperature-regulated chaperone.* EMBO J, 1999. **18**(23): p. 6744-51.
137. van den Oetelaar, P.J., et al., *A dynamic quaternary structure of bovine alpha-crystallin as indicated from intermolecular exchange of subunits.* Biochemistry, 1990. **29**(14): p. 3488-93.
138. Garrido, C., et al., *Heat shock proteins 27 and 70: anti-apoptotic proteins with tumorigenic properties.* Cell Cycle, 2006. **5**(22): p. 2592-601.
139. Lee, G.J., N. Pokala, and E. Vierling, *Structure and in vitro molecular chaperone activity of cytosolic small heat shock proteins from pea.* J Biol Chem, 1995. **270**(18): p. 10432-8.
140. Koteiche, H.A. and H.S. McHaourab, *Mechanism of chaperone function in small heat-shock proteins. Phosphorylation-induced activation of two-mode binding in alphaB-crystallin.* J Biol Chem, 2003. **278**(12): p. 10361-7.
141. Bova, M.P., et al., *Subunit exchange of alphaA-crystallin.* J Biol Chem, 1997. **272**(47): p. 29511-7.
142. Bova, M.P., et al., *Subunit exchange, conformational stability, and chaperone-like function of the small heat shock protein 16.5 from Methanococcus jannaschii.* J Biol Chem, 2002. **277**(41): p. 38468-75.
143. Regini, J.W., et al., *Structural changes in alpha-crystallin and whole eye lens during heating, observed by low-angle X-ray diffraction.* J Mol Biol, 2004. **336**(5): p. 1185-94.
144. Benesch, J.L., et al., *Small heat shock protein activity is regulated by variable oligomeric substructure.* J Biol Chem, 2008. **283**(42): p. 28513-7.
145. Sugiyama, Y., et al., *Muscle develops a specific form of small heat shock protein complex composed of MKBP/HSPB2 and HSPB3 during myogenic differentiation.* J Biol Chem, 2000. **275**(2): p. 1095-104.
146. Suzuki, K., et al., *Overexpressed heat shock protein 70 attenuates hypoxic injury in coronary endothelial cells.* J Mol Cell Cardiol, 1998. **30**(6): p. 1129-36.
147. Kato, K., et al., *Dissociation as a result of phosphorylation of an aggregated form of the small stress protein, hsp27.* J Biol Chem, 1994. **269**(15): p. 11274-8.
148. Shemetov, A.A., et al., *Phosphorylation by cyclic AMP-dependent protein kinase inhibits chaperone-like activity of human HSP22 in vitro.* Biochemistry (Mosc), 2008. **73**(2): p. 200-8.
149. Landry, J., et al., *Human HSP27 is phosphorylated at serines 78 and 82 by heat shock and mitogen-activated kinases that recognize the same amino acid motif as S6 kinase II.* J Biol Chem, 1992. **267**(2): p. 794-803.

150. Zantema, A., et al., *Heat shock protein 27 and alpha B-crystallin can form a complex, which dissociates by heat shock.* J Biol Chem, 1992. **267**(18): p. 12936-41.
151. Arata, S., S. Hamaguchi, and K. Nose, *Inhibition of colony formation of NIH 3T3 cells by the expression of the small molecular weight heat shock protein HSP27: involvement of its phosphorylation and aggregation at the C-terminal region.* J Cell Physiol, 1997. **170**(1): p. 19-26.
152. Mehlen, P., et al., *Tumor necrosis factor-alpha induces changes in the phosphorylation, cellular localization, and oligomerization of human hsp27, a stress protein that confers cellular resistance to this cytokine.* J Cell Biochem, 1995. **58**(2): p. 248-59.
153. Garrido, C., et al., *Heat shock protein 27 enhances the tumorigenicity of immunogenic rat colon carcinoma cell clones.* Cancer Res, 1998. **58**(23): p. 5495-9.
154. den Engelsman, J., et al., *Mimicking phosphorylation of the small heat-shock protein alphaB-crystallin recruits the F-box protein FBX4 to nuclear SC35 speckles.* Eur J Biochem, 2004. **271**(21): p. 4195-203.
155. Michaud, S., et al., *Cell-specific expression and heat-shock induction of Hsps during spermatogenesis in Drosophila melanogaster.* J Cell Sci, 1997. **110 (Pt 17)**: p. 1989-97.
156. Wu, C., *Heat shock transcription factors: structure and regulation.* Annu Rev Cell Dev Biol, 1995. **11**: p. 441-69.
157. Lis, J. and C. Wu, *Protein traffic on the heat shock promoter: parking, stalling, and trucking along.* Cell, 1993. **74**(1): p. 1-4.
158. Morimoto, R.I., *Cells in stress: transcriptional activation of heat shock genes.* Science, 1993. **259**(5100): p. 1409-10.
159. Morimoto, R.I., *Regulation of the heat shock transcriptional response: cross talk between a family of heat shock factors, molecular chaperones, and negative regulators.* Genes Dev, 1998. **12**(24): p. 3788-96.
160. Hu, Z., et al., *Structure, function, property, and role in neurologic diseases and other diseases of the sHsp22.* J Neurosci Res, 2007. **85**(10): p. 2071-9.
161. Kappe, G., et al., *Characterization of two novel human small heat shock proteins: protein kinase-related HspB8 and testis-specific HspB9.* Biochim Biophys Acta, 2001. **1520**(1): p. 1-6.
162. Benndorf, R., et al., *HSP22, a new member of the small heat shock protein superfamily, interacts with mimic of phosphorylated HSP27 ((3D)HSP27).* J Biol Chem, 2001. **276**(29): p. 26753-61.
163. Kim, M.V., et al., *Some properties of human small heat shock protein Hsp22 (H11 or HspB8).* Biochem Biophys Res Commun, 2004. **315**(4): p. 796-801.
164. Kasakov, A.S., et al., *Effect of mutations in the beta5-beta7 loop on the structure and properties of human small heat shock protein HSP22 (HspB8, H11).* FEBS J, 2007. **274**(21): p. 5628-42.

165. Kazakov, A.S., et al., *Thermally induced structural changes of intrinsically disordered small heat shock protein Hsp22.* Biophys Chem, 2009. **145**(2-3): p. 79-85.
166. Uversky, V.N., C.J. Oldfield, and A.K. Dunker, *Showing your ID: intrinsic disorder as an ID for recognition, regulation and cell signaling.* J Mol Recognit, 2005. **18**(5): p. 343-84.
167. Kim, M.V., et al., *Structure and properties of K141E mutant of small heat shock protein HSP22 (HspB8, H11) that is expressed in human neuromuscular disorders.* Arch Biochem Biophys, 2006. **454**(1): p. 32-41.
168. Cantin, G.T., et al., *Combining protein-based IMAC, peptide-based IMAC, and MudPIT for efficient phosphoproteomic analysis.* J Proteome Res, 2008. **7**(3): p. 1346-51.
169. Dephoure, N., et al., *A quantitative atlas of mitotic phosphorylation.* Proc Natl Acad Sci U S A, 2008. **105**(31): p. 10762-7.
170. Villen, J., et al., *Large-scale phosphorylation analysis of mouse liver.* Proc Natl Acad Sci U S A, 2007. **104**(5): p. 1488-93.
171. Rikova, K., et al., *Global survey of phosphotyrosine signaling identifies oncogenic kinases in lung cancer.* Cell, 2007. **131**(6): p. 1190-203.
172. Depre, C., et al., *H11 kinase is a novel mediator of myocardial hypertrophy in vivo.* Circ Res, 2002. **91**(11): p. 1007-14.
173. Smith, C.C., et al., *A novel human gene similar to the protein kinase (PK) coding domain of the large subunit of herpes simplex virus type 2 ribonucleotide reductase (ICP10) codes for a serine-threonine PK and is expressed in melanoma cells.* J Biol Chem, 2000. **275**(33): p. 25690-9.
174. Hanks, S.K. and A.M. Quinn, *Protein kinase catalytic domain sequence database: identification of conserved features of primary structure and classification of family members.* Methods Enzymol, 1991. **200**: p. 38-62.
175. Mymrikov, E.V., et al., *The pivotal role of the beta 7 strand in the intersubunit contacts of different human small heat shock proteins.* Cell Stress Chaperones, 2010. **15**(4): p. 365-77.
176. Sanbe, A., et al., *Protective effect of geranylgeranylacetone via enhancement of HSPB8 induction in desmin-related cardiomyopathy.* PLoS One, 2009. **4**(4): p. e5351.
177. Chavez Zobel, A.T., et al., *Distinct chaperone mechanisms can delay the formation of aggresomes by the myopathy-causing R120G alphaB-crystallin mutant.* Hum Mol Genet, 2003. **12**(13): p. 1609-20.
178. Carra, S., et al., *HspB8, a small heat shock protein mutated in human neuromuscular disorders, has in vivo chaperone activity in cultured cells.* Hum Mol Genet, 2005. **14**(12): p. 1659-69.
179. Fontaine, J.M., et al., *Interactions of HSP22 (HSPB8) with HSP20, alphaB-crystallin, and HSPB3.* Biochem Biophys Res Commun, 2005. **337**(3): p. 1006-11.

180. Sun, X., et al., *Interaction of human HSP22 (HSPB8) with other small heat shock proteins.* J Biol Chem, 2004. **279**(4): p. 2394-402.
181. Sun, X., M.J. Welsh, and R. Benndorf, *Conformational changes resulting from pseudophosphorylation of mammalian small heat shock proteins--a two-hybrid study.* Cell Stress Chaperones, 2006. **11**(1): p. 61-70.
182. Verschuure, P., et al., *Expression of small heat shock proteins HspB2, HspB8, Hsp20 and cvHsp in different tissues of the perinatal developing pig.* Eur J Cell Biol, 2003. **82**(10): p. 523-30.
183. Carra, S., S.J. Seguin, and J. Landry, *HspB8 and Bag3: a new chaperone complex targeting misfolded proteins to macroautophagy.* Autophagy, 2008. **4**(2): p. 237-9.
184. Crippa, V., et al., *The small heat shock protein B8 (HspB8) promotes autophagic removal of misfolded proteins involved in amyotrophic lateral sclerosis (ALS).* Hum Mol Genet, 2010. **19**(17): p. 3440-56.
185. Carra, S., et al., *HspB8 participates in protein quality control by a non-chaperone-like mechanism that requires eIF2{alpha} phosphorylation.* J Biol Chem, 2009. **284**(9): p. 5523-32.
186. Carra, S., *The stress-inducible HspB8-Bag3 complex induces the eIF2alpha kinase pathway: implications for protein quality control and viral factory degradation?* Autophagy, 2009. **5**(3): p. 428-9.
187. Takayama, S. and J.C. Reed, *Molecular chaperone targeting and regulation by BAG family proteins.* Nat Cell Biol, 2001. **3**(10): p. E237-41.
188. Rosati, A., et al., *Apoptosis inhibition in cancer cells: a novel molecular pathway that involves BAG3 protein.* Int J Biochem Cell Biol, 2007. **39**(7-8): p. 1337-42.
189. Takayama, S., Z. Xie, and J.C. Reed, *An evolutionarily conserved family of Hsp70/Hsc70 molecular chaperone regulators.* J Biol Chem, 1999. **274**(2): p. 781-6.
190. Briknarova, K., et al., *Structural analysis of BAG1 cochaperone and its interactions with Hsc70 heat shock protein.* Nat Struct Biol, 2001. **8**(4): p. 349-52.
191. Wang, H.G., et al., *Bcl-2 interacting protein, BAG-1, binds to and activates the kinase Raf-1.* Proc Natl Acad Sci U S A, 1996. **93**(14): p. 7063-8.
192. Doong, H., A. Vrailas, and E.C. Kohn, *What's in the 'BAG'?--A functional domain analysis of the BAG-family proteins.* Cancer Lett, 2002. **188**(1-2): p. 25-32.
193. Takayama, S., et al., *BAG-1 modulates the chaperone activity of Hsp70/Hsc70.* EMBO J, 1997. **16**(16): p. 4887-96.
194. Zeiner, M. and U. Gehring, *A protein that interacts with members of the nuclear hormone receptor family: identification and cDNA cloning.* Proc Natl Acad Sci U S A, 1995. **92**(25): p. 11465-9.
195. Townsend, P.A., et al., *BAG-1: a multifunctional regulator of cell growth and survival.* Biochim Biophys Acta, 2003. **1603**(2): p. 83-98.
196. Townsend, P.A., et al., *BAG-1: a multi-functional pro-survival molecule.* Int J Biochem Cell Biol, 2005. **37**(2): p. 251-9.

197. Schulz, J.B., et al., *Cooperative interception of neuronal apoptosis by BCL-2 and BAG-1 expression: prevention of caspase activation and reduced production of reactive oxygen species.* J Neurochem, 1997. **69**(5): p. 2075-86.
198. Takaoka, A., et al., *Anti-cell death activity promotes pulmonary metastasis of melanoma cells.* Oncogene, 1997. **14**(24): p. 2971-7.
199. Luders, J., J. Demand, and J. Hohfeld, *The ubiquitin-related BAG-1 provides a link between the molecular chaperones Hsc70/Hsp70 and the proteasome.* J Biol Chem, 2000. **275**(7): p. 4613-7.
200. Gamerdinger, M., et al., *Protein quality control during aging involves recruitment of the macroautophagy pathway by BAG3.* EMBO J, 2009. **28**(7): p. 889-901.
201. Behl, C., *BAG3 and friends: co-chaperones in selective autophagy during aging and disease.* Autophagy, 2011. **7**(7): p. 795-8.
202. Gamerdinger, M., et al., *BAG3 mediates chaperone-based aggresome-targeting and selective autophagy of misfolded proteins.* EMBO Rep, 2011. **12**(2): p. 149-56.
203. Gout, E., et al., *Co-chaperone BAG3 and adenovirus penton base protein partnership.* J Cell Biochem, 2010. **111**(3): p. 699-708.
204. Iwasaki, M., et al., *BAG3 directly associates with guanine nucleotide exchange factor of Rap1, PDZGEF2, and regulates cell adhesion.* Biochem Biophys Res Commun, 2010. **400**(3): p. 413-8.
205. Doong, H., et al., *CAIR-1/BAG-3 forms an EGF-regulated ternary complex with phospholipase C-gamma and Hsp70/Hsc70.* Oncogene, 2000. **19**(38): p. 4385-95.
206. Chang, J.S., et al., *Pleckstrin homology domains of phospholipase C-gamma1 directly interact with beta-tubulin for activation of phospholipase C-gamma1 and reciprocal modulation of beta-tubulin function in microtubule assembly.* J Biol Chem, 2005. **280**(8): p. 6897-905.
207. Kochl, R., et al., *Microtubules facilitate autophagosome formation and fusion of autophagosomes with endosomes.* Traffic, 2006. **7**(2): p. 129-45.
208. Arndt, V., et al., *Chaperone-assisted selective autophagy is essential for muscle maintenance.* Curr Biol, 2010. **20**(2): p. 143-8.
209. Franceschelli, S., et al., *Bag3 gene expression is regulated by heat shock factor 1.* J Cell Physiol, 2008. **215**(3): p. 575-7.
210. Bruno, A.P., et al., *Identification of a synaptosome-associated form of BAG3 protein.* Cell Cycle, 2008. **7**(19): p. 3104-5.
211. Fuchs, M., et al., *Identification of the key structural motifs involved in HspB8/HspB6-Bag3 interaction.* Biochem J, 2010. **425**(1): p. 245-55.
212. McCollum, A.K., G. Casagrande, and E.C. Kohn, *Caught in the middle: the role of Bag3 in disease.* Biochem J, 2010. **425**(1): p. e1-3.
213. Bjorkoy, G., et al., *p62/SQSTM1 forms protein aggregates degraded by autophagy and has a protective effect on huntingtin-induced cell death.* J Cell Biol, 2005. **171**(4): p. 603-14.

214. Pankiv, S., et al., *p62/SQSTM1 binds directly to Atg8/LC3 to facilitate degradation of ubiquitinated protein aggregates by autophagy.* J Biol Chem, 2007. **282**(33): p. 24131-45.
215. Ichimura, Y., et al., *Structural basis for sorting mechanism of p62 in selective autophagy.* J Biol Chem, 2008. **283**(33): p. 22847-57.
216. Kabeya, Y., et al., *LC3, a mammalian homologue of yeast Apg8p, is localized in autophagosome membranes after processing.* EMBO J, 2000. **19**(21): p. 5720-8.
217. Mizushima, N., et al., *In vivo analysis of autophagy in response to nutrient starvation using transgenic mice expressing a fluorescent autophagosome marker.* Mol Biol Cell, 2004. **15**(3): p. 1101-11.
218. Mizushima, N., T. Yoshimori, and B. Levine, *Methods in mammalian autophagy research.* Cell, 2010. **140**(3): p. 313-26.
219. Li, F., et al., *C terminus of Hsc70-interacting protein promotes smooth muscle cell proliferation and survival through ubiquitin-mediated degradation of FoxO1.* J Biol Chem, 2009. **284**(30): p. 20090-8.
220. Dai, Q., et al., *CHIP activates HSF1 and confers protection against apoptosis and cellular stress.* EMBO J, 2003. **22**(20): p. 5446-58.
221. Mymrikov, E.V., A.S. Seit-Nebi, and N.B. Gusev, *Large potentials of small heat shock proteins.* Physiol Rev, 2011. **91**(4): p. 1123-59.
222. White, B.G., et al., *Small heat shock protein 27 (Hsp27) expression is highly induced in rat myometrium during late pregnancy and labour.* Reproduction, 2005. **129**(1): p. 115-26.
223. White, B.G. and D.J. MacPhee, *Distension of the uterus induces HspB1 expression in rat uterine smooth muscle.* Am J Physiol Regul Integr Comp Physiol, 2011. **301**(5): p. R1418-26.
224. Cross, B.E., H.M. O'Dea, and D.J. MacPhee, *Expression of small heat shock-related protein 20 (HSP20) in rat myometrium is markedly decreased during late pregnancy and labour.* Reproduction, 2007. **133**(4): p. 807-17.
225. Williams, S.J., et al., *Spatiotemporal expression of alpha(1), alpha(3) and beta(1) integrin subunits is altered in rat myometrium during pregnancy and labour.* Reprod Fertil Dev, 2010. **22**(4): p. 718-32.
226. Baulieu, E.E., *Contragestion and other clinical applications of RU 486, an antiprogesterone at the receptor.* Science, 1989. **245**(4924): p. 1351-7.
227. Laemmli, U.K., *Cleavage of structural proteins during the assembly of the head of bacteriophage T4.* Nature, 1970. **227**(5259): p. 680-5.
228. Fort, P., et al., *Various rat adult tissues express only one major mRNA species from the glyceraldehyde-3-phosphate-dehydrogenase multigenic family.* Nucleic Acids Res, 1985. **13**(5): p. 1431-42.
229. Condon, J., et al., *Telomerase immortalization of human myometrial cells.* Biol Reprod, 2002. **67**(2): p. 506-14.
230. Bradford, M.M., *A rapid and sensitive method for the quantitation of microgram quantities of protein utilizing the principle of protein-dye binding.* Anal Biochem, 1976. **72**: p. 248-54.

231. Geisterfer, A.A., M.J. Peach, and G.K. Owens, *Angiotensin II induces hypertrophy, not hyperplasia, of cultured rat aortic smooth muscle cells.* Circ Res, 1988. **62**(4): p. 749-56.
232. McKay, S., et al., *Angiotensin II induces hypertrophy of human airway smooth muscle cells: expression of transcription factors and transforming growth factor-beta1.* Am J Respir Cell Mol Biol, 1998. **18**(6): p. 823-33.
233. Gibbons, G.H., R.E. Pratt, and V.J. Dzau, *Vascular smooth muscle cell hypertrophy vs. hyperplasia. Autocrine transforming growth factor-beta 1 expression determines growth response to angiotensin II.* J Clin Invest, 1992. **90**(2): p. 456-61.
234. Depre, C., et al., *H11 kinase prevents myocardial infarction by preemptive preconditioning of the heart.* Circ Res, 2006. **98**(2): p. 280-8.
235. Takayama, S., et al., *Expression and location of Hsp70/Hsc-binding anti-apoptotic protein BAG-1 and its variants in normal tissues and tumor cell lines.* Cancer Res, 1998. **58**(14): p. 3116-31.
236. Carra, S., et al., *HspB8 chaperone activity toward poly(Q)-containing proteins depends on its association with Bag3, a stimulator of macroautophagy.* J Biol Chem, 2008. **283**(3): p. 1437-44.
237. Wareham, A.L., *Expression of Small Heat Shock Protein B8 (HspB8) in Rat Uterine Smooth Muscle During Pregnancy and Labour*, in *Biochemistry*. 2008, Memorial University: St. John's.
238. Wang, H.Q., et al., *Characterization of BAG3 cleavage during apoptosis of pancreatic cancer cells.* J Cell Physiol, 2010. **224**(1): p. 94-100.
239. Du, Z.X., et al., *Caspase-dependent cleavage of BAG3 in proteasome inhibitors-induced apoptosis in thyroid cancer cells.* Biochem Biophys Res Commun, 2008. **369**(3): p. 894-8.
240. Sun, X., et al., *Induction of Hsp22 (HspB8) by estrogen and the metalloestrogen cadmium in estrogen receptor-positive breast cancer cells.* Cell Stress Chaperones, 2007. **12**(4): p. 307-19.
241. Chowdary, T.K., et al., *Interaction of mammalian Hsp22 with lipid membranes.* Biochem J, 2007. **401**(2): p. 437-45.
242. Simon, S., et al., *Myopathy-associated alphaB-crystallin mutants: abnormal phosphorylation, intracellular location, and interactions with other small heat shock proteins.* J Biol Chem, 2007. **282**(47): p. 34276-87.
243. Pagliuca, M.G., et al., *Regulation by heavy metals and temperature of the human BAG-3 gene, a modulator of Hsp70 activity.* FEBS Lett, 2003. **541**(1-3): p. 11-5.
244. Ferri, K.F. and G. Kroemer, *Organelle-specific initiation of cell death pathways.* Nat Cell Biol, 2001. **3**(11): p. E255-63.
245. Liao, Q., et al., *The anti-apoptotic protein BAG-3 is overexpressed in pancreatic cancer and induced by heat stress in pancreatic cancer cell lines.* FEBS Lett, 2001. **503**(2-3): p. 151-7.
246. Lee, J.H., et al., *Bis, a Bcl-2-binding protein that synergizes with Bcl-2 in preventing cell death.* Oncogene, 1999. **18**(46): p. 6183-90.

247. Earnshaw, W.C., L.M. Martins, and S.H. Kaufmann, *Mammalian caspases: structure, activation, substrates, and functions during apoptosis.* Annu Rev Biochem, 1999. **68**: p. 383-424.
248. Hong, S.K., et al., *Effect of glycine on recovery of bladder smooth muscle contractility after acute urinary retention in rats.* BJU Int, 2005. **96**(9): p. 1403-8.
249. Charpentier, A.H., et al., *Effects of estrogen on global gene expression: identification of novel targets of estrogen action.* Cancer Res, 2000. **60**(21): p. 5977-83.
250. Gober, M.D., et al., *Forced expression of the H11 heat shock protein can be regulated by DNA methylation and trigger apoptosis in human cells.* J Biol Chem, 2003. **278**(39): p. 37600-9.
251. Perkins, D., et al., *The herpes simplex virus type 2 R1 protein kinase (ICP10 PK) blocks apoptosis in hippocampal neurons, involving activation of the MEK/MAPK survival pathway.* J Virol, 2002. **76**(3): p. 1435-49.
252. Yang, C., et al., *Identification of cyclin D1- and estrogen-regulated genes contributing to breast carcinogenesis and progression.* Cancer Res, 2006. **66**(24): p. 11649-58.
253. Gober, M.D., S.Q. Wales, and L. Aurelian, *Herpes simplex virus type 2 encodes a heat shock protein homologue with apoptosis regulatory functions.* Front Biosci, 2005. **10**: p. 2788-803.
254. Chiappetta, G., et al., *The antiapoptotic protein BAG3 is expressed in thyroid carcinomas and modulates apoptosis mediated by tumor necrosis factor-related apoptosis-inducing ligand.* J Clin Endocrinol Metab, 2007. **92**(3): p. 1159-63.
255. Liu, P., et al., *BAG3 gene silencing sensitizes leukemic cells to Bortezomib-induced apoptosis.* FEBS Lett, 2009. **583**(2): p. 401-6.
256. Jacobs, A.T. and L.J. Marnett, *HSF1-mediated BAG3 expression attenuates apoptosis in 4-hydroxynonenal-treated colon cancer cells via stabilization of anti-apoptotic Bcl-2 proteins.* J Biol Chem, 2009. **284**(14): p. 9176-83.
257. Wang, H.Q., et al., *Inhibition of the JNK signalling pathway enhances proteasome inhibitor-induced apoptosis of kidney cancer cells by suppression of BAG3 expression.* Br J Pharmacol, 2009. **158**(5): p. 1405-12.
258. Festa, M., et al., *BAG3 protein is overexpressed in human glioblastoma and is a potential target for therapy.* Am J Pathol, 2011. **178**(6): p. 2504-12.
259. Ammirante, M., et al., *IKK{gamma} protein is a target of BAG3 regulatory activity in human tumor growth.* Proc Natl Acad Sci U S A, 2010. **107**(16): p. 7497-502.
260. Jung, S.E., et al., *Down-modulation of Bis sensitizes cell death in C6 glioma cells induced by oxygen-glucose deprivation.* Brain Res, 2010. **1349**: p. 1-10.
261. Cesaro, E., et al., *WT1 protein is a transcriptional activator of the antiapoptotic bag3 gene.* Leukemia, 2010. **24**(6): p. 1204-6.
262. Bonelli, P., et al., *BAG3 protein regulates stress-induced apoptosis in normal and neoplastic leukocytes.* Leukemia, 2004. **18**(2): p. 358-60.

263. Fang, X., S. Wong, and B.F. Mitchell, *Effects of RU486 on estrogen, progesterone, oxytocin, and their receptors in the rat uterus during late gestation.* Endocrinology, 1997. **138**(7): p. 2763-8.
264. Cox, B.E., et al., *Tissue specific expression of vascular smooth muscle angiotensin II receptor subtypes during ovine pregnancy.* Am J Physiol, 1996. **271**(1 Pt 2): p. H212-21.
265. Heenan, A.P., et al., *Effects of human pregnancy on fluid regulation responses to short-term exercise.* J Appl Physiol (1985), 2003. **95**(6): p. 2321-7.
266. Cui, X.L., B. Chang, and L. Myatt, *Expression and distribution of NADPH oxidase isoforms in human myometrium--role in angiotensin II-induced hypertrophy.* Biol Reprod, 2010. **82**(2): p. 305-12.
267. Shvets, E., E. Fass, and Z. Elazar, *Utilizing flow cytometry to monitor autophagy in living mammalian cells.* Autophagy, 2008. **4**(5): p. 621-8.
268. Blommaart, E.F., et al., *The phosphatidylinositol 3-kinase inhibitors wortmannin and LY294002 inhibit autophagy in isolated rat hepatocytes.* Eur J Biochem, 1997. **243**(1-2): p. 240-6.
269. Matsunaga, K., et al., *Two Beclin 1-binding proteins, Atg14L and Rubicon, reciprocally regulate autophagy at different stages.* Nat Cell Biol, 2009. **11**(4): p. 385-96.
270. Lenne, C. and R. Douce, *A Low Molecular Mass Heat-Shock Protein Is Localized to Higher Plant Mitochondria.* Plant Physiol, 1994. **105**(4): p. 1255-61.
271. Morrow, G., et al., *The small heat shock protein Hsp22 of Drosophila melanogaster is a mitochondrial protein displaying oligomeric organization.* J Biol Chem, 2000. **275**(40): p. 31204-10.
272. Morrow, G., et al., *Overexpression of the small mitochondrial Hsp22 extends Drosophila life span and increases resistance to oxidative stress.* FASEB J, 2004. **18**(3): p. 598-9.

From: Jacques.Landry@fmed.ulaval.ca
To: d42nlm@mun.ca
Subject: Figure for thesis
Date: July 9th/2012

Dear Ms Marsh,

Yes, you can use it. No problem. Good luck with your thesis.

JL

Jacques Landry, Ph.D.
Centre de recherche en cancérologie de l'Université Laval
Centre hospitalier universitaire de Québec
L'Hôtel-Dieu de Québec
9, rue McMahon
Québec, CANADA G1R 2J6

tél: (418) 525-4444 poste 15155
fax: (418) 691-5439

Avis relatif à la confidentialité / Notice of Confidentiality / Advertencia de confidencialidad
<http://www.rec.ulaval.ca/lce/securite/confidentialite.htm>

From: d42nlm@mun.ca
To: Jacques.Landry@fmed.ulaval.ca
Subject: Figure for thesis
Date: July 9th/2012

Dr. Landry:

My name is Noelle Marsh and I am a graduate student in a reproductive physiology lab in Memorial University. I am currently writing my thesis and I was wondering if I could use Figure 2A from your paper "Identification of the key structural motifs involved in HspB8/HspB6-Bag3 interaction". I will be using it to briefly explain where the interaction between HspB8 and Bag3 has been found to occur in my introduction. Thank you for your time.

Sincerely,

Noelle